~~A STUDY OF~~ SOME Surface PROPERTIES OF SILVER AND GOLD ~~SURFACES~~

By

Christopher Geoffrey Hart.

A Thesis presented to the University of London in partial fulfilment of the requirements for the degree of Doctor of Philosophy.

The Sir Christopher Ingold Laboratories,

Department of Chemistry.

University College, London.

September 1974

Abstract

Clean silver and gold surfaces were prepared under ultra high vacuum by the deposition of films of the metals onto pyrex or B37 glass substrates. The adsorption of hydrogen, xenon and carbon monoxide was studied on these films. Measurements of surface potential, equilibrium pressure and rates of adsorption were made as a function of coverage of the surface by the adsorbate. Certain of the properties of the films towards these gases were found to be dependent on the choice of glass substrate.

Xenon surface potentials of 480mV for silver and 470mV for gold were recorded, and the form of the surface potential vs coverage curves discussed in terms of some simple models. The occurrence of a phase change near the half monolayer is postulated for this system. Surface potential data for carbon monoxide included maximum values of 460mV on silver and 660mV on gold, and for hydrogen included maximum values of -320mV on Ag/pyrex and -265mV on Ag/B37: on gold the surface potential reached a maximum value of -100mV near half coverage and subsequently fell to near -70mV at full coverage.

Surface potential and adsorption rate data indicated the occurrence of interactions between hydrogen atoms and xenon or carbon monoxide pre-adsorbed on these surfaces. Some features of these are discussed in terms of a simple hydrogen atom recombination model. The reported desorption of hydrogen on adding xenon to a hydrogen covered surface is also implicit in this model.

Acknowledgements

I should like to express my thanks and appreciation to Dr.M.H.B.Stiddard, my supervisor, for his continual advice, helpful criticism and encouragement throughout this study,

to Dr.A.G.Knapp for his interest in the project and for many helpful and often hilarious discussions,

to my wife Tessa, for her considerable help with the typescript and for her patience and understanding,

and to my parents for their continual interest and encouragement.

The award of a Research Studentship by the Science Research Council is also gratefully acknowledged.

Contents

Chapter 1

Experimental

1.1

In order to prepare a clean surface and to investigate its properties, an apparatus capable of maintaining pressures in the ultra-high-vacuum (UHV) range (less than 10^{-9}torr) is essential. Surfaces prepared or maintained at appreciably higher pressures may be covered to an unknown and significant extent with a layer of adsorbed gas. Surfaces may either be freshly prepared under UHV conditions for example by evaporation or cleavage; or an initially contaminated surface may be cleaned for example by heating or ion bombardment. In this study clean silver and gold surfaces were prepared by evaporation onto glass substrates. In this chapter the construction, operation and calibration of the vacuum system, which was capable of attaining pressures below 4×10^{-10}torr, is described. The preparation of the silver and gold surfaces and the specialised apparatus and techniques used in the investigation of their properties are described.

1.2 Vacuum System

In any vacuum system the ultimate pressure attainable is determined by the equilibrium between the rate of influx of gas from all sources and its rate of removal by pumping. Small and simple pumps of low pumping speed can achieve UHV conditions if the rate of influx of gas is maintained at a very low level. The choice of type of pump is determined by the nature of the experiment; in

this case the pumps are required to remove hydrogen and inert gases and this requirement is most economically met by diffusion pumps backed by a rotary backing pump. Contamination by hydrocarbons has particularly to be avoided thus making mercury diffusion pumps the most suitable choice.

1.3

Sources of residual gas other than those gases introduced experimentally include the following (1).

(a) Real leaks

(b) Diffusion of gas through the vacuum envelope

(c) Vapour and dissociation pressures

(d) Desorption of previously adsorbed gas

(e) Diffusion of gas from inside solids

(f) Re-emission of gas previously pumped by ion pumping in gauges.

1.4

The detection and elimination of leaks is discussed in the sections describing the operation of the system (1.11). (b) is the largest single source of gas in a borosilicate glass system due to the permeation of atmospheric helium (1). The use of aluminosilicate glass reduces the permeation rate by several orders of magnitude but since it is much more difficult to work it is rarely used. (c) prohibits the use of any material in the construction of the system which shows significant vapourisation or decomposition at temperatures encountered in the system, for example brass in the bake out zones. Sources (d), (e)

and (f) can be efficiently reduced by baking critical portions of the system at approximately 400°C. (limit for borosilicate glass) since the rate of these processes increases exponentially with temperature. On subsequent cooling to room temperature the gas influx rate from these sources can be reduced by many orders of magnitude. The techniques used are described in sections discussing system operation (1.11).

The vacuum apparatus constructed therefore consists of a small borosilicate glass system whose UHV section could be heat treated at approximately 400°C. and subsequently protected by cold traps: pumped by mercury diffusion pumps and backed by a rotary pump it is shown diagrammatically in fig. 1.1.

1.5

For ease of description the system may be divided into three sections:

(a) Backing line and diffusion pumps

(b) Gas dosing system

(c) UHV section.

(a) <u>Backing line and diffusion pumps.</u>

The system is rough pumped by an AEI GDR1 2 stage gas ballasted rotary pump arranged to pump through an Edwards automatic air admittance valve which isolates the vacuum system (maintaining backing pressure) and admits air to the backing pump should the pump fail. Reservoir R1 buffers the system from the effects of the periodic pumping action of a rotary pump and serves as an

Fig.1.1 VACUUM SYSTEM

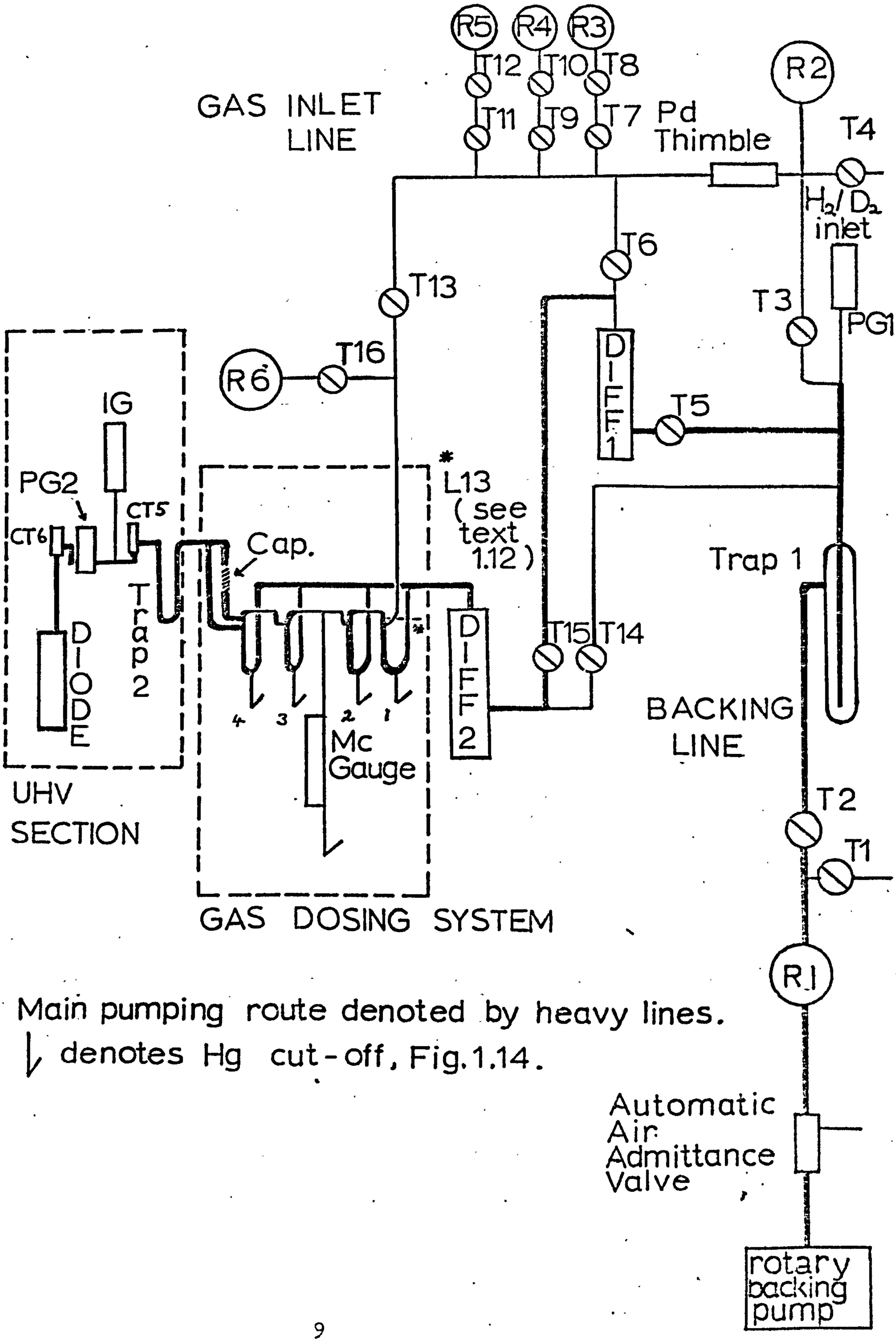

Main pumping route denoted by heavy lines.
⌊ denotes Hg cut-off, Fig.1.14.

emergency catchpot for oil in the event of catastrophic failure of the mechanical pump. Tap T2 allows the system to be isolated from the backing pump and air can be admitted through tap T1.*

Cold trap 1 prevents the diffusion of oil vapour into the system and mercury into the rotary pump. The pressure in the backing line was monitored using PG1, an Edwards G6A pirani gauge, with its control unit a Vacuum Generators IGP3.

Two two stage diffusion pumps, Jencons type 1, were arranged for series or parallel operation. They were usually operated in series i.e. tap T14 closed, tap T15 open as this conferred a greater resistance to back diffusion of gases from the backing line and hence a lower ultimate pressure. The gas inlet line was evacuated when necessary by opening tap T6; taps T14 and T15 were both temporarily closed during this procedure to prevent the critical backing pressure of diffusion pump 2 being exceeded.

(b) Gas dosing system.

This consists of a gas inlet line defined by taps T6, T13,

---

* These two taps could with advantage be sited on the backing pump side of R1, allowing the system to be isolated from the backing pump for long periods, the diffusion pumps exhausting into R1. They were always placed in this position in subsequent systems.

T8, T10, T12 and a palladium thimble, and a dosing system comprising a set of mercury cut offs (2) and a McLeod gauge. It is shown in fig. 1.1 and in greater detail in figs. 1.13 and 1.14.* Hydrogen or deuterium could be admitted to the gas inlet line through the palladium thimble which was heated electrically. This procedure also purifies the gas. Impure hydrogen or deuterium was stored in reservoir R2 which could be evacuated through tap T3 and filled from a cylinder through tap T4. Purified hydrogen or deuterium was stored in reservoir R6 which was placed below tap T13 in order that more than one gas could be handled by the inlet line simultaneously. Other gases, BOC Grade X, were stored in reservoirs R3, R4 and R5. These were fitted with glass break seals and magnetic hammers in the tubes between the bulbs and taps T8, T10 and T12. The operation of the gas dosing system is detailed in section 1.12. The system is terminated in cut off CT4 by two tubes leading to the UHV section, one having a reduced bore (capillary approximately 0.5mm. diameter) the other

---

* Smooth operation of the mercury cut offs is only possible if the small tubes entering the cut off sides are arranged to have steeply sloping shoulders as shown in fig. 1.13, ensuring that the mercury always returns to the main tube on lowering the mercury reservoir.

of normal diameter (approximately 1cm.) arranged so that by adjusting the mercury level in CT4 either the capillary route alone, or both tubes could be opened to the UHV section. By this means gases could be admitted quickly or at a much reduced rate to the UHV section as required.

(c) UHV Section.

Shown in figs. 1.2, 1.3 and 1.6, it consists of a U-tube cold trap which prevents the diffusion of condensible material (chiefly mercury) into the section, two cone and socket cut offs, a Mullard IOG12 ion gauge, a fast response pirani gauge head (fig 1.3) and the diode cell used for the experimental measurements. (The diode cells were mounted so that the bulb could be immersed in liquid nitrogen during adsorption experiments.) The UHV section could be baked in three zones to 400°C. using electric ovens. Details of its operation are included in sections 1.11 and 1.14. Pressures in the UHV section were routinely measured using the IOG12 gauge operated by a Vacuum Generators control unit IGP3. Pressures could be measured between 5×10^{-3} and 1×10^{-10} torr. Emission currents of less than 1mA. were always used. The gauge was calibrated for carbon monoxide and xenon using the McLeod gauge; hydrogen pressures could only be measured if the high pumping speed of the gauge for hydrogen was reduced by first saturating it with the gas. The gauge was rarely used in this manner. Indicated pressures of less than 1×10^{-9} torr are highly inaccurate as the gauge is then operating near its X-ray limit of 1×10^{-10} torr

Fig.1.2 UHV SECTION

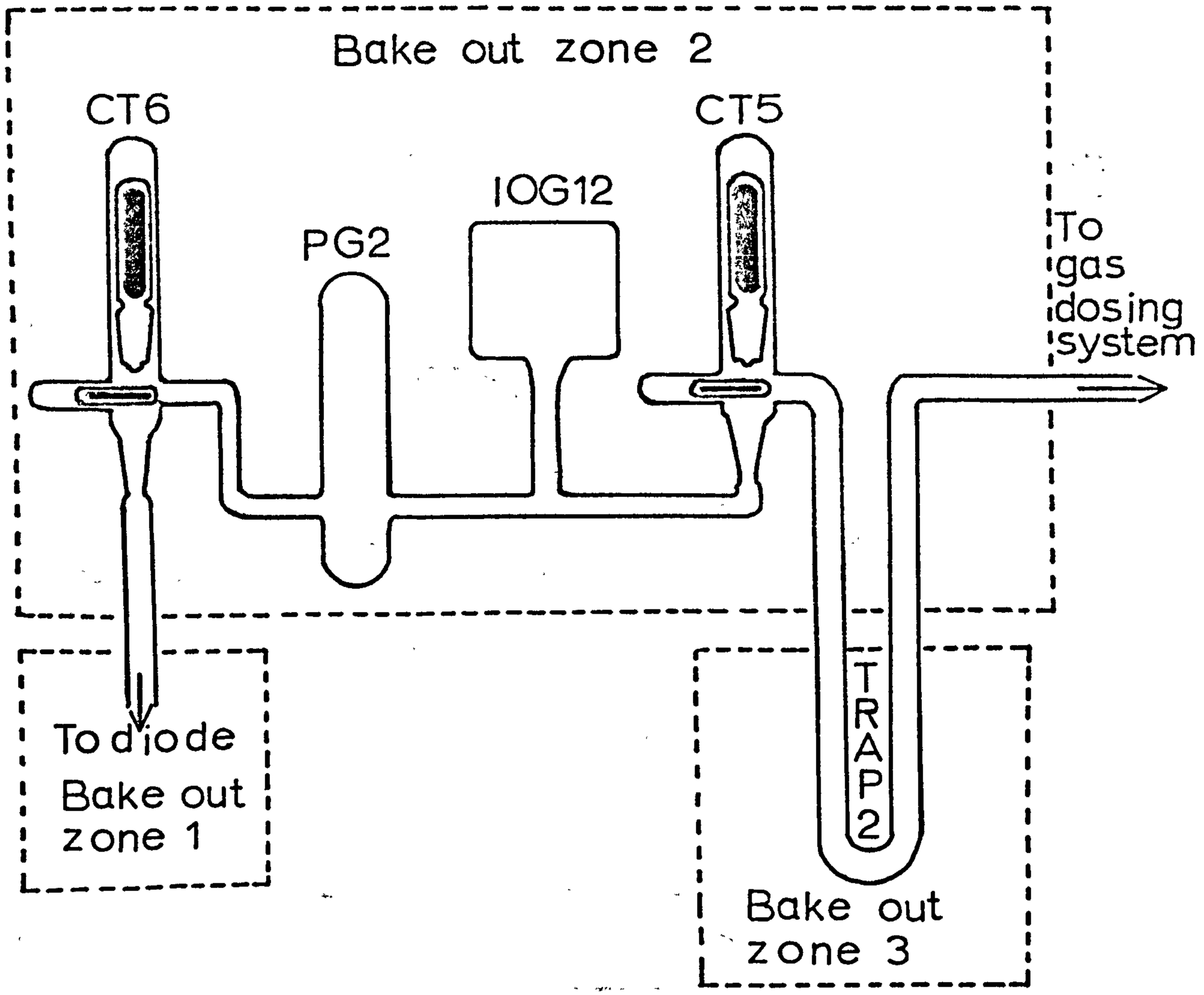

and they are best regarded as an indication of the consistency of performance of the system (3).

1.6 Pirani Gauge.

The pirani gauge was particularly used for measuring the rapid changes of pressure observed during hydrogen adsorption. It was specially constructed and operated so as to have a high sensitivity and fast response. The gauge is shown in fig.1.3, and its operating circuit in fig. 1.4. The gauge consisted of a length of about 30cm. of 0.01mm. diameter tungsten wire, openly coiled and spot welded via short 0.1mm. wires in order to reduce thermal

Fig.1.3 FAST RESPONSE PIRANI GAUGE

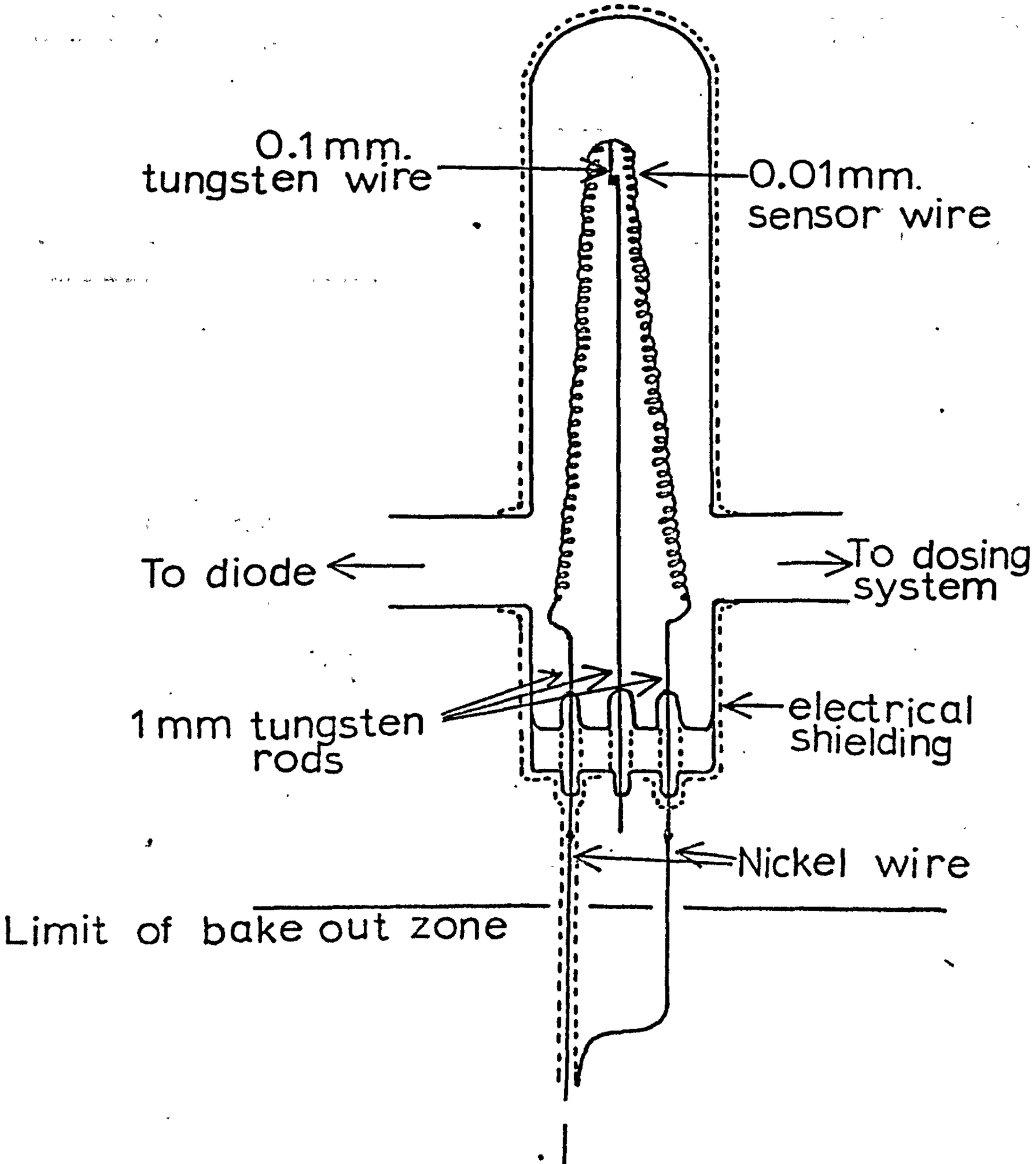

inertia, to three 1mm. tungsten rods. Nickel wires were welded to the two rods supporting the ends of the sensing wire outside the vacuum envelope, and were used to take the connections outside the bake out area in order to reduce thermal noise due to corroded contacts. The gauge head was electrically shielded to reduce electrical "pick-up" and to permit higher amplification in the control unit. The device was placed in the vacuum line rather than tubulated off the line in order to reduce conductance effects.

The control unit maintains the wire at constant temperature, the output from the device being derived from the adjustment to the current needed to maintain this constant temperature as the heat losses from the sensor wire change with varying gas pressure. Operating in this manner increases the rate of response of the gauge and results in an output which over a wide range of pressures is proportional to the pressure (4). The control unit operates as follows:

R1, R2, R3 and the gauge head form a Wheatstone bridge supplied with current through TR1. If the bridge is out of balance due to a change in pressure then a voltage develops between the junctions of R2/R3 and R1/gauge. This out of balance voltage is amplified and inverted by the operational amplifier OP1 which controls TR1 so as to rebalance the bridge by altering the current flowing through it. This restores the gauge wire temperature and consequently its resistance to the balanced bridge

condition. The voltage across the bridge is amplified by OP2, R4 acting as a back off to permit the sensitivity of the recorder to be increased. The output of OP2 is fed to the recorder. The rate of response of the control unit/ gauge head is determined by the thermal inertia of the sensor wire and by the gain of the servo loop formed by OP1, TR1 and the bridge circuit R1, R2, R3 and the gauge head. Very high gain (approximately 1000 times) plus minimal thermal inertia result in rapid response to pressure change.

1.7

Since the gauge wire is held at constant temperature, after equilibrium heat flow conditions have been reached, the power dissipated in the wire will be the sum of two factors (a) the constant heat loss due to radiation and conduction through the wire supports and (b) that due to the thermal conductivity of the gas at pressure P. At low pressures this conductivity is proportional to P.

Hence

$$W_p = KP + W_o$$

$$KP = W_p - W_o \qquad \text{——— (1)}$$

where

W_o = power dissipated at P = 0

(i.e. due to (a))

W_p = power dissipated at pressure P

(i.e. (a) + (b))

K is a constant for a given gas.

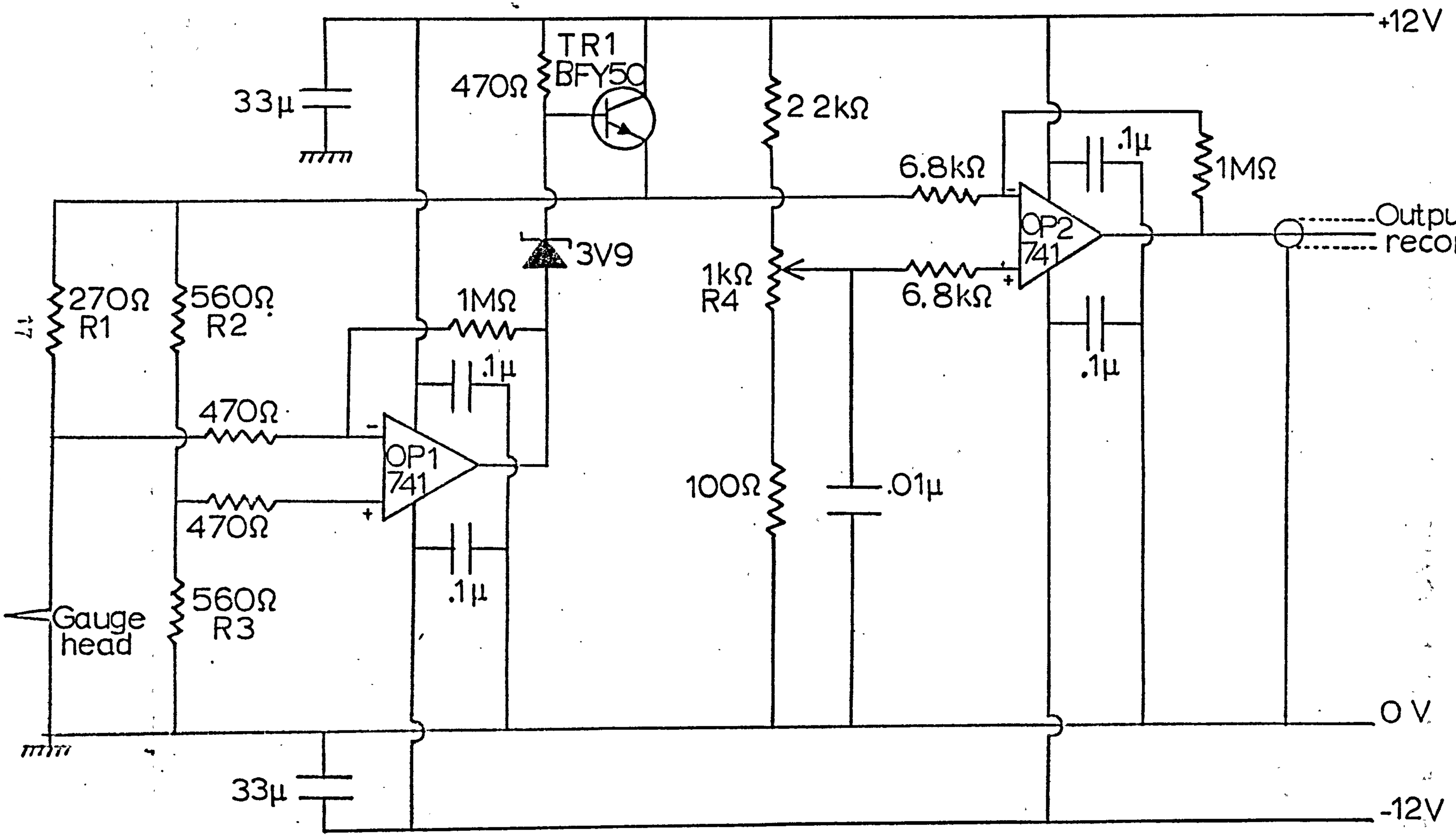

Fig.1.4 FAST PIRANI OPERATING CIRCUIT

Fig.1.5 PIRANI GAUGE CALIBRATION CURVE (Nov 1973)

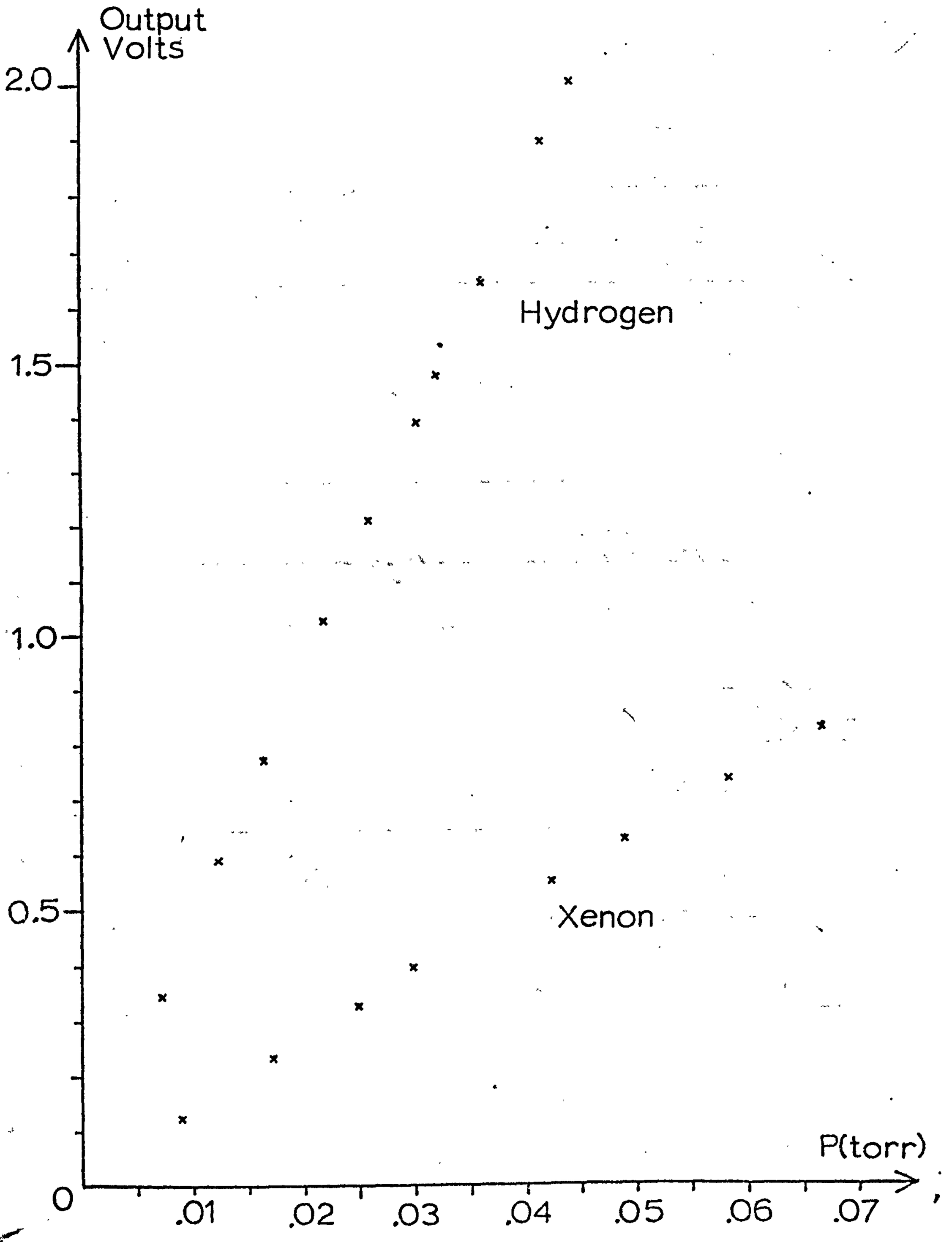

Now let the value of the bridge voltage at P = 0 be V_o and at pressure P be V_p. Since $W = \frac{V^2}{R}$

$$W_o = \frac{V_o^2}{R}$$

$$W_p = \frac{V_p^2}{R}$$

where $$R = \frac{(R_1 + R_{gauge})(R_2 + R_3)}{(R_{gauge} + R_1 + R_2 + R_3)}$$

Therefore substituting in (1)

$$K P = \frac{(V_p^2 - V_o^2)}{R}$$

Now let $V_p - V_o = \Delta V$ and, since ΔV is small at low pressures, by neglecting terms in ΔV^2 we have:

$$KP = \frac{2V_o \cdot \Delta V}{R}$$

Therefore

$$V = \left[\frac{K.R}{2V_o}\right] P$$

Hence ΔV is proportional to P at low pressures.

The gauge was calibrated for various gases several times during the course of experiments and a typical example in fig. 1.5 shows the expected linear behaviour at low pressures.

1.8 Diode Cell

The diode cell used for surface potential and rate of adsorption experiments is shown in fig. 1.6 and the electrical circuits associated with it in figs. 1.7, 1.8 and 1.9.

Two types of diode were used during the series of experiments differing only in that type 1 was constructed from B37 glass while type 2 was constructed from pyrex except for the glass metal seals which were B37. One of these latter diodes was modified by the addition of a large flat ground glass flange (shown dotted in fig. 1.6) which mated with a specially constructed dewar vessel. When filled with liquid nitrogen coolant this combination could be partially evacuated in order to reduce the boiling point of the liquid nitrogen. This technique was used during experiments with krypton. The filament and hook were 0.1mm diameter tungsten wire spot welded via nickel tabs to 1mm diameter tungsten supporting rods. These rods which also brought heating current to the filament were cooled by a thermostatted water jacket in order to maintain their resistance constant (see section 1.9). Electrical connections were made to them by welded nickel wires which were taken outside the bake out area, in order to reduce thermal noise due to corroded contacts. Operating techniques and details of the procedure used to evaporate gold and silver films onto the inside surface of the bulb are given in sections 1.14 and 1.15. Electrical contact with the film was achieved via a strip of platinum foil sealed to the

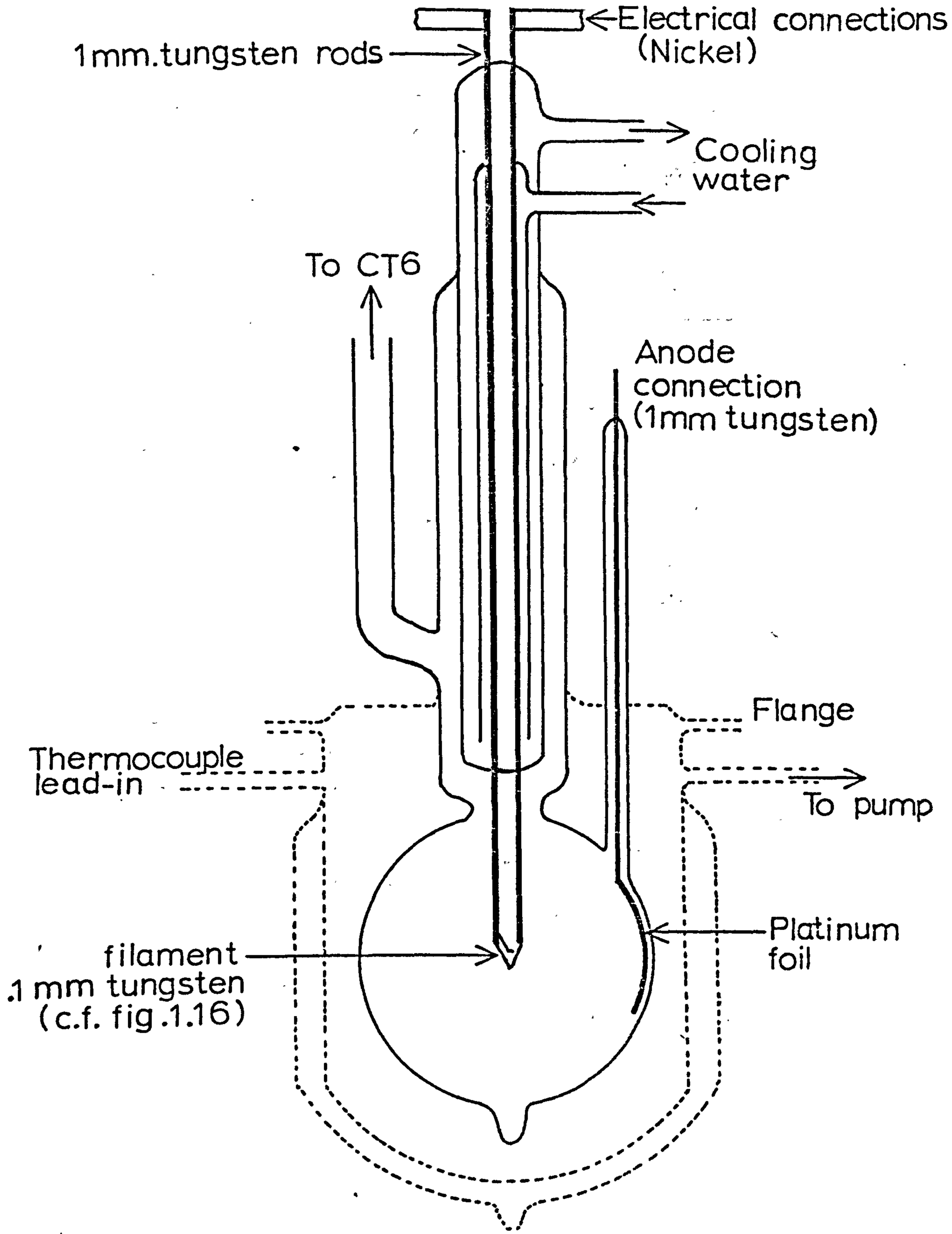

------ = Dewar vessel
(Kr adsorption only)

Fig. 1.6 DIODE CELL

Fig. 1.7 DIODE CELL - ELECTRICAL

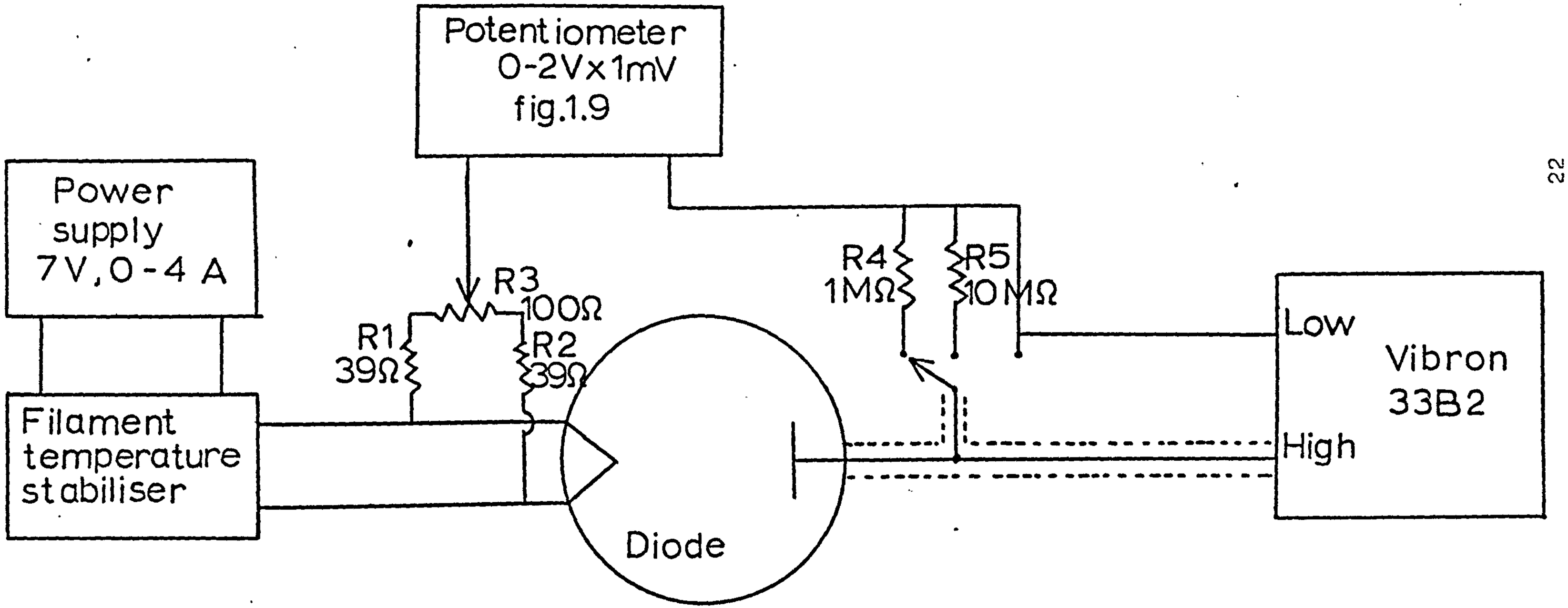

diode wall and welded to a 1mm. tungsten rod sealed through the wall of the bulb.* Since the bulb of the diode was immersed in liquid nitrogen during measurements, the anode (film) contact was arranged so that connection could be made to it above the liquid nitrogen level as this reduced electrical noise from the connection.

1.9

The electrical circuits associated with the diode perform the following functions.

Since the diode I_a vs V_a characteristics are highly dependent on the filament temperature, this is automatically stabilised. The circuit used is shown in fig. 1.8. It operates in essentially identical manner to the constant temperature pirani gauge sensing unit, sensing the resistance of the filament (function of temperature) and maintaining it constant. Transistor 2N3055 is added to enable higher currents to be controlled. Potentiometer R1 (10 turn helipot) enables the position of balance of the bridge to be altered and so varies the filament temperature.

The potentiometer supplies a variable anode voltage of between $\pm$ 2 volts in 1mv. steps. Its circuit is shown in fig. 1.9. Its output voltage is set to correspond to that indicated by the decade resistors by adjusting the power

---

*It is important that this anode connection is not placed in the plane of the filament supporting rods as shading from these rods during evaporation can result in poor electrical contact to the film.

supply voltage and measuring the potentiometer output using a digital voltmeter. The calibration was rechecked at intervals.

The potentiometer was connected to the diode filament via the isolating circuit R1, R2, R3 (fig. 1.7). R3 was adjusted until the anode current was unaltered by reversing the polarity of the filament power supply. R4 and R5 are the anode load resistors for the diode (R4 normally used). The anode current was measured by monitoring the voltage across the anode load resistor using the Vibron electrometer:

Fig.1.8 DIODE FILAMENT TEMPERATURE STABILIZER

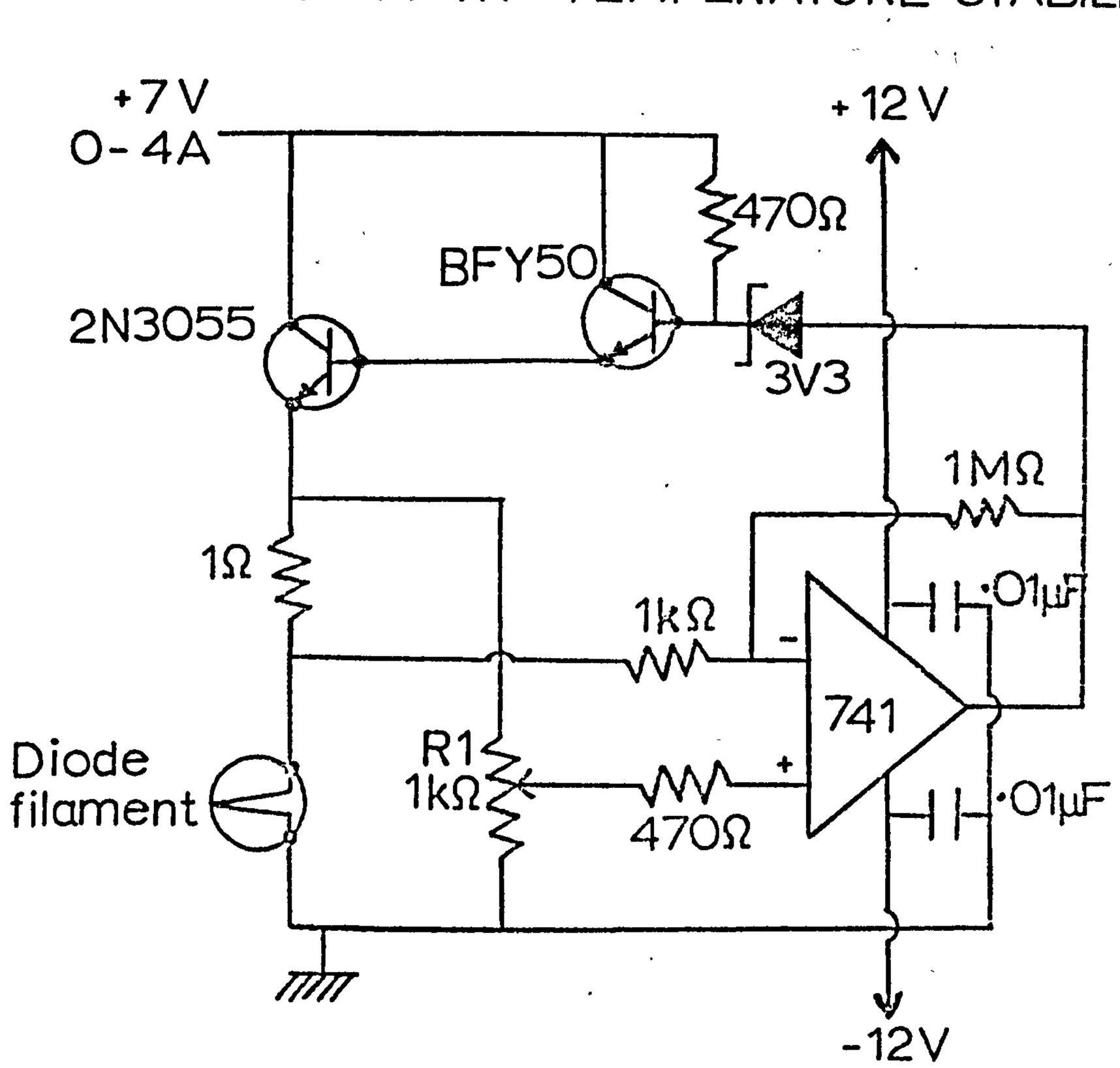

Fig. 1.9 POTENTIOMETER

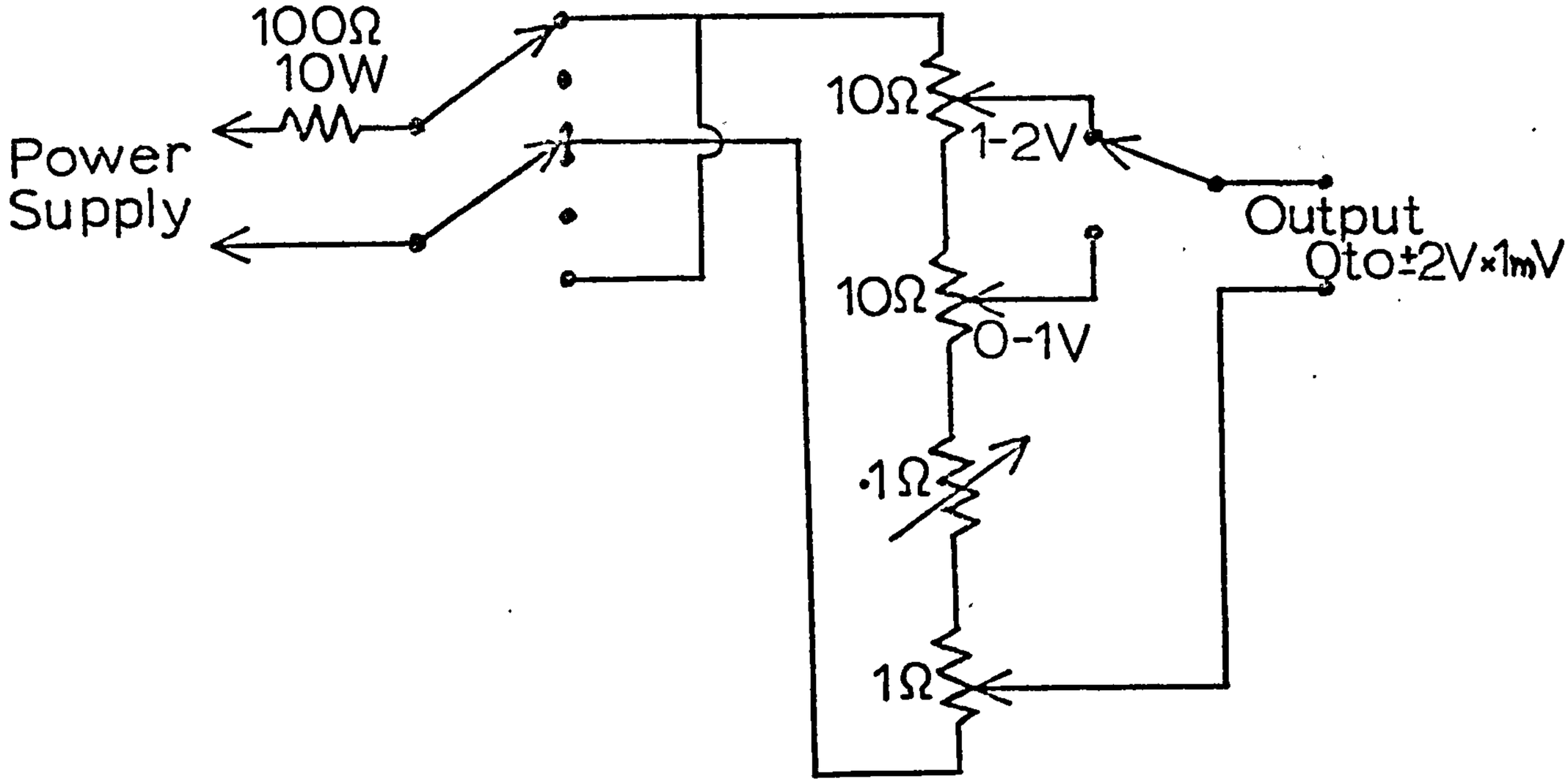

10 step decade resistors

$$I_a = V_{R_a} / R_a$$

$$V_a = V + V_{R_a}$$

where I_a = anode current

V_{R_a} = voltage across anode load

R_a = anode load resistor (R4 or R5)

V_a = anode voltage

V = output voltage of potentiometer.

Using these two relationships the I_a / V_a characteristics of the diode could be plotted.

Surface potentials may be measured as follows (section 2.10): After evaporating a film the filament temperature was set so that I_a = 100nA. when V_a was -1.101V. Surface potentials were then obtained by adjusting V_a using the potentiometer so that I_a remained constant during the adsorption process.

I_a could be monitored very accurately using the back-off facility of the Vibron electrometer to obtain maximum sensitivity. I_a could be maintained constant to $\pm$ 0.5nA. and hence surface potentials measured to $\pm$ 0.5mV.

1.10

Two simple ancillary pieces of apparatus remain to be described.

(a) Automatic cold trap filler: this apparatus maintains the level of liquid nitrogen in a cold trap within prescribed limits. It is shown in fig. 1.10 and functions as follows: When the tube is partially immersed in liquid nitrogen the oxygen of the air in it condenses. This lowers the pressure in the device. The mercury manometer is drawn towards the sensing tube and contact between pin A and B is broken. The transfer pump is switched off. As the liquid nitrogen level falls below the end of the tube, the air in the tube evaporates, contact is made between pins A and C as the mercury moves in response to the increased pressure and the transfer pump is switched on. Pin B acts as a maintaining contact. Sufficient current flows through resistor R to hold the relay on but not to energise it from the fully off position. Thus the relay only switches on when contact is made between A and C and only switches off when contact is lost between A and B. This prevents the relay chattering and prematurely switching off due to liquid nitrogen splashing during pumping. Adjustment to the position of contact C alters the liquid nitrogen level at which the pump is switched on relative to the end of the sensing tube.

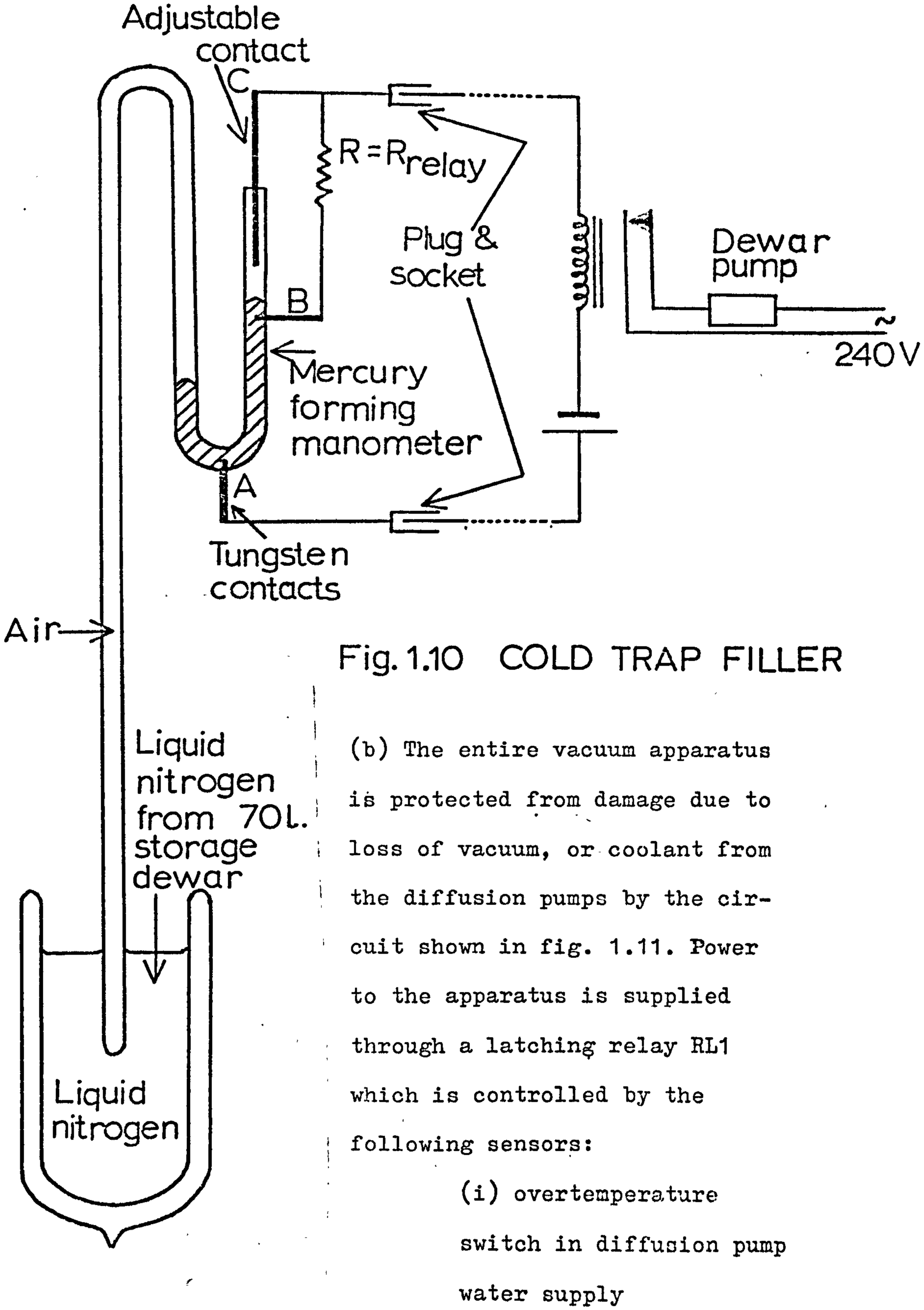

Fig. 1.10 COLD TRAP FILLER

(b) The entire vacuum apparatus is protected from damage due to loss of vacuum, or coolant from the diffusion pumps by the circuit shown in fig. 1.11. Power to the apparatus is supplied through a latching relay RL1 which is controlled by the following sensors:

(i) overtemperature switch in diffusion pump water supply

(ii) pressure switch in diffusion pump water supply

(iii) sensitive manometric switch (± .5torr) monitoring rough vacuum, shown in fig 1.11(a).

Power is not restored to the apparatus after power cuts or

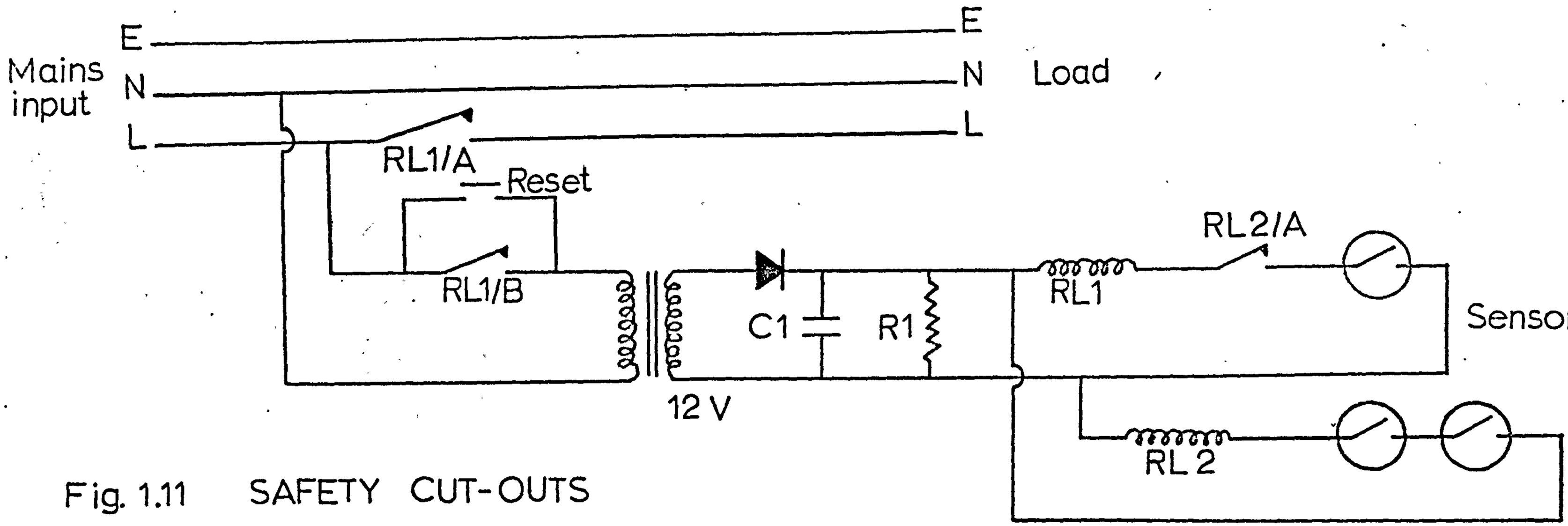

Fig. 1.11 SAFETY CUT-OUTS

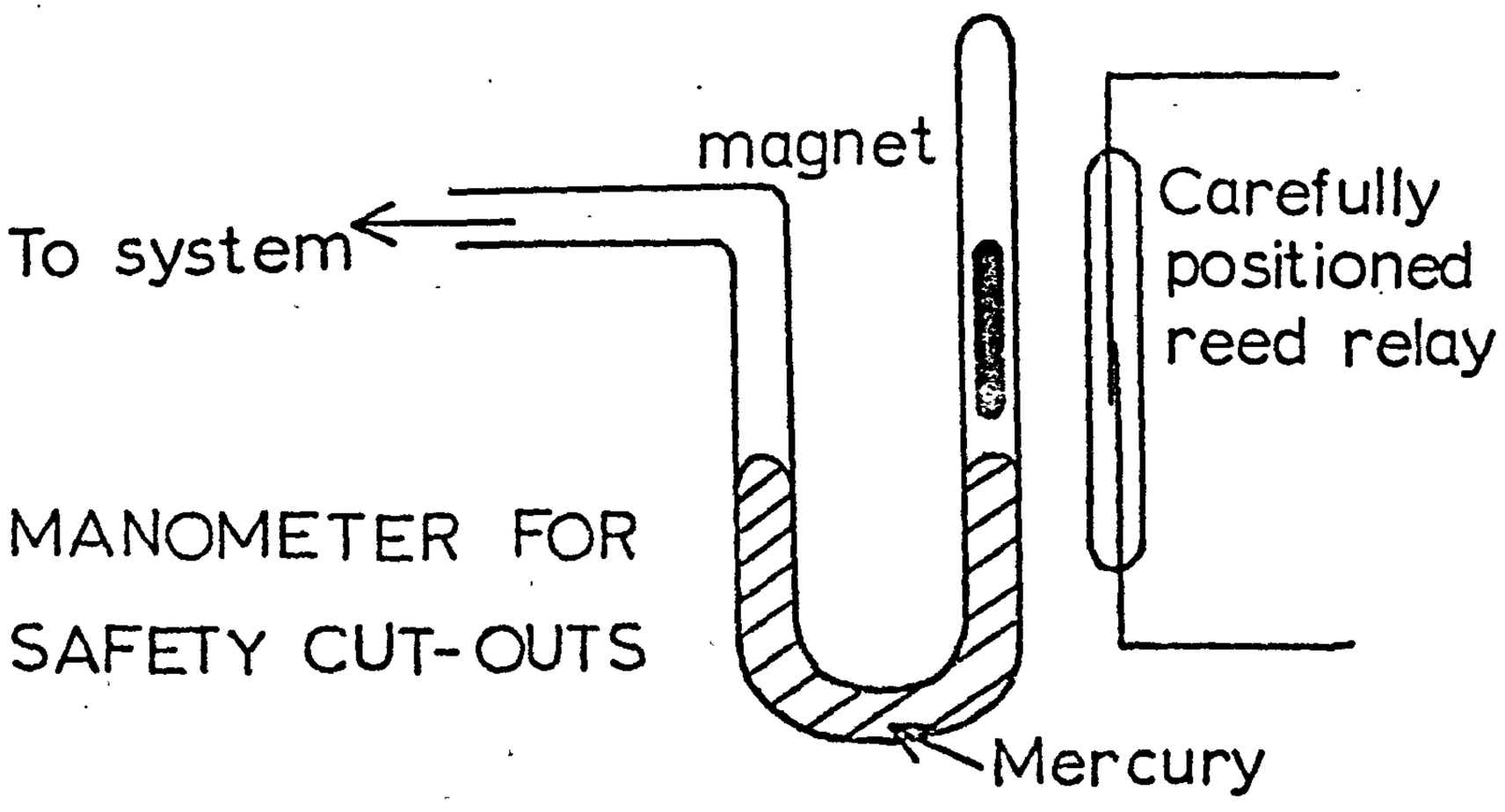

Fig. 1.11(a) MANOMETER FOR SAFETY CUT-OUTS

in the event of one of the sensors resetting e.g. as the diffusion pumps cool down, due to the action of the main latching relay. The time constant of C1/R1 is chosen to avoid a shutdown due to momentary fluctuations in mains voltage.

System Operation

1.11 Pump Down

After initial pump down the system was always let down to dry nitrogen rather than air as this greatly reduced subsequent pump down times, chiefly by reducing the quantity of water vapour which was adsorbed onto the walls of the system. Before evacuation the diode was prepared as detailed in section 1.14. The mercury reservoirs for the gas dosing system were lowered to their fullest extent. All taps and cut offs were opened except for T1, T4 and taps T8, T10 and T12 after the seals on reservoirs R3, R4 and R5 had been opened. The evacuation procedure was then as follows (fig. 1.12). Pump down was most economically commenced at about 2pm. The system was first evacuated using the rotary pump, on gas ballast for the first few minutes to speed removal of water vapour. When a pressure of less than 10^{-2}torr was indicated by PG1 trap 1 was cooled in liquid nitrogen whereupon the pressure would immediately fall to less than 10^{-3}torr. The system was always pumped at this pressure for a few more minutes; trap 2 was then cooled in liquid nitrogen, taps T13 and T14 were closed and the diffusion pumps started. After some fifteen minutes the

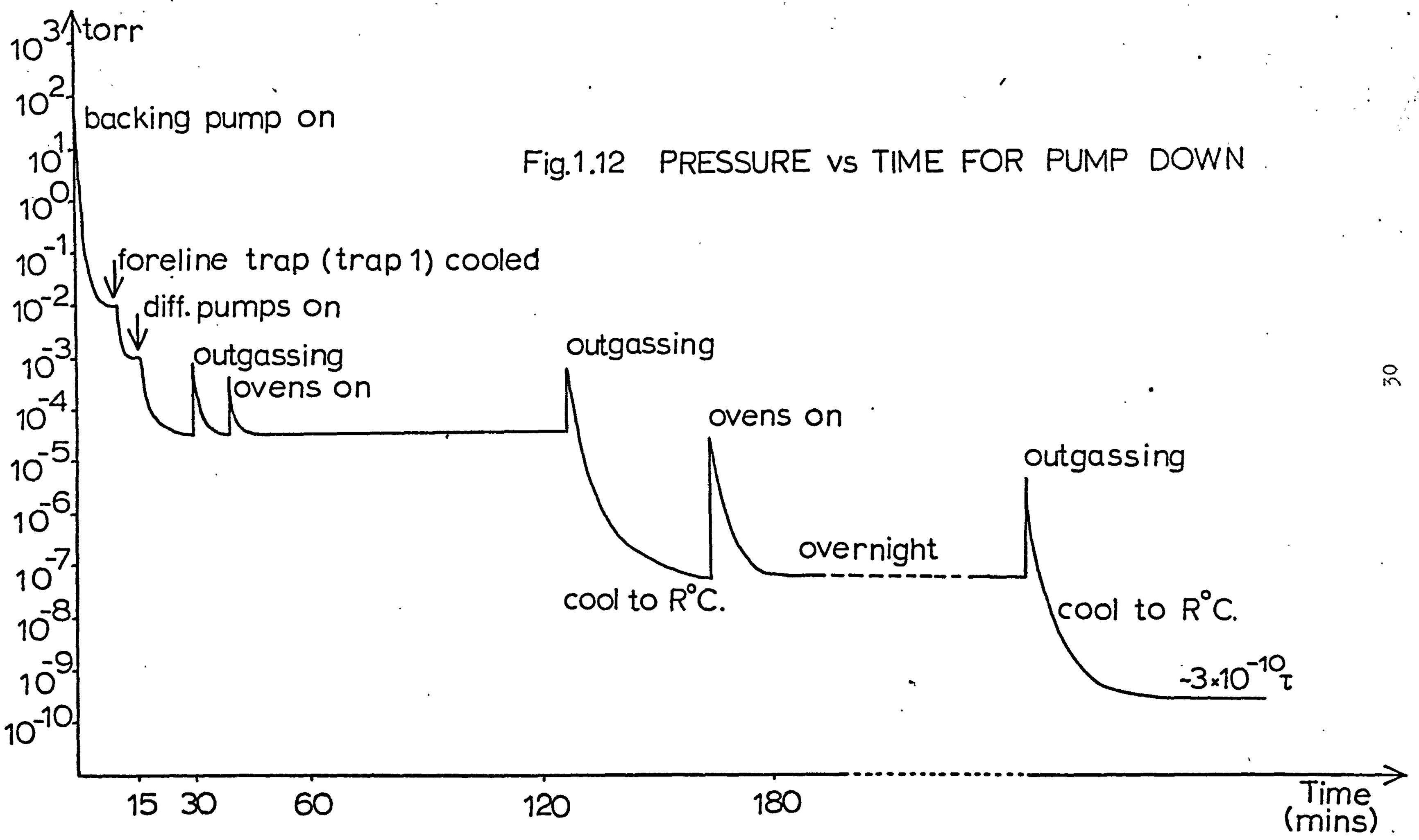

Fig.1.12 PRESSURE vs TIME FOR PUMP DOWN

pressure as indicated by the McLeod gauge would fall to below 10^{-4}torr. The mercury in cut offs CT1-4 and the McLeod gauge was then raised to levels L11, L21, L31, L41 and LMC1 respectively (fig. 1.13). The ion gauge could then be switched on and the filament was lightly outgassed by operating the gauge for a few minutes at 0.1mA., 1mA. and then 10mA. emission current. The diode filament was also lightly outgassed by operating it at a bright yellow heat. Outgassing was continued for about ten minutes. The UHV section was then baked out for about two hours as follows. Ovens were placed round the diode and UHVsection, excepting trap 2,i.e. bake out ovens 1 and 2 (fig. 1.2), and their temperature raised to 200°C. over a period of approximately twenty minutes. The liquid nitrogen coolant was removed from trap 2, an oven placed around it (no. 3) and the temperature of all the ovens raised to 350°C. After about one and a half hours the capillary and wide bore tubes leading from CT4 to the UHV section, and the upper part of CT4 were heated using a gas-air hand torch for about fifteen minutes. After a further fifteen minutes bake out, oven 3 was switched off and removed and trap 2 cooled in liquid nitrogen. Ovens 1 and 2 were then switched off and allowed to cool. When their temperatures had fallen to 200°C. they were removed and vigorous outgassing of the ion gauge and diode filament commenced immediately, while the glass walls of the UHV section were still hot. Outgassing was continued for about one hour whereupon, after cleaning trap 2 of condensible material by closing cut off CT5, warming the

diode side only of the trap to room temperature, recooling the trap to -196°C. and re-opening CT5, the pressure indicated by the ion gauge would typically fall to 5 x 10^{-8}torr. It was often found advantageous to clean trap 2 several times during outgassing. The UHV section was then baked out overnight using a procedure similar to that of the "short bake out" above. The liquid nitrogen coolant of trap 1 was replaced by solid carbon dioxide/acetone at this point, the mercury mirror condensed by the liquid nitrogen remaining and increasing the effectiveness of the trap. Vigorous outgassing of the ion gauge and diode filament was carried out on cool down in the morning terminating before the glass walls of the UHV section had cooled to room temperature. The diode filament was flashed to white heat several times. After cleaning trap 2 the pressure normally fell to around 2 x 10^{-9}torr and dropped further to about 3 x 10^{-10}torr over the next hour. At these pressures the major components of the residual gas in a system of this type are hydrogen, helium and carbon monoxide. (1),(5).

Real leaks are suspected by a failure at any stage to maintain this pump down schedule (fig. 1.12). They are detected by the following procedure: sections of the system are first isolated and any pressure changes observed are indicative of the general location of a leak. Large leaks, especially pin-holes may then be found using a Tesla high frequency tester. Smaller leaks are best searched for using distilled water. On drenching a leak with distilled water a dramatic rise in pressure is first observed as water vapourises in the

system followed by an equally dramatic fall as the water freezes and blocks the leak. (The pumps are usually well able to remove the small quantity of water vapour released by the ice in the leak). Acetone may also be used to search for leaks of intermediate size. The smallest leaks may be detected using a jet of hydrogen, a rise in pressure being observed due to the higher flow rate of hydrogen through the leak.

After an experiment the system was let down to nitrogen as noted above. The diffusion pumps were always cooled to room temperature before let-down and all mercury reservoirs returned to their lowest positions. Traps 1 and 2 were warmed to room temperature after let-down (permissible in a nitrogen atmosphere) as this was found to minimise diffusion of their contents through the system.

Operation and Calibration of the Gas Dosing System

1.12

This is shown in fig. 1.1 and in greater detail in figs. 1.13 and 1.14. This system was used to introduce small known quantities of gas into the UHV section during surface potential and rate of adsorption experiments. It functions by utilising mercury cut offs to define a series of known volumes between which a quantity of gas is shared to produce a sample of appropriate volume and pressure, which could then be admitted to the UHV section. The volumes defined were as follows (* denotes calibrated volume).

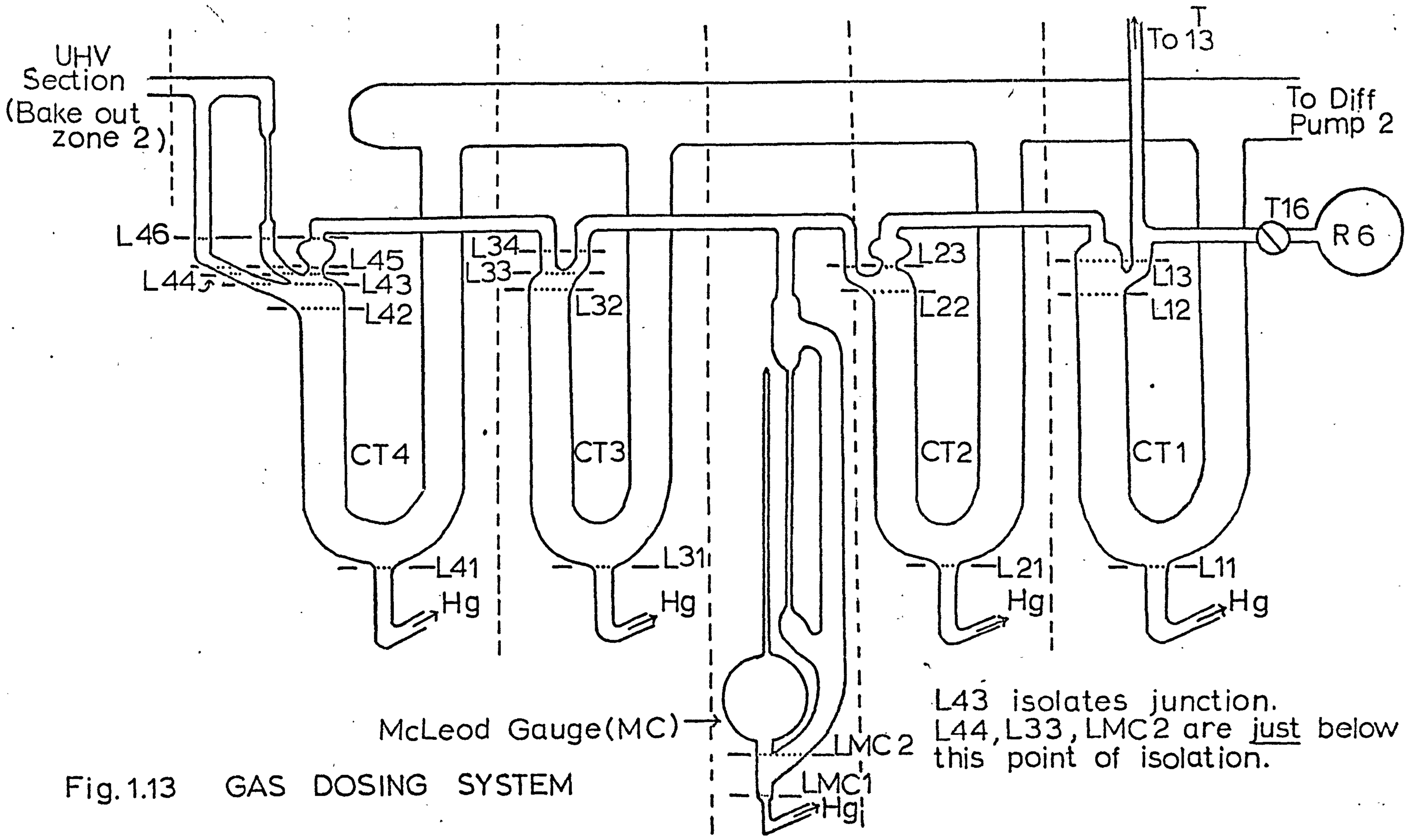

Fig. 1.13 GAS DOSING SYSTEM

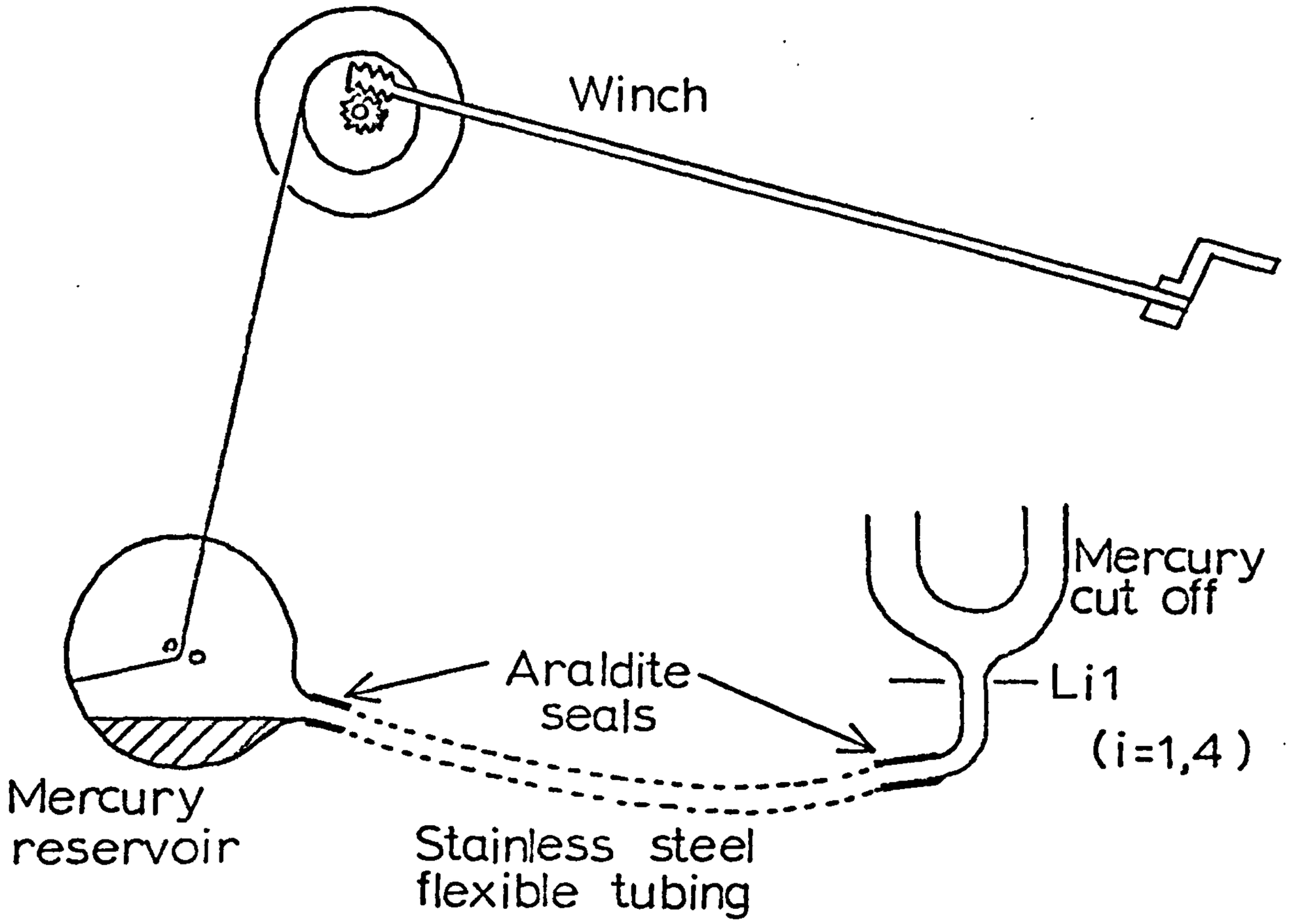

Fig. 1.14 ADJUSTABLE MERCURY RESERVOIRS

V_1 volume between L13, T16, T13 (mercury levels L13 etc. shown in fig. 1.13).

V_2 volume between L13 and L23

*V_3 volume of McLeod gauge, defined by LMC2

*V_4 volume defined by LMC2, L23, L33 and McLeod gauge (i.e. mercury at LMC2 just isolating McLeod gauge)

*V_5 volume between L33 and L45 (i.e. mercury at L33 just isolating the junction)

*V_6 volume between L33 and L46

*V_7 volume of UHV section, defined by L44.

Hydrogen was admitted to the gas inlet line in controlled amounts through a palladium thimble. It was stored in reservoir R6 which was filled as follows. Taps T7, T9 and T11

were closed. Taps T6, T13 and T16 were opened to allow the inlet line to be evacuated (close T14, T15 see section 1.5). T6 was then closed and mercury raised in CT1 to level L13 where it formed a small manometer allowing pressure in the inlet line to be monitored. Mercury in CT2 was set to L21 and in CT4 to L45 to prevent surges of gas to the UHV section in case of accidental release of gas past the manometer. The temperature of the palladium thimble was then raised to approximately 250°C. and hydrogen/deuterium allowed to diffuse into the inlet line and R6 until the pressure reached approximately 10torr. Taps T13 and T16 were then closed and the thimble cooled. The hydrogen above L13 was normally used immediately. Other gases were used directly from the inlet line which was filled as follows: after initially evacuating the entire inlet line including the tubes between taps T8, T10 and T12 and the glass seals of reservoirs R3, R4 and R5, T6 to T13 were closed and the reservoir seals broken using magnetic hammers. A similar procedure was then followed for R3, R4 or R5, for example R3; T8 was opened and closed filling the volume T7→T8 with gas. T7 was opened and closed filling the inlet line with gas at a reduced pressure. Known doses of gas could then be admitted to the UHV section either from the inlet line or from reservoir R6 using the mercury cut offs to define appropriate quantities.

Gas was first admitted to V_1 either via T13 or T16 using CT1 as a manometer to obtain a suitable pressure. CT2 and CT4 were set as above in case of an accident.

CT2 was then raised to L23, CT1 lowered to L12 and returned to L13 allowing gas to expand into V_2.

CT3 was set to L34, MC to LMC1, CT2 lowered to L22 and returned to L23, sharing gas into V_4 . The pressure of this gas was measured using the McLeod gauge (Ptorr).

CT4 was set either to L45 or L46. CT3 was lowered to L32 and returned to L34 sharing a known portion of the gas in V_4 into either V_5 or V_6. This dose of gas was then admitted to the UHV section by lowering CT4 to L42. From the McLeod gauge reading and the calibrated volumes V_3, V_4, V_5 and V_6 the amount of gas G (litre.microns) in this dose could be calculated from the expression

$$G = \frac{P.V_{5/6}.V_4}{V_4 + V_{5/6}}$$

{volumes in cm^3
{P in torr
{G in litre.microns.

Iin some experiments gas was admitted slowly but continuously from $(V_4 + V_5)$ through the capillary tube by setting CT3 to L32 and CT4 to L43.

1.13

The gas dosing system was calibrated in two stages

(i) The volume V_3 and the bore of the McLeod gauge capillary were obtained by direct measurement and hence a pressure calibration for the McLeod gauge established.

(ii) Volumes $V_4 \rightarrow V_7$ were obtained by a series of gas sharing experiments relying on the calibration of the McLeod gauge.

(i) V_3, the volume of the gauge, was obtained from the weight of distilled water at a known temperature needed to fill the

volume. The mean of four determinations gave a value for V_3 of 141.7 cm.

The McLeod gauge capillary was formed from a length of 1mm. internal diameter precision bore tubing. The tube was selected for uniform bore before gauge construction by measuring the length of a column of mercury of a given weight at varying positions along the tube. The bore was calibrated after construction of the gauge by filling it with various weights of mercury and measuring the length of the resulting mercury column. These results were used to compute a table of pressure (torr) against scale reading (mm.) at 0.2mm. intervals.

(ii) A series of gas sharing experiments was then carried out to determine $V_4 \rightarrow V_7$. These determinations were repeated at intervals throughout the life of the vacuum system. The gas used was always hydrogen.

Volume V_4

The McLeod gauge (V_3) was filled with hydrogen at a pressure (P_3) which was carefully determined. CT2 was set to L23 and CT3 set to L34, thus defining volume V_4. (L33 could not be used to define V_4 for this determination as the mercury level could not be maintained accurately at this position during the procedure. The volume between L33 and L34 (V_4') was carefully measured and found to be 1.25cm^3 : its value was added to the measured value of V_4). MC was lowered to LMC1 and the system allowed to come to equilibrium. The mercury in the McLeod gauge was then very slowly raised to LMC2 and then further raised to measure the equilibrium gas pressure in the new volume (P_4).

Then:

$$V_4 = \frac{P_3 V_3}{P_4}$$

This determination was repeated many times using varying pressures for P_3 of between 10^{-1} and 10^{-2}torr, resulting in a mean value for V_4 (including V_4') of 175.8cm^3.

Volumes V_5 and V_6

A multiple sharing technique was used to measure these since their volumes were very small. An essentially identical procedure was used to determine both. That for V_5 will be described.

V_4 was filled with hydrogen at a known pressure of between 10^{-1} and10^{-2}torr (P_0). The following sequence of operations was then carried out n times where n varied between 5 and 20 for different determinations:-

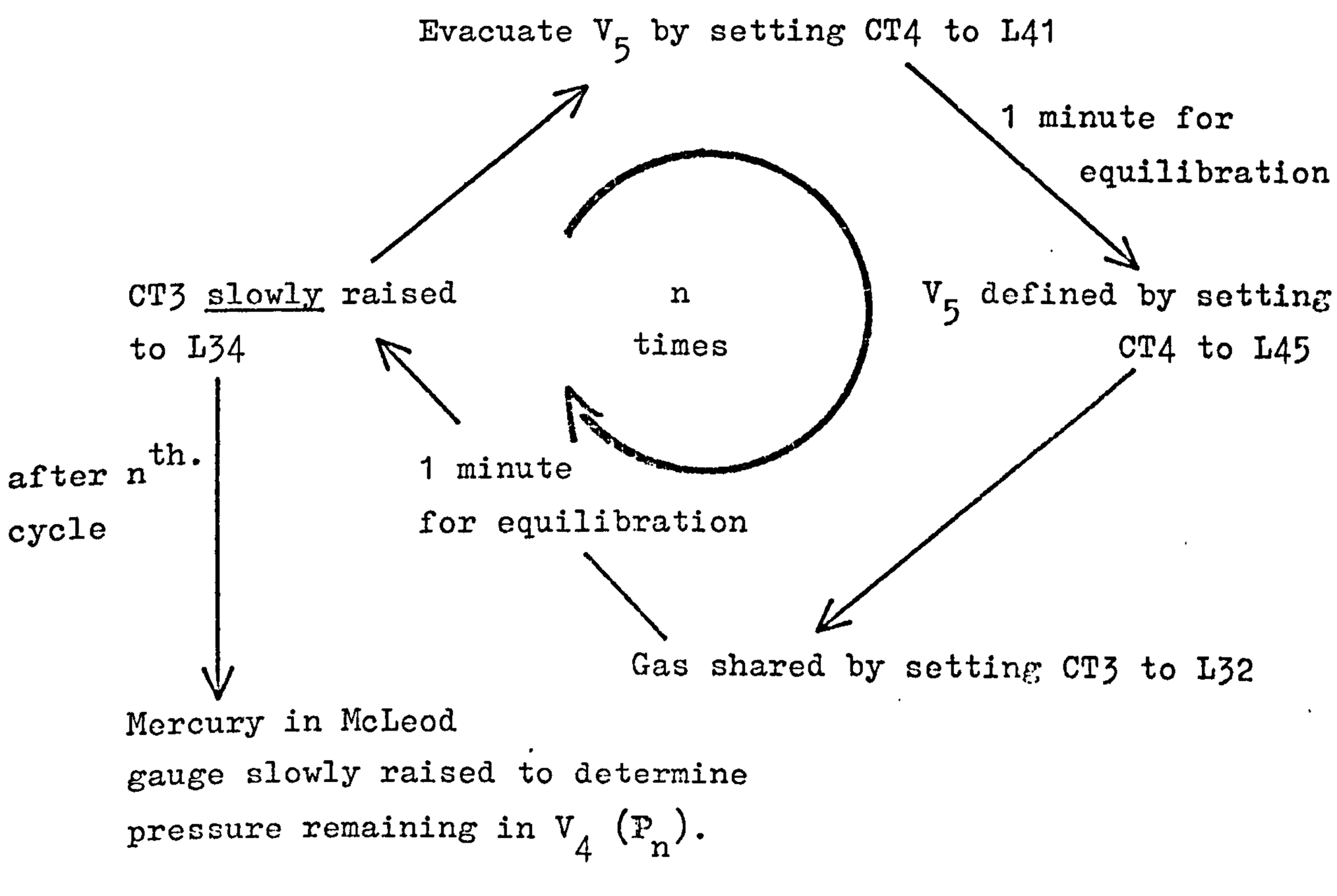

V_5 may be calculated from the measured values of n, P_0 and P_n as follows:

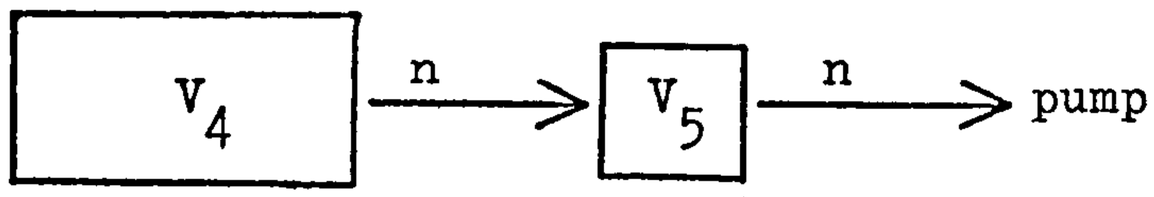

Initially = P_0

After n cycles = P_n

After one cycle $$P_1 = \frac{P_0 V_4}{V_4+V_5}$$

After two cycles $$P_2 = P_1\left[\frac{V_4}{V_4+V_5}\right] = P_0\left[\frac{V_4}{V_4+V_5}\right]^2$$

After n cycles $$P_n = P_0\left[\frac{V_4}{V_4+V_5}\right]^n$$

And hence $$V_5 = V_4\left[\sqrt[n]{\frac{P_0}{P_n}} - 1\right]$$

For minimum errors P_0 should be as large as possible and $n = \frac{V_4}{V_5}$.

The multiple sharing experiment was repeated four times yielding a mean value for V_5 of 2.3cm^3. An exactly similar series of experiments gave a value for V_6 of 1.4cm^3.

As a check on these results an alternative method of measuring V_5 and V_6 was also used which was carried out as follows:

(i) V_4 and V_5(or V_6) were filled with hydrogen at a known pressure of between 10^{-1} and 10^{-2}torr.

(ii) V_5 (or V_6) was then isolated and V_4 evacuated via CT2.

(iii) CT2 was set to L23 and CT3 lowered to L32. One minute was allowed for equilibration.

(iv) CT2 and MC were then raised slowly in order to reach L33 and LMC2 simultaneously.

MC was then further raised to measure the new pressure $P_{(4+5/6)}$.

Essentially the procedure consists of expanding a known pressure of gas in V_5 or V_6 into volume $V_4 + V_{(5or6)}$

Volume $V_{(5or6)}$ is then given by

$$V_{(5or6)} = \frac{V_4}{\frac{P_{5/6}}{P_{(4+5/6)}} - 1}$$

The experiment was repeated on numerous occasions and yielded values for V_5 and V_6 substantially in agreement with the multiple sharing technique above.

Volume V_7

This volume varied during the course of a series of experiments as alterations to the dimensions of the UHV section were made by changing diode cells, pressure gauges etc. Consequently it was remeasured as and when required. As the volume of this section is large, a single sharing experiment was used, hydrogen being shared from V_4 into $(V_7+V_5+V_x)$. V_x is the volume of the tubes between L44 and L45. This volume which is quite small (approximately $1cm^3$.) also varied from experiment to experiment and was measured carefully each time.

1.14 The Evaporation of Silver and Gold Films

The diode cell used in these studies is shown in fig. 1.6. Metal films were evaporated onto the inside surface of the

spherical diode by heating a sample of the metal on the diode filament. The procedure was as follows. Before pump down a weighed length of gold or silver wire (Johnson Matthey 99.999%) was formed into the shape shown in fig. 1.15 using forceps.

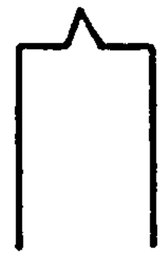

Fig. 1.15

The pip on the bottom of the diode bulb was blown off and the length of wire hung on the hook above the filament as shown in fig. 1.16.

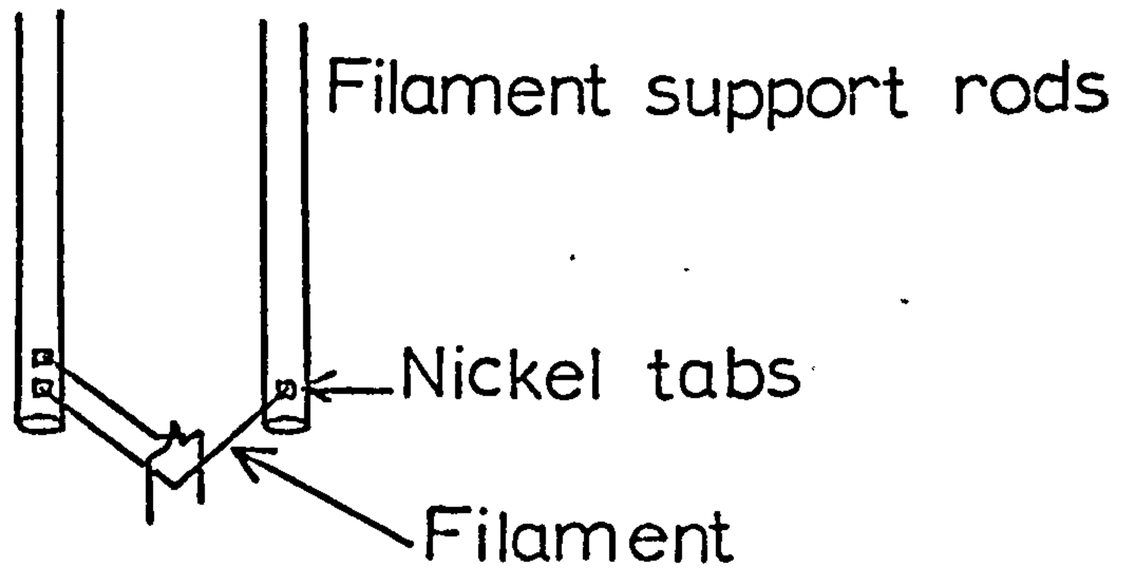

Fig. 1.16

The pip was then resealed and UHV conditions established as detailed in section 1.11. A smart tap on the bulb of the diode would then result in the metal wire falling onto the filament which must of course be cold. The filament temperature was then raised slowly until the gold or silver melted and formed a bead surrounding the "V" of the filament. The filament was very rapidly cooled to prevent premature evaporation of the gold or silver which occurs rapidly at these filament temperatures. The filament temperature normally has to be raised to a value

well above the melting point of gold or silver in order to melt the wire due to the poor thermal contact between the filament and the wire. The bead was then remelted several times, alternatively in approximately .1torr hydrogen and in UHV, to remove dissolved oxygen. The system was baked between each cycle. Finally after restoring UHV conditions the metal was evaporated by heating the gold to a bright yellow heat, or the silver to a dull yellow heat. Evaporation occurred over a period of about forty five minutes. The pressure rose during evaporation to approximately 4×10^{-8}torr but always fell to approximately 5×10^{-10}torr immediately afterwards. The bulb of the diode was always at room temperature during evaporation.

1.15

The adsorption of simple gases was then studied on these evaporated films as follows:

(i) The liquid nitrogen coolant for trap 2 was replaced by solid carbon dioxide/acetone. Care was taken to ensure that the mercury mirror condensed on the inside of the trap by the liquid nitrogen was retained as this increases the effectiveness of the trap.

(ii) The bulb of the diode was cooled in liquid nitrogen under atmospheric pressure (i.e. -196°C.) during the measurements, except for those involving krypton in which a lower temperature was needed. This was obtained by reducing the pressure above the liquid nitrogen using a rotary pump. The temperature resulting was measured

using a thermocouple.

(iii) Studies were made of the variation of surface potential (section 2.9) with adsorption of hydrogen, deuterium, xenon, krypton and carbon monoxide on both gold and silver. Small doses of the gas in question were admitted to the diode using the gas dosing system as described in section 1.12. After each dose the equilibrium pressure of the gas was measured and the surface potential determined as outlined in section 1.9.

The pip of the diode was always pre-cooled in liquid nitrogen before cooling the whole bulb of the diode in order to adsorb any residual gas remaining from previous experiments onto a part of the film in poor electrical contact with the anode i.e. that on the bottom surface of the pip. A small fall in pressure with no change in surface potential was normally observed.

(iv) In order to provide a check on the validity of the surface potentials measured, the diode I_a/V_a characteristic was frequently measured for the clean film and for the film and adsorbed gas. As described in section 2.10 these characteristics should always remain parallel for a given film. The characteristics were measured over a range of I_a from 1nA. to 500nA. and fig. 1.17 shows a typical result. The plots were always found to be parallel to within $\pm$ .5 mV.

(v) The rate of adsorption of a gas (most frequently hydrogen) was followed by monitoring the change in pressure during the adsorption of a dose using the fast response pirani

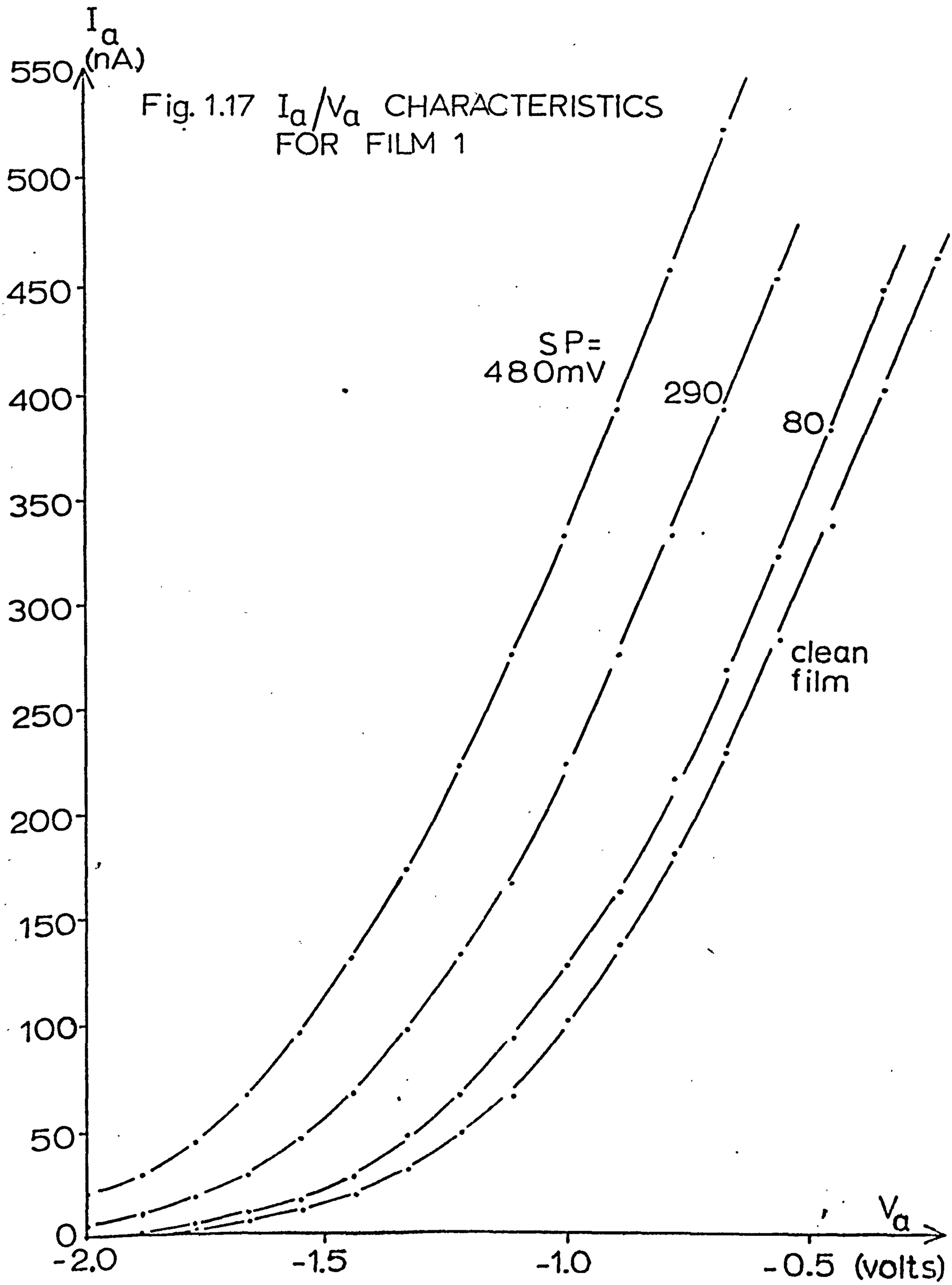

Fig. 1.17 I_a/V_a CHARACTERISTICS FOR FILM 1

gauge PG2 and a Servoscribe chart recorder. A typical plot of P vs Time for one dose is shown in fig. 1.18.

Fig. 1.18

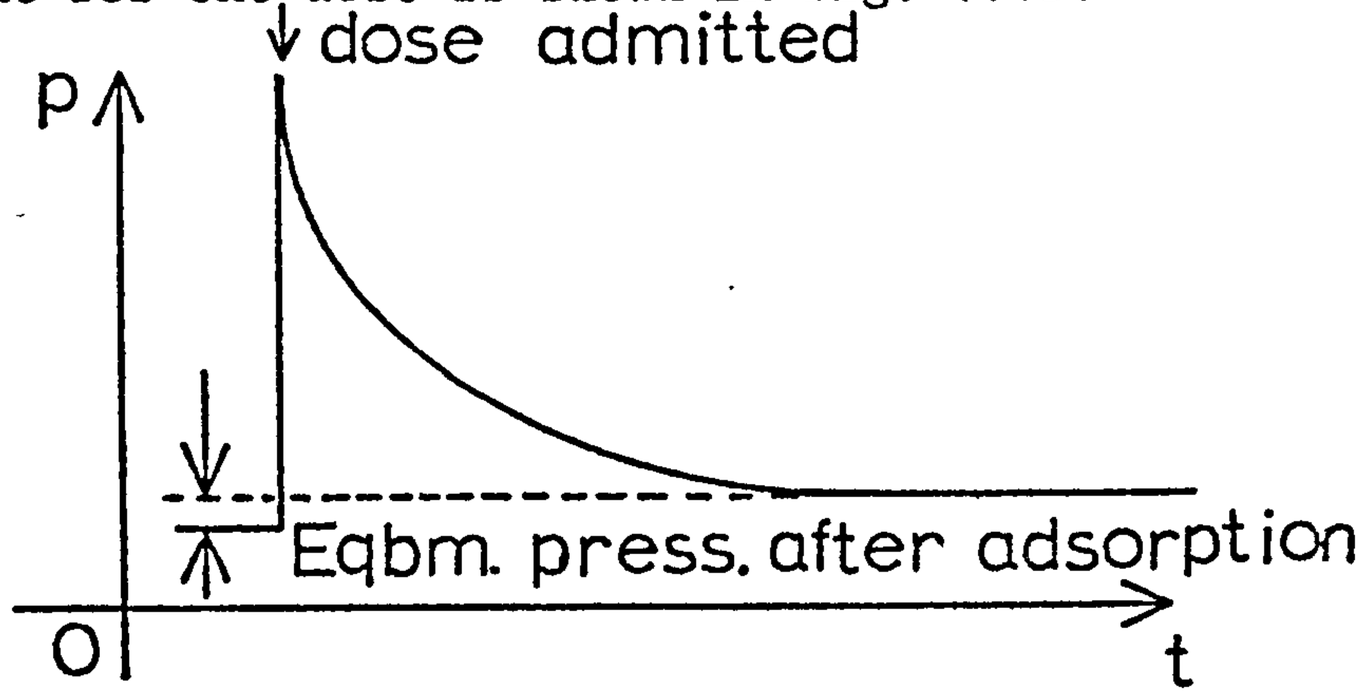

These experiments were normally combined with those in section (iii). Blank experiments i.e. in which adsorption did not occur were also performed in order to determine the effects of recorder and pirani responses on the shape of these experimental plots. The analysis of these is described in chapter four.

References

(1) P.A. Redhead; E.V. Kornelsen and J.P. Hobson
Can. J. Phys. 40, 1814, (1962)

(2) J. Pritchard. J. Sci. Instr. 44, 652, (1967)

(3) V.G. Technical Bulletin "Pressure Measurement"

(4) R.A.E. Farnborough, Technical Report No. 68146

(5) A.G. Knapp. Thesis, U. of L. (1971)

Chapter 2

Theoretical

2.1

The apparatus and techniques described in chapter 1 were used to study the interactions between simple gases and clean silver and gold surfaces. In this chapter the nature of these surfaces will be considered. The theory underlying the surface potential measurements used in this study will be described, and their possible interpretation considered.

The Nature of the Surface

2.2

Two factors make the use of thin films for the preparation and study of metal surfaces particularly attractive.

(i) UHV evaporations from a pure and well degassed source yield films with a surface substantially free of adsorbed gas atoms. The gettering action of the metal results in the surface being the cleanest part of the film.

(ii) The surface to volume ratio is large in a film, resulting in an increased tolerance of subsequent contamination. The structure of a film however, is frequently quite different from that of the bulk material and is heavily dependent on the nature of the substrate and the conditions during evaporation, in particular substrate temperature and deposition rate. The nucleation and growth of thin films has been discussed by many authors including Rhodin and Walton (1) and Neugebauer (2). The topic has been discussed at symposia (3). More recently Cinti and Chakraverty (4) have investigated the silver/silica system under conditions

of low supersaturation, although their conclusions appear to have wider generality; Lewis and Campbell (5) have considered the high supersaturation case. Kakati and Wilman (6) have investigated the structure of silver, gold and copper films on stainless steel and glass substrates in some detail and Walton (7) has considered the role of nucleation in determining orientation.

2.3

In the early stages of film deposition, metal atoms arriving at the substrate surface must take part in one of three competitive processes:-

(i) the atom may be captured by a stable nucleus. Coalescence of these nuclei during later film growth leads to the grains (crystalites) of the continuous film

(ii) nucleation may occur i.e. the atom may combine with another single atom or critical nucleus to form a stable nucleus

(iii) the atom may complete its lifetime on the surface before being captured and hence evaporate.

The nuclei referred to in (i) and (ii) are small clusters of atoms adsorbed on the substrate surface which grow or decay by the addition or loss of single atoms. Condensation of permanent metal films onto glass and other inert substrates which have a low heat of adsorption for metal atoms will only occur via the formation of these aggregates. However, their formation is energetically unfavourable up to a certain critical size, after which further growth becomes favoured. The critical nucleus comprises one less

atom than the smallest stable nucleus. Experimentally (8) and from theoretical estimates, albeit using bulk data (5), the upper limit for the size of the smallest stable nucleus for silver on glass at room temperature and for similar systems is known to be small, of the order of a few atoms.

The stability of these very small nuclei and hence the size of the smallest stable nucleus is strongly dependent on their structure, in particular the number of bonds limking each individual atom to the cluster. Thus we can imagine a stability series, beginning:-

Fig. 2.1

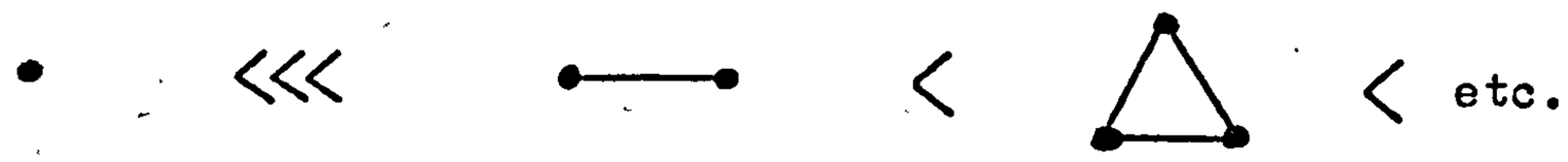

bonds to substrate only | 1 bond per atom | 2 bonds per atom

In addition the substrate surface may alter this series by imposing its geometry on the embryo nucleus, for example perhaps making

Fig. 2.2

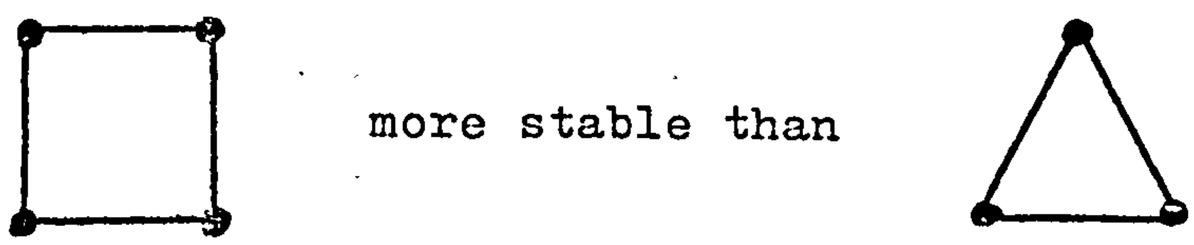

more stable than both structures however allowing two bonds per ad-atom.

A cluster will only grow if the lifetime of an atom attached to it is sufficient for the rate at which atoms arrive at the cluster to exceed the rate at which others leave. Hence the size and structure of the smallest stable nucleus will be a function of the film material and substrate (i.e. bond strengths and geometry), substrate temperature

(i.e. leaving rate) and deposition rate (i.e. arrival rate). Since the clusters must contain an integral number of atoms, a critical nucleus of a particular size will result from quite a wide range of deposition conditions.Walton (7) sees here the origin of epitaxy, smallest stable nuclei of two atoms leading to total misorientation, three atoms to (111) planes parallel to the substrate and four atoms to (100) (for fcc metals).

Fig. 2.3

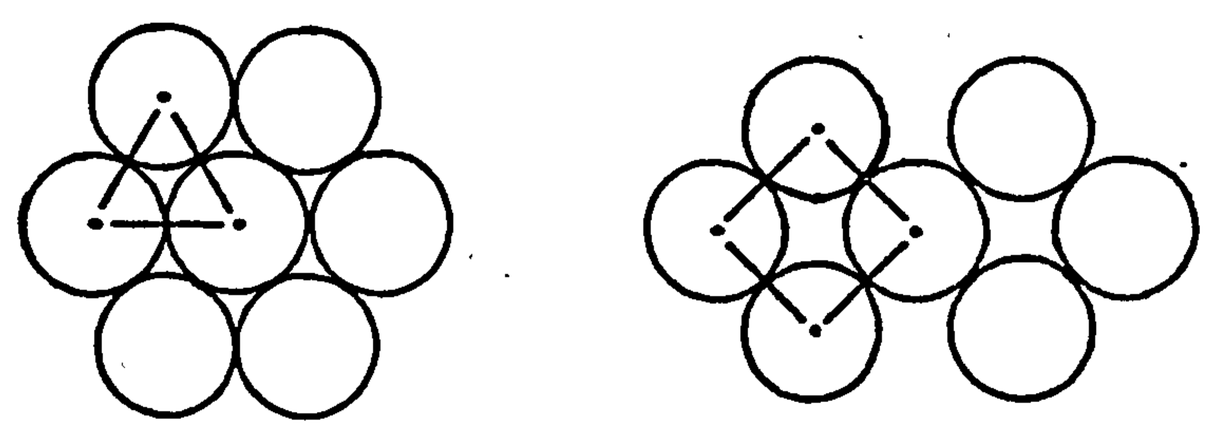

Evaporated films having crystalites orientated with (111) planes parallel to the substrate are common (9). Kakati and Wilman (6) have observed (111) orientations in silver and gold films of a few hundred angstroms thickness evaporated onto glass or stainless steel at pressures of less than 2×10^{-7} torr. Films prepared in this study are probably either entirely disorientated or at least partially orientated with (111) faces parallel to the substrate (section 1.14 and 3.5 ff.).

2.4

It is likely however, that the properties of evaporated metal films are influenced at least as much by the defects in the film as by the predominating crystal faces. LEED (10) and FEM (11) studies for example suggest that adsorbate

atoms interact much more strongly with stepped surfaces than with surfaces exposing low index planes only. FEM photographs show otherwise mobile adatoms to be trapped by irregularities. The concentration of these defects in a thin film surface is a function of the number and location of the stable nuclei formed during initial deposition. Under conditions where the substrate temperature is low and the rate of impingement of atoms high enough, statistical variations in the concentration of the adatoms may be expected to lead to the formation of critical nuclei. This is probably the case in Kakati and Wilman's experiments where a high deposition rate of 30Å/sec. was used. Films prepared in this way will consist of many small crystalites whose number and distribution is insensitive to substrate heterogeneity. At lower super-saturations however, i.e. higher substrate temperatures or substantially lower impingement rates; Cinti and Chakraverty's experiments and this study (section 1.14), the rate of evaporation of metal atoms will be more significant. Stable nuclei will be formed preferentially on areas of the substrate where the lifetime of the adsorbed single atom is increased. In such areas the crystalites formed will be greater in number and smaller in size than elsewhere on the substrate. Electron micrographs of very low thickness films show enhanced nucleation occurring at such features as cleavage steps (12). Decoration phenomena are well known (13). Dixit (3, page 29) suggests that micro temperature wells may cause preferential nucleation.

However it seems reasonable to associate areas of enhanced nucleation on glass substrates with crystal defects, recrystalisation points and impurities often observed on glass surfaces. Films can be anticipated therefore to show properties which reflect both the nature and the heterogeneity of the substrate when the deposition rate is low.

Two factors may however reduce this sensitivity to substrate heterogeneity.

(i) Contaminants: since these are most strongly bound to the same sites that we have identified as causing enhanced nucleation, and will tend to reduce their effectiveness, only films prepared under UHV will show this sensitivity to surface detail.

(ii) Annealing: during annealing larger crystalites grow at the expense of small ones and hence tend to remove the consequences of the initial distribution of crystalites.

2.5 Summary

(i) Vacuum deposited films are preparitively attractive but frequently show structure quite different from bulk material.

(ii) In this study the films are probably unorientated or orientated with (111) planes parallel to the substrate.

(iii) The defect density influences the properties of the film and is a reflection of the substrate and deposition conditions.

(iv) Incompletely annealed films prepared under UHV can be expected to show differences in properties which reflect micro dissimilarities in substrate, between different types

of glass for example.

(v) A very slow drift in the properties of a film is anticipated due to contamination, annealing and recrystalisation. Recrystalisation is known to be promoted by the presence of water vapour (14) always present in systems handling hydrogen atoms (15).

Surface Potentials and Work Function

2.6

It has been observed by numerous authors (16) that the work function (ϕ) of a metal (or semiconductor) is altered by the adsorption of a gas onto its surface. This work function change is termed a surface potential (SP), and its measurement provides a useful means of following an adsorption process.

2.7

The work function may be loosely defined as the energy, expressed in electron volts or volts, necessary to remove an electron from just inside to just outside a metal surface. Herring and Nichols (17) give a more rigorous definition:-

$$\phi \text{ (volts)} = -\Phi_o - \frac{\bar{\mu}}{e}$$

where $\bar{\mu}$ = electrochemical potential of electrons just inside the metal. $\left[= \left[\frac{\partial G}{\partial n_e} \right]_{T,P} \right]$

Φ_o = electrostatic potential of electrons just outside the surface.

we may further define $\bar{\mu}$ by

$$\bar{\mu} = \mu - e\Delta\Phi$$

where μ = chemical potential of electrons inside metal - independent of surface

and $\Delta\Phi$ = electrostatic potential difference across surface (section 2.8ii)

hence
$$\phi = -\Phi_o + \Delta\Phi - \frac{\mu}{e} \qquad (1)$$

The term Φ_o is known to be a function of the distance (r) of the electron from the surface of the metal, given to a very good approximation by the image potential:

$$V(r) = \frac{-e}{16\pi\varepsilon_o r} = \Phi_o(r) \qquad (2)$$

provided that r is greater than a few angstroms, that external fields are absent and $\Delta\Phi$ is assumed equal to zero. The distance r_o from the surface of which the work function is effectively measured must therefore be defined and clearly the most convenient distance will be that at which Φ_o is reduced to zero.

i.e. At $r = r_o$, $\Phi_o = 0$

and hence
$$\phi = -\frac{\bar{\mu}}{e} \qquad (3)$$

In the simplest possible system of an infinite single crystal surface with no external electric fields,

$$\Phi_o \longrightarrow 0 \quad \text{as} \quad r \longrightarrow \infty$$

and we therefore define r_o as infinity (fig. 2.4).

Fig. 2.4

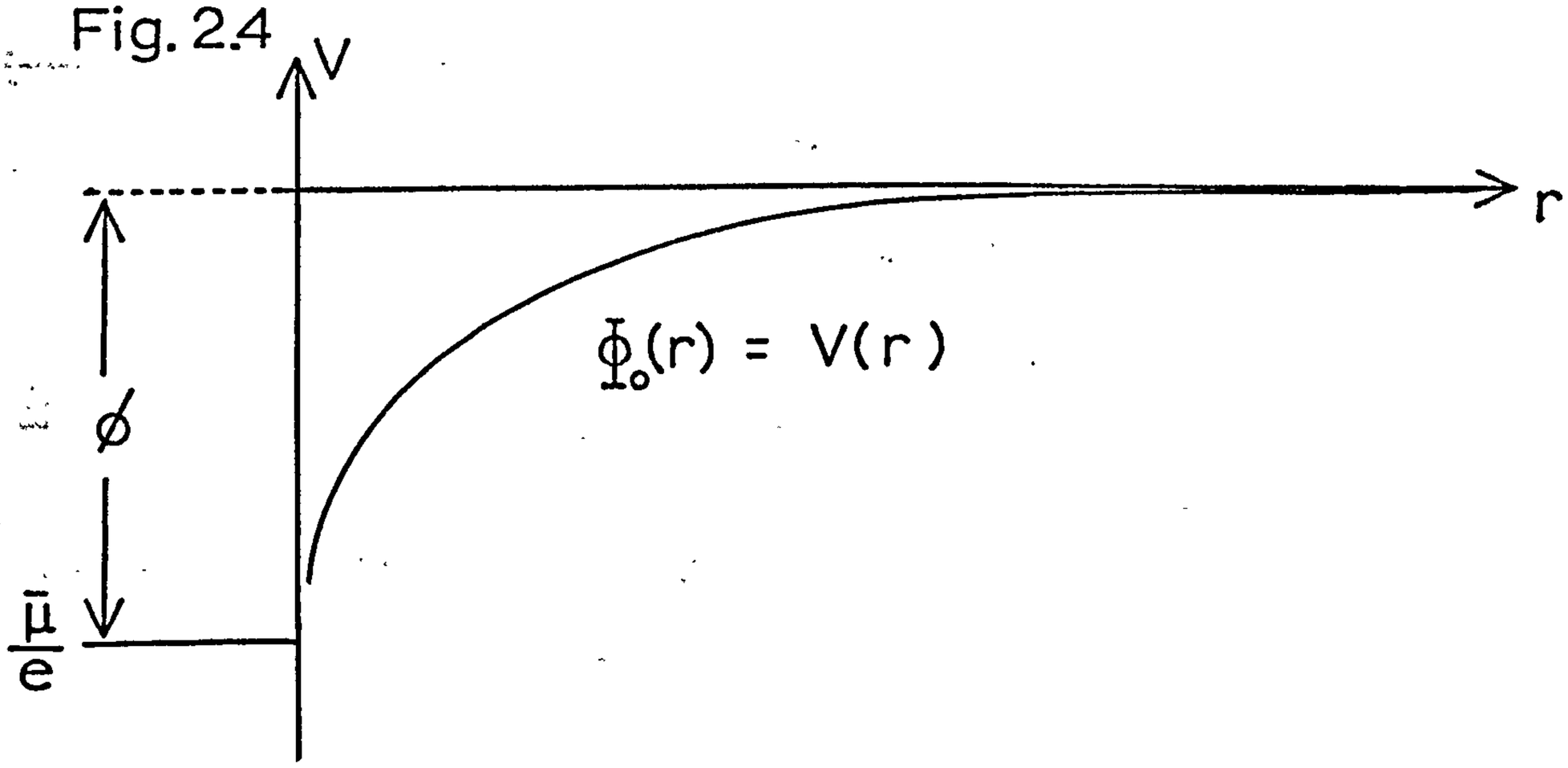

This ideal case is not realised in any practical determination of work function (or surface potential). In particular when using the diode method to measure the SP of gases adsorbed onto evaporated films the following deviations from ideality occur:

(i) An electric field is applied (sections 1.9, 2.8 and 2.9)

(ii) The metal surface no longer consists of a single crystal face.

2.8

(i) In this study the diode was always operated in the retarding field mode (section 2.9) i.e. the anode of the diode was held negative with respect to the filament. The effect of this on the field close to the metal surface of the film (anode) is shown in fig. 2.5. The electrostatic potential $\Phi_o(r)$ experienced by an electron at a distance from the surface will be the algebraic sum of the image potential due to the applied field ($\Delta\Phi = 0$)

$$\Phi_o(r) = -Er - \frac{e}{16\pi\varepsilon_o r} \qquad (4)$$

Fig. 2.5

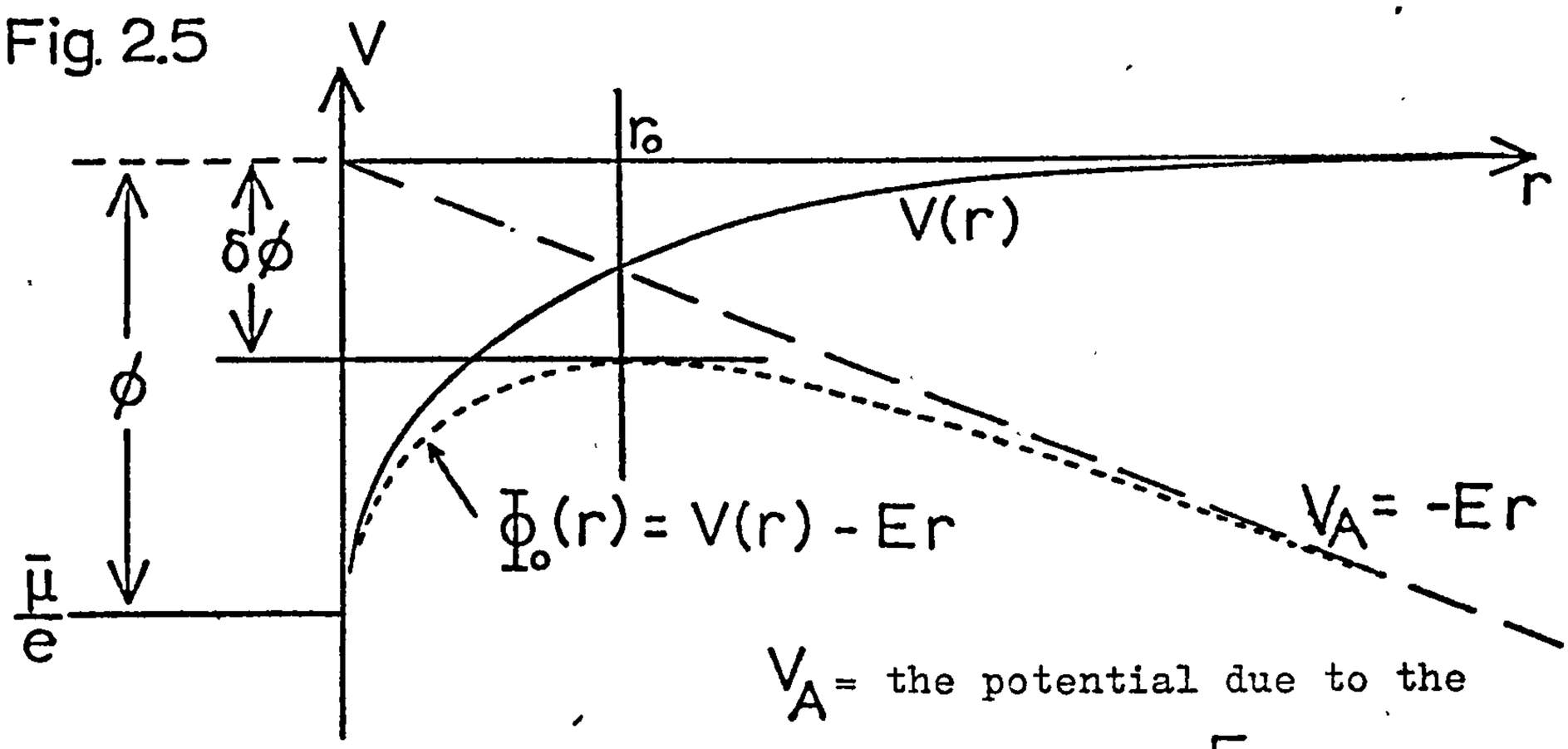

V_A = the potential due to the applied field E

The effective work function will be reduced by the presence of this external field by an amount $\delta\phi$, (Schottky effect), and the position of the barrier which the electrons must cross,in order to enter or leave the surface, defined by the maximum in this potential function $\Phi_o(r)$.

At this maximum

$$\left[\frac{d\Phi_o(r)}{dr}\right]_{r=r_o} = 0 \qquad \text{——————(5)}$$

hence

$$\left[\frac{e}{16\pi\varepsilon_o r_o^2}\right] - E = 0 \qquad \text{——————(6)}$$

and on rearrangement

$$r_o = \left[\frac{e}{16\pi\varepsilon_o E}\right]^{\frac{1}{2}} \qquad \text{——————(7)}$$

The decrease in work function is given by

$$\delta\phi = -\Phi_o(r_o) = \left[\frac{eE}{4\pi\varepsilon_o}\right]^{\frac{1}{2}} \qquad \text{——————(8)}$$

In a diode cell of radius approximately 2cm. with a potential difference between filament and film of approximately 1volt the position of the potential barrier will be

approximately 10^{-5}m. from the surface and the lowering of the work function approximately 10mV.

(ii) There are two further contributions to the work function in addition to $\frac{\mu}{e}$ which cause the electrostatic potential across the surface $(\Delta\Phi)$ to be non-zero (18) (19).

(a) Electrons spread beyond the surface of the metal as defined by the position of the ion cores, fig. 2.6.

Fig. 2.6

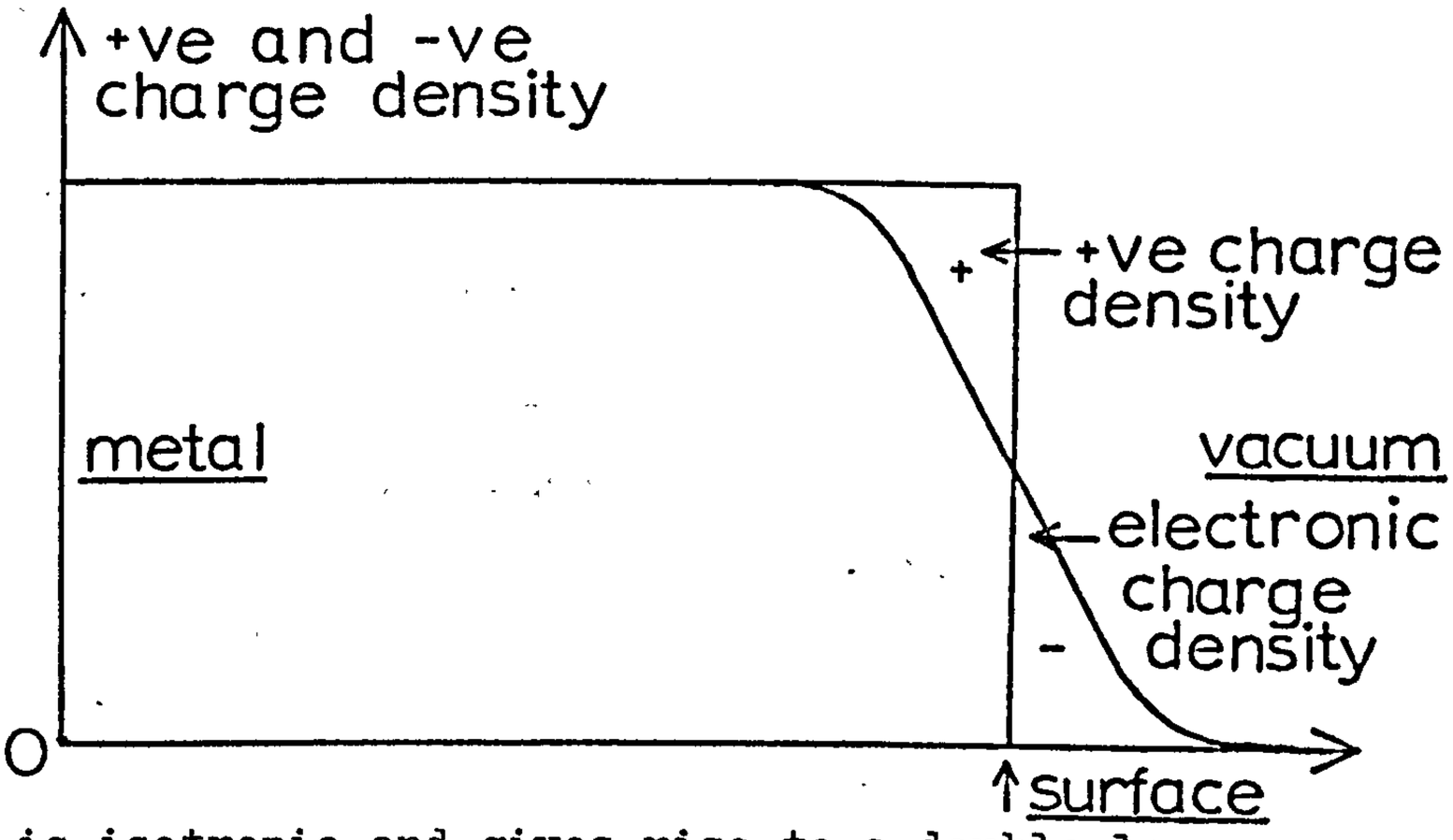

This effect is isotropic and gives rise to a double layer as shown. Double layers at the surface are always described by the sign of the charge on the outer or vacuum side of the charge layer, hence this effect produces a negative double layer. It results in an increase in the electrostatic potential drop across the surface, equal to the potential difference between two points on opposite sides of the double layer, and hence causes an increase in the work function.

(b) A positive double layer arises from the smoothing of the electronic surface with respect to the ion cores and this reduces the work function. (fig. 2.7)

Fig. 2.7

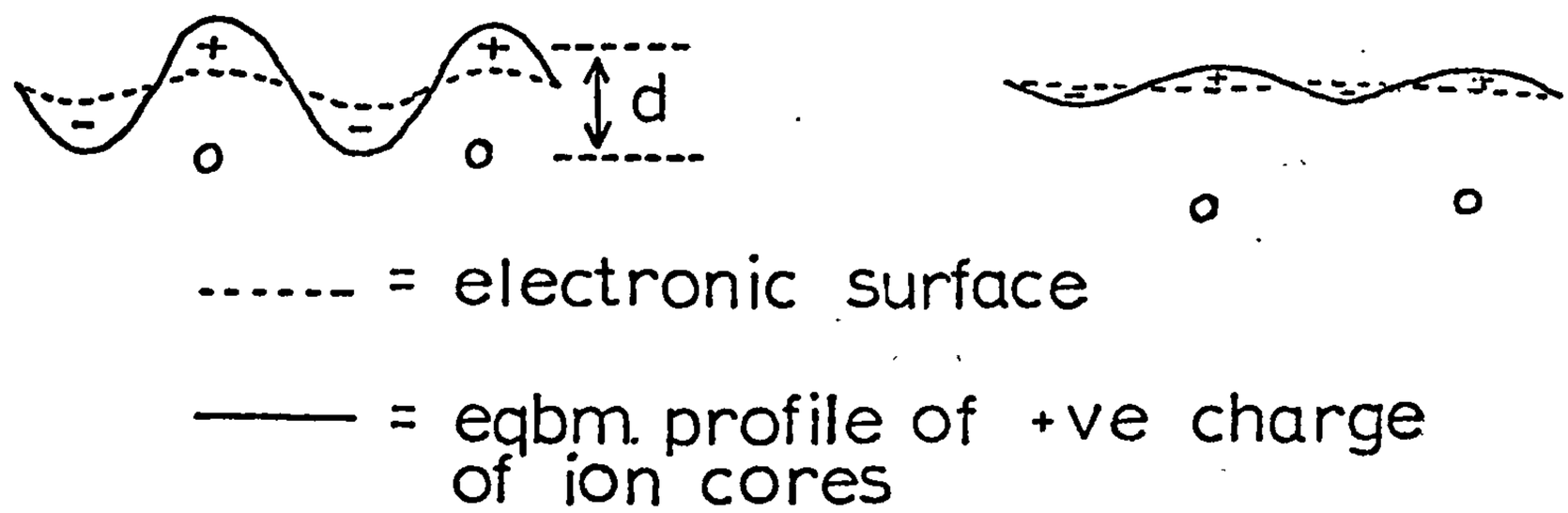

The magnitude of this double layer is sensitive to the roughness of the surface on an atomic scale and will therefore be different for surfaces exposing different crystal planes. This is experimentally confirmed by numerous authors (19). Differences in work function for various crystal planes for the same metal are typically 0.1V - 1V, ϕ being highest for the smoothest i.e. most close packed surfaces. A polycrystaline evaporated film (section 2.5) can therefore be expected to consist of small areas each having a different work function. Each individual area of substantially uniform ϕ is called a patch and each will have a work function which is uniquely a property of that patch if its dimensions are large compared to the distance r_{oi} at which ϕ for the patch i is defined. r_{oi} is a function of the field E_p experienced by each patch in the absence of applied fields as a consequence of their differences in work function and is given by equation(7).

Hence

$$r_{oi} = \left[\frac{e}{16\pi\varepsilon_o}\right]^{\frac{1}{2}} E_p^{-\frac{1}{2}} \quad \text{metres} \qquad (9)$$

$$= 17 \times 10^{-5} \times E_p^{-\frac{1}{2}} \quad \text{metres}$$

E_p will be of the order of $\left[\frac{\Delta\phi}{d}\right]$ where $\Delta\phi$ = the difference between the work function of a patch and the mean of those of the patches surrounding it (approximately .1 - 1volt)

d = patch width

and consequently this condition $r_{oi} \ll d$ is always fulfilled.

Herring and Nichols (17) have shown however that at distances that are large compared to the size of the patches Φ_o will reach an average value $\overline{\Phi}_o$ given by

$$\overline{\Phi}_o = \sum_i f_i \Phi_{oi}$$

where f_i = fractional area of patch

and since $\frac{\bar{\mu}}{e}$ is independent of i (equation(1)), the work function will reach an average value ϕ at the same distance. Providing that the value of r_o is large compared to the size of the patches, electrons entering or leaving the surface must pass over a barrier whose height is dependent on $\overline{\phi}$ and consequently the value of ϕ_i will have no significance except insofar as it influences the value of $\overline{\phi}$. An example is shown in fig. 2.8.

ϕ_1, ϕ_2 and ϕ_3 are the work functions of patches 1, 2 and 3. The work function is equal to $\left[-\Phi_d(r)-\frac{\mu}{e}\right]$ plus the potential difference across any double layer present at the patch surface.

Fig. 2.8

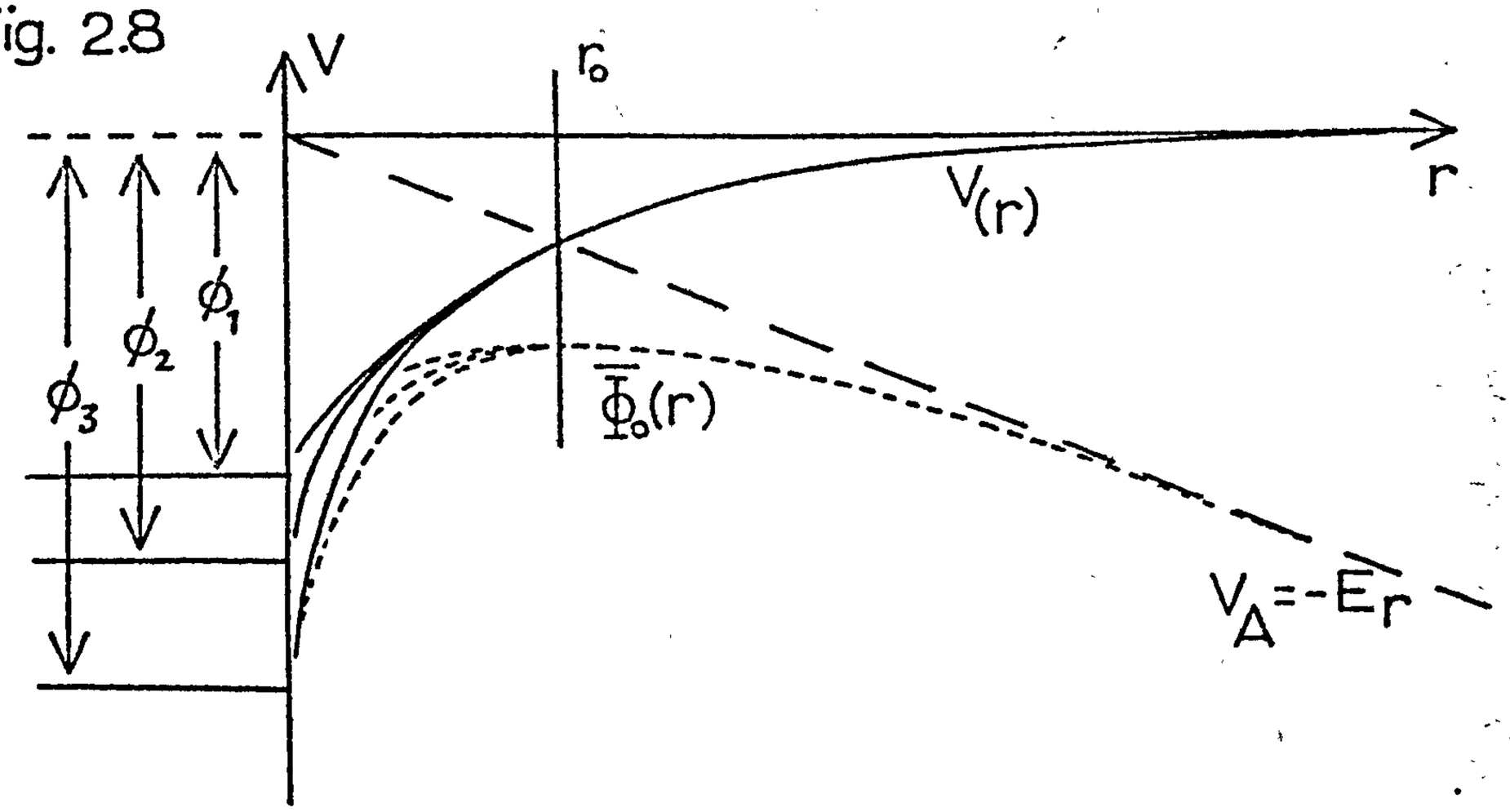

There is good evidence that the retarding field diode is sensitive only to the mean work function, provided by the substantial agreement between SP measurements made using a retarding field diode and vibrating capacitor by Ford (20) and Anderson (21). The vibrating capacitor almost certainly responds to the true average work function. Since r_o is approximately equal to 1000Å (section 2.8(i)) this observation implies an upper limit to the size of the patches or alternatively that either

(a) the work function for these polycrystaline surfaces is substantially uniform across the surface or

(b) the SP due to an adsorbed gas is insensitive to the work function of the patches.

2.9 Surface Potentials

A surface potential is defined as the change in the work function of a metal produced by an adsorbate.

$$\Delta V = \phi_o - \phi_1 \qquad (11)$$

where ΔV = surface potential

ϕ_o = work function of clean surface

ϕ_1 = work function of surface + adsorbate

It is caused by the presence of dipoles in the adsorbed atoms or molecules (section 2.11) which alter the work function in the same way as the double layers described in 2.8(ii). The magnitude of the SP will be a function of the magnitude of the dipoles (σ) and the number of dipoles per unit area (n) and will be equal to the potential difference across the dipole layer if it is assumed that the array of dipoles behaves as an infinite and continuous layer of charge. This may then be considered as a capacitor of C farads $m.^{-1}$ having plates l metres apart each carrying charge q coulombs. Then:

$$n\sigma = q\,l \qquad \text{——————(12)}$$

and

$$C = \frac{\varepsilon_o}{l} \qquad \text{——————(13)}$$

hence

$$\Delta V = \frac{q}{C} = \frac{n\sigma}{\varepsilon_o} \qquad \text{——————(14)}$$

ΔV is defined as having a sign equal to that of the side of the dipole layer further from the metal surface i.e. a positive SP implies a lowered work function.

Gomer (22) has considered the effect of the dipole layer being composedof discrete dipoles rather than a continuous layer, and his conclusions are illustrated schematically in fig. 2.9.

The value for the potential due to a layer of discrete dipoles

rises to that of the ideal continuous sheet at a distance from the surface which is dependent on the number of dipoles per unit area.

Fig. 2.9

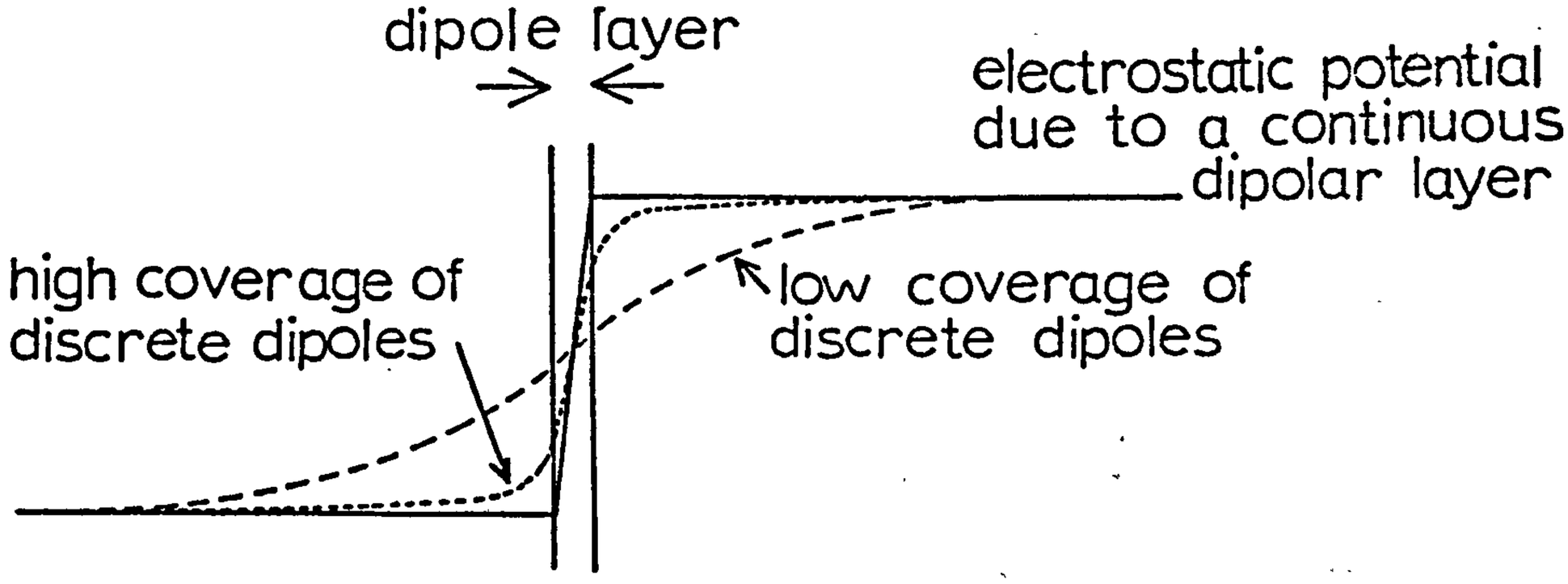

When measuring SP's by a method which is dependent on Φ_o at some little distance from the surface i.e. diode or capacitor methods, this correction will be of little significance except perhaps at very low coverages. The effect of the surface not being infinite has been considered by Knapp (23). He concludes that at distances from the surface that are not large compared to the surface dimensions, equation (14) gives a good approximation to the surface. The inside surface of a sphere (diode) would appear to present a particularly favourable approximation to an infinite sheet.

2.10 The Use of the Diode to Measure Surface Potentials

The diode cell used to measure surface potentials has been described in section 1.8 and follows a design due to Pritchard (24). Essentially it consists of an evacuated sphere, on the inside surface of which is the evaporated film forming the anode, and a centrally mounted filament

which forms the cathode. The device was always operated as a retarding field diode in which the anode voltage, after correcting for the contact potential between anode and cathode, was held negative with respect to the cathode ($-V_a$). The potential energy diagram for an electron crossing from cathode to anode is shown in fig. 2.10. Average work functions are indicated since the anode surface in particular will be polycrystaline.

Fig. 2.10

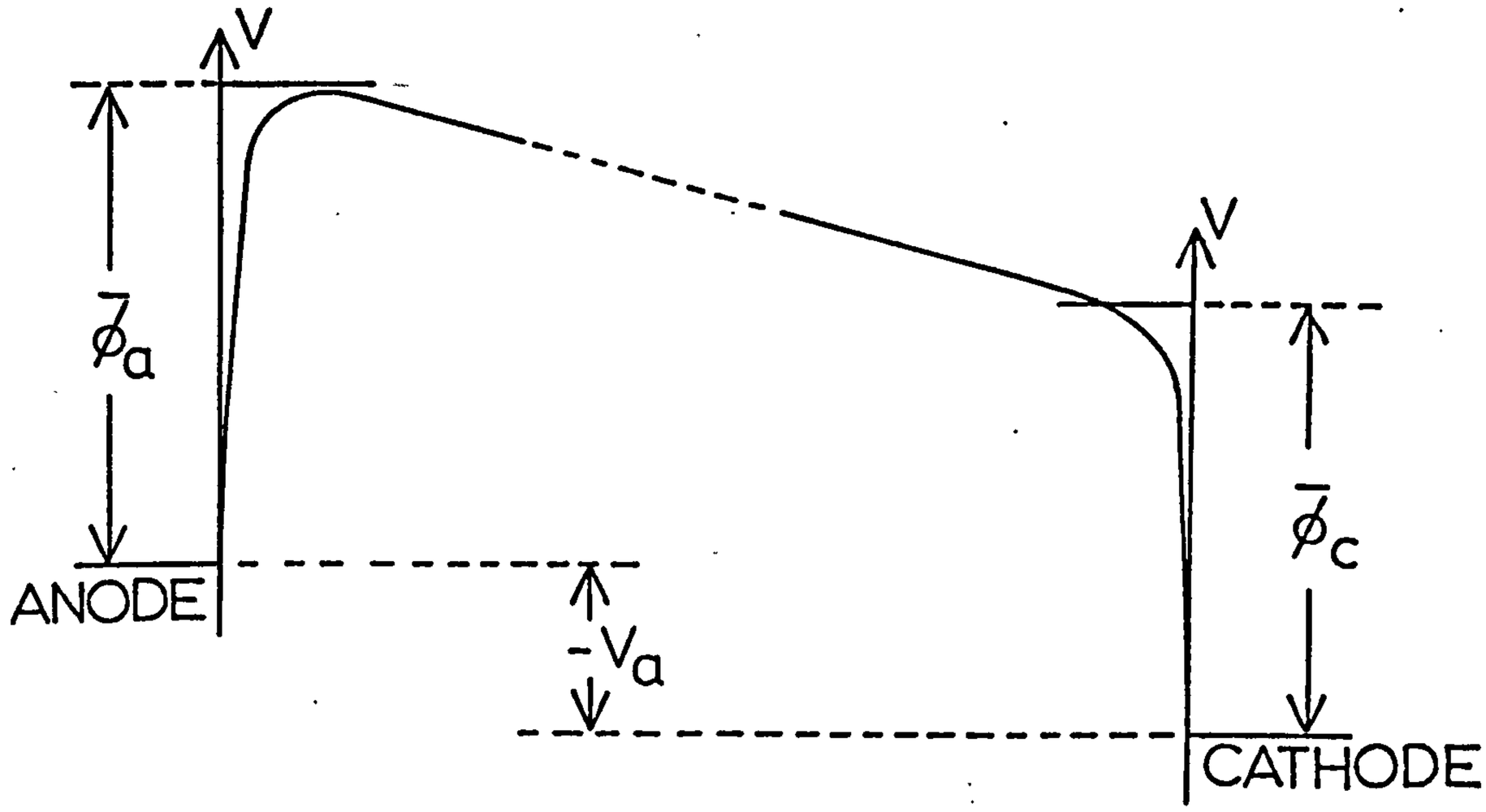

The potential barrier to electrons entering the anode from the cathode is $(\bar{\phi}_a - V_a)$ and hence the anode current for a diode operated in this manner is given by:

$$I_a = A(1-\bar{r})(\bar{T}_f)^2 \exp\left[(V_a - \bar{\phi}_a)/k\bar{T}_f\right] \text{——(15)}$$

where V_a = anode voltage

I_a = anode current

A = constant

$\bar{r}$ = reflection coefficient for electrons at the anode

$\bar{T}_f$ = average filament temp.

This expression is derived from that used to calculate saturated emission current from a metal surface (25) by the replacement of the potential barrier ϕ_c with $(\bar{\phi}_a - V_a)$ and the addition of the term $(1-\bar{r})$. This term is assumed independent of the energy of the electrons and tends to 1 (i.e. $\bar{r} \rightarrow 0$) for an ideally spherical diode.

Three conclusions may be drawn fromthis expression:

(i) I_a is a monotonic function of $(V_a - \bar{\phi}_a)$; thus for a clean film

$$I_a = f(V_a - \bar{\phi}_a) \qquad \text{——————————} (16)$$

A plot of I_a against V_a to give a curve of function f is termed an I_a/V_a characteristic of the diode. A second plot of I_a against V_a made after an adsorption process has occurred may be represented by

$$I'_a = f'(V'_a - \bar{\phi}'_a) \qquad \text{——————————} (17)$$

If these two curves are parallel then $f' = f$ i.e. function f has not been altered by the adsorbate e.g. fig. 1.17. In every situation where this is true, the change in anode work function due to the presence of an adsorbate may be obtained from the displacement of these curves along any line intersecting the curves which is parallel to the V_a axis. At the intersections of this line and the curves,

$I_a = I'_a$

Therefore $\quad V_a - \bar{\phi}_a = V'_a - \bar{\phi}'_a \qquad (f = f')$

The surface potential ΔV is thus given by

$$\Delta V = \bar{\phi}_a - \bar{\phi}'_a = V_a - V'_a \qquad \text{——————————} (18)$$

(ii) The anode current and hence any measurement of SP is independent, at least to a first approximation, of the cathode work function. In addition since the cathode is maintained at a high temperature, adsorption on its surface which may change ϕ_c is unlikely to occur.

(iii) I_a is strongly dependent on $\overline{T}_f$ and therefore this must be automatically stabilised (section 1.9).

The diode method is a simple and effective method of measuring SP's. There are however two serious restrictions on its use.

(i) High gas pressures (greater than 10^{-3}torr) cause changes in the form of the function f, restricting the technique to lower pressures. The form of f may however be checked at any time by plotting the I_a/V_a characteristic in order to test the validity of an SP measurement.

(ii) Certain gases present problems as adsorbates as they react with the heated cathode.

2.11 Interpretation of Surface Potential Measurements

The SP arises from the presence of dipoles in the adsorbate layer whose origin is due to one or more of the following:

(i) An adsorbed molecule may possess a permanent dipole. This will produce an SP whose magnitude is a function of the orientation of the dipole with respect to the surface.

(ii) A chemical bond (chemisorption) may be formed between the surface metal atoms and the adsorbate and this may be polar. Ionic bonding occurs, for example, when alkali metals are adsorbed on tungsten. Covalent bonding results in a dipole whose magnitude and direction will be a function of

the electron affinity of the metal and adsorbate (26).

(iii) The electric field at the metal surface may polarise the adsorbed atom or molecule and hence induce a dipole in it. For a purely physically adsorbed species this dipole will always be positive. Attempts have been made to calculate the SP due to this effect for a purely physically adsorbed gas (27).

In addition the adsorbed atoms or molecules may interact. Long range repulsive forces are known to exist between adsorbed atoms or molecules due at least in part to dipole-dipole interactions. The effect of these interactions is complex in the case of chemisorption, but in purely physisorbed adsorbates results in mutual depolarisation. It was anticipated that this simple depolarisation would be described by the equation derived by Knapp (23) from the Topping formula for point dipoles (28).

$$1 + 9n_o^{\frac{3}{2}}\theta^{\frac{3}{2}} = \sigma_o n_o \theta \Big/ \varepsilon_o \Delta V \qquad (19)$$

A plot of $\frac{\theta}{\Delta V}$ vs $\theta^{\frac{3}{2}}$ will result in a straight line in cases where this simple depolarisation occurs. An example of a system in which verification of this model has been attempted is xenon adsorbed on palladium (100). (29) (section 3.7)

The simultaneous operation of these effects and their interdependence and reflection of the nature of the surface can produce a rich complexity of behaviour. In the simplest possible instance of a species having a permanent or induced dipole being adsorbed, having no sensitivity to surface

heterogeneity and no mutual interactions, a plot of SP against the number of atoms adsorbed may be expected to produce a straight line. In this study the SP vs coverage plots recorded will be discussed in terms of deviations from this ideal linear behaviour.

References

(1) T.N. Rhodin and D. Walton: Trans. 9th. Natl. Vac. Soc. L.A. (1962) Macmillan N.Y.

(2) C.A. Neugebauer: Physics of Thin Films. 2 , 1, (1964).

(3) Int. Symp. Basic Probs. of Thin Film Physics. Vandenhoeck and Ruprecht, Gottingen (1966).

(4) R.C. Cinti and B.K. Chakraverty: Surface Sci. 30, 109+125 (1972).

(5) B. Lewis and D.S. Campbell: J. Vac. Sci. Tech. 4, 209. (1967).

(6) K.K.Kakati and H.Wilman: J. Phys. D: Appl. Phys. 6, 1307, (1973).

(7) D. Walton: Phil. Mag. 7, 1671, (1962).
J. Chem. Phys. 37, 2182, (1962).

(8) L. Yang, G.E. Birchenall, G.M. Pound and M.T. Simnad: Acta Met. 2, 463, (1954).

(9) D.W. Pashley: Adv. in Phys. 5, 173, (1956).
H. Mayer: Physik Dünner Schichten (Stuttgart) (1955). pp. 108, 124, 125

(10) B. Lang, R.W. Joyner and G.A. Somorjai: Surface Sci. 30, 454, (1972).

(11) G. Ehrlich and F.G. Hudda: J. Chem. Phys. 30, 493, (1959).

(12) G.A. Basset, J.W. Menter and D.W. Pashley: "Structure and properties of thin films" Wiley N.Y.(1959).p.423.

(13) B.K. Chakraverty and G.M. Pound: Acta Met. 12, 851, (1964).
C.H. Sholl and N.H. Fletcher: Acta Met. 18, 1083, (1970).

(14) L. Bachmann and H. Hilbrand: Ref.(3) p.77.

(15) B.J. Hopkins and S. Ussami: Surface Sci. 23, 423, (1970).

(16) J.C.P. Mignollet: Discuss. Faraday Soc. 8, 105, (1950).
R. Suhrmann: J. Am. Chem. Soc. 53, 15, (1956).

(17) C. Herring and M.H. Nichols: Rev. Mod. Phys. 21, 185, (1949).

(18) R. Smolnchowski: Phys. Rev. 60, 661, (1941).

(19) J. Müller: Surface Sci. 42, 525, (1974).

(20) R.R. Ford: Ph.D Thesis, U. of L. (1966).

(21) P.A. Anderson: Phys. Rev. 88, 655, (1952).

(22) R. Gomer: J. Chem. Phys. 21, 1869, (1953).

(23) A.G. Knapp: Surface Sci. 34, 289, (1973).

(24) J. Pritchard: Trans. Faraday Soc. 51, 457, (1965).

(25) C. Kittel: Intro. to Solid State Phys. 3rd. Ed. p.246, (1968).

(26) B.J. Hopkins and C.W. Jowett: Surface Sci. 22, 392, (1970).

(27) J.R. Smith: Phys. Rev. 181, 522, (1969).

(28a) J. Topping: Proc. Roy. Soc. A114, 67, (1927).

(28b) A.R. Miller: Proc. Camb. Phil. Soc. 42, 292, (1946).

(29) P. W. Palmberg: Surface Sci. 25, 598, (1971).

Chapter 3

Surface Potential Measurements

3.1

Chapters 1 and 2 have been devoted to a description of the apparatus and techniques used in this study, and to a discussion of the nature of the surfaces studied and the measurements of surface potentials. In chapters 3 and 4 the results of the experimental work will be described and discussed.

The gold and silver films were evaporated onto either pyrex or B37 glass substrates as described in section 1.14 and sequences of small doses of gas admitted to the cooled surface (section 1.12): the gases used were chiefly xenon, carbon monoxide or hydrogen, either singly or in sequence. During the addition of gas to the surface two types of measurement were made:

(i) The rate at which each dose of gas was adsorbed onto the surface was followed as described in section 1.15. The results of these measurements and their evaluation are discussed in chapter 4.

(ii) After the addition of each dose, the system was allowed to come to equilibrium and the surface potential and equilibrium pressure of gas over the surface was then measured. The results of these measurements are recorded and discussed in this chapter.

3.2 Xenon Adsorption - Results

The adsorption of inert gases onto group 1b metal surfaces has been a source of interest for some years and a number of

studies of this phenomenon have been made, both on single crystal surfaces (1) and on evaporated films (2). In this investigation the adsorption of xenon was studied on four systems.

Silver films evaporated onto (i) pyrex

and (ii) B37 substrates

Gold films evaporated onto (iii) B37

and (iv) pyrex

(i) Silver evaporated onto pyrex.

Xenon adsorption was studied on four films evaporated onto pyrex. A typical example of the SP data collected is tabulated in fig. 3.1 and shown graphically in fig. 3.2. The number of atoms adsorbed was calculated from the dimensions of the gas dosing system and corrected for the equilibrium pressure of gas over the surface where this was significant. Exactly analogous tables and graphs were drawn for each adsorption experiment.

The graphs of surface potential and equilibrium pressure against coverage for each of the four films had the characteristic shape typified by fig. 3.2 which may be described as follows:-

Surface Potential vs Coverage

(a) A maximum surface potential of +470 to 490mV.

(b) A maximum uptake of approximately 7×10^{16} atoms measured at the point where the SP vs coverage graph becomes horizontal and the equilibrium pressure is rising rapidly. This point is equated with the completion of a monolayer (3). The films all had a geometric surface area of approximately

Fig 3.1 ADSORPTION DATA FOR FILM 1—(day 1)

Dose No:	Potentiometer Voltage (V)	SP(mV)	ΔSP(mV)	Pressure (torr)	No. of xenon ats.ads.($\times 10^{-16}$)
0	-1.101	0	0	3×10^{-8}	0.0
1	-1.109	8	8	2×10^{-7}	0.452
2	-1.127	26	18	3×10^{-7}	0.950
3	-1.162	61	35	5×10^{-7}	1.442
4	-1.202	101	40	6×10^{-7}	1.925
5	-1.242	141	40	7×10^{-7}	2.334
6	-1.285	184	43	1×10^{-6}	2.826
7	-1.323	222	41	1×10^{-6}	3.276
8	-1.358	257	35	1×10^{-6}	3.724
9	-1.389	288	31	1×10^{-6}	4.076
10	-1.420	319	31	1×10^{-6}	4.568
11	-1.454	353	33	1×10^{-6}	5.039
12	-1.485	384	31	1×10^{-6}	5.452
13	-1.514	413	29	1×10^{-6}	5.871
14	-1.540	439	26	1×10^{-6}	6.266
15	-1.560	459	20	1×10^{-6}	6.680
16	-1.570	469	10	2×10^{-6}	7.082
17	-1.576	475	6	5×10^{-6}	7.463
18	-1.580	479	4	1×10^{-5}	7.802
19	-1.584	483	4	5×10^{-5}	8.200
*	-1.581	480	-1		

* Pump for 10 minutes at $77^{\circ}K$.

Fig 3.2 SP and EQUILIBRIUM PRESSURE vs Xe COVERAGE – film 1

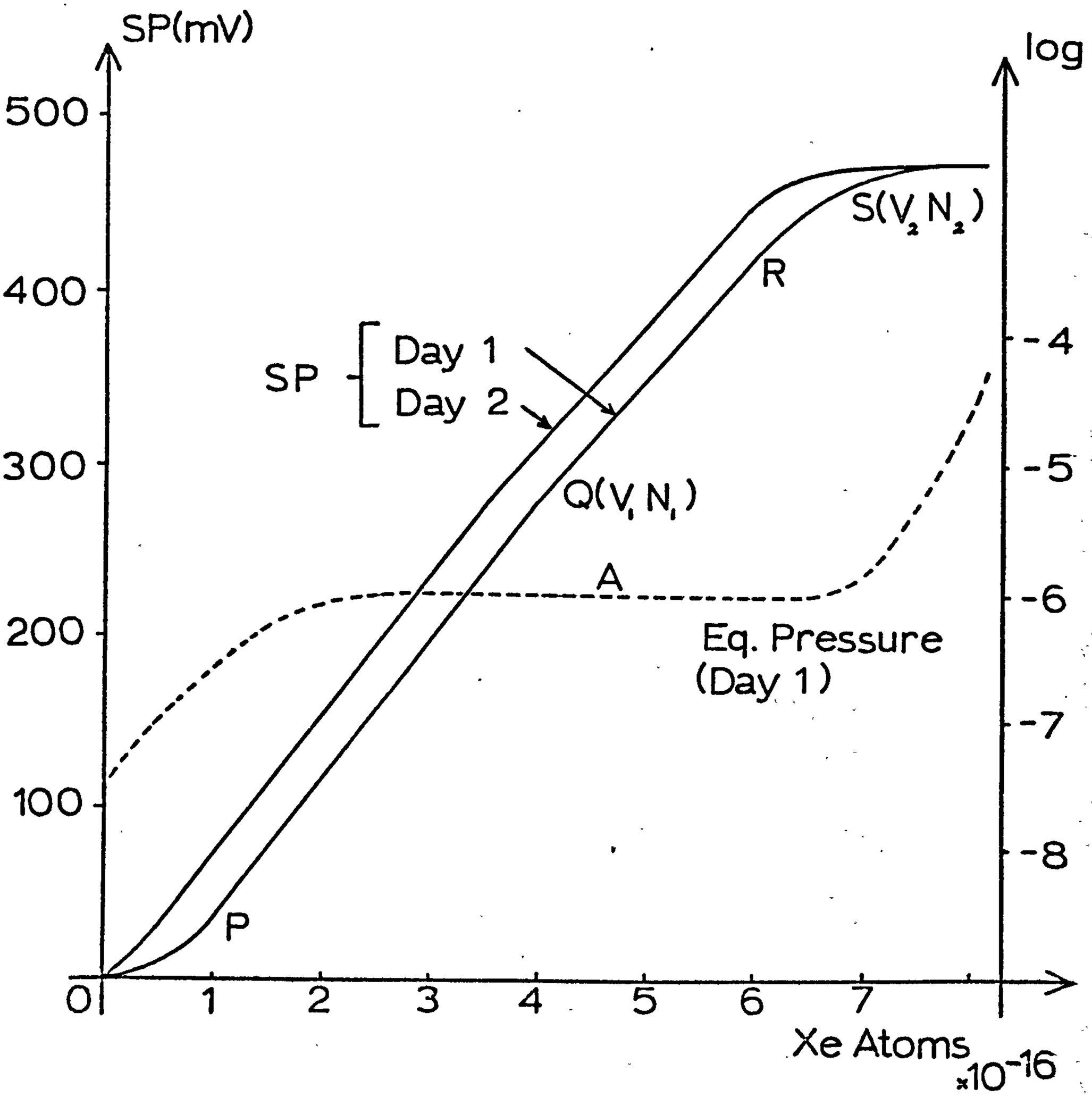

100cm².

(c) A curved section OP at very low coverages (less than 1×10^{16} atoms), the shape of which changed during the life of the film.

(d) Two intersecting straight lines PQ and QR. The intersection was always clearly marked with no indication of a curved intermediate section. The slope of each section

remained constant for a given film despite changes in the shape of OP.

(e) A curved section at high coverages (RS) leading to a horizontal line at approximately 7 x 10^{16} atoms.

Equilibrium Pressure vs Coverage

(a) Initially at the background pressure of the system, the pressure rose rapidly to between 8 x10^{-8} and 1 x 10^{-6}torr after the addition of approximately 2 x 10^{16}atoms xenon.

(b) The pressure then remained constant at this value which however, while always lying between these limits, varied from film to film. (Region A).

(c) After the addition of an amount of xenon corresponding to point R on the SP vs coverage graph the pressure again rose rapidly to reach approximately 10^{-4}torr as the SP rose to its maximum value.

(d) The addition of further xenon resulted in a further large increase in pressure but this was not accompanied by any significant change in SP.

The form of these graphs is in substantial agreement with Knapp and Stiddard (2a) and with other published values of maximum surface potentials of xenon on silver (2b). The curved section of the surface potential plot (OP) is also reported to occur in some cases by Knapp (4). A particular study was made of the variation in shape of this sectionOP as the age of the film increased. The form of the variation was the same for each film and is typified by the results for film four shown in fig. 3.3. The initially strongly marked curvature diminished as the age of the film

Fig 3.3 THE VARIATION IN SHAPE OF SECTION OP

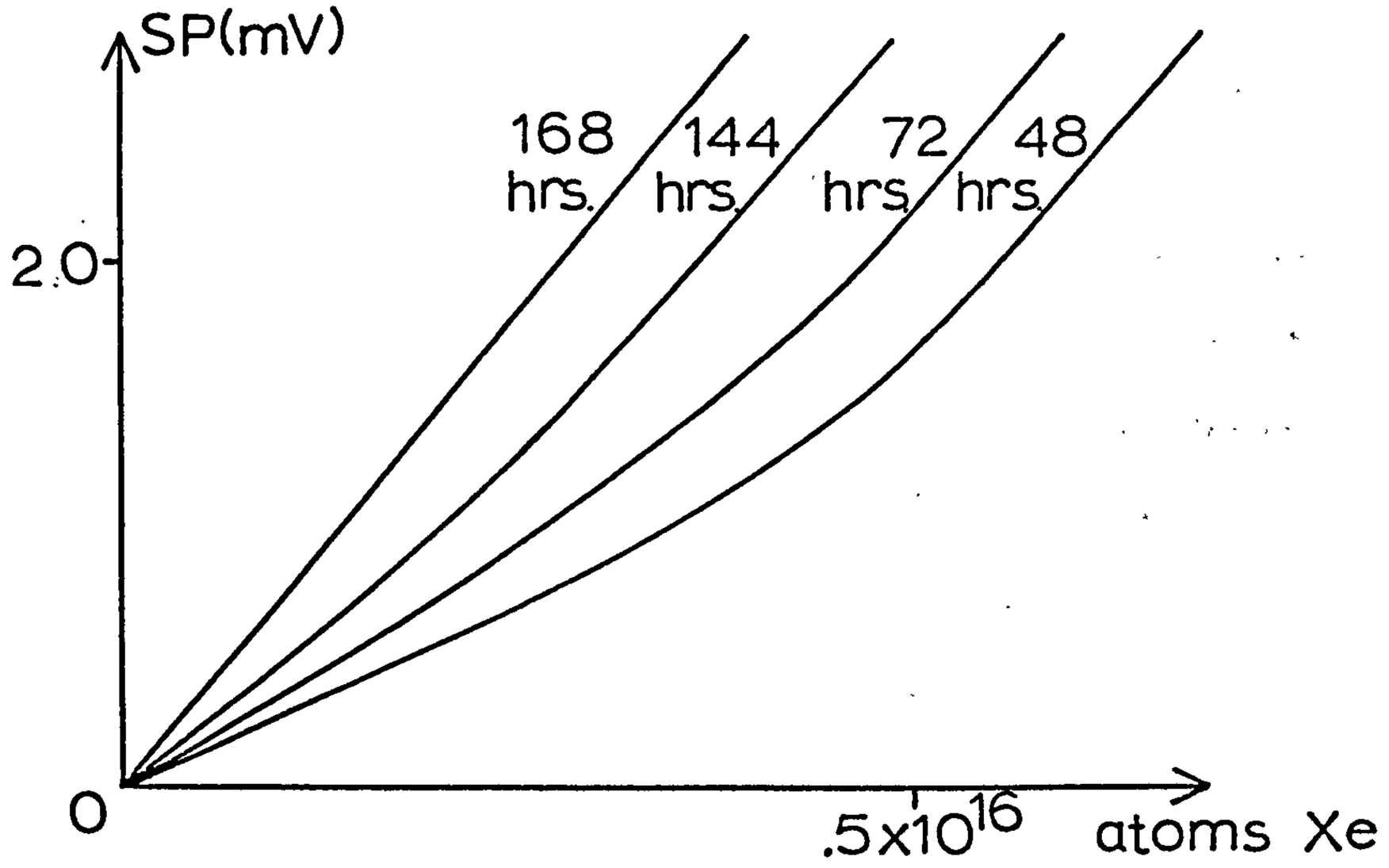

increased. The remainder of the plot was displaced (fig.3.2).

Variations in the observed behaviour for individual films fell into two categories:

(a) The magnitude of the initial effect varied, point P initially occurring between $.5x10^{16}$ atoms and $1x10^{16}$ atoms. The surface potential at point P was always about 20 to 25mV.

(b) The rate at which this curve was removed was not constant, ranging from complete removal in one day, to over four days.

There was no correlation between (a) and (b) or between either of these and any other property of the film, including their weight.

A summary of the surface potential data for the four films is tabulated in fig. 3.4.

The maximum surface potential (V_2) remained approximately constant throughout the life of the films, as did V_1 the

surface potential at the point of intersection of the two straight line sections of the graph. Values of N_1 and N_2 however decreased by approximately $.5x10^{16}$ atoms as the age of the film increased (fig. 3.2) as a consequence of the disappearance of the curved section OP.

Values recorded are those late in the life of the film.

Fig. 3.4 SP DATA FOR Ag FILMS EVAPORATED ONTO PYREX

Film No:	Weight (mg.)	Sub-strate	$SP(V_2)$ (mV)	N_2 ($x10^{-16}$ats)	$Q(V_1)$ (mV)	$Q(N_1)$ ($x10^{-16}$ats)
1	5.3	pyrex	+480	7	+285	3.5
2	5.8	"	+490	7	+260	3.5
3	8.6	"	+470	7.5	+260	3.75
4	9.4	"	+475	7.5	+270	3.5

(ii) Silver evaporated onto B37

Xenon adsorption was studied on three silver films evaporated onto B37 glass, one of these being devoted solely to the investigation of the behaviour at very low coverages. Again the SP against coverage plots always had a characteristic shape, shown in fig. 3.5.

Fig. 3.5

SP vs COVERAGE – Xe on Ag/B37

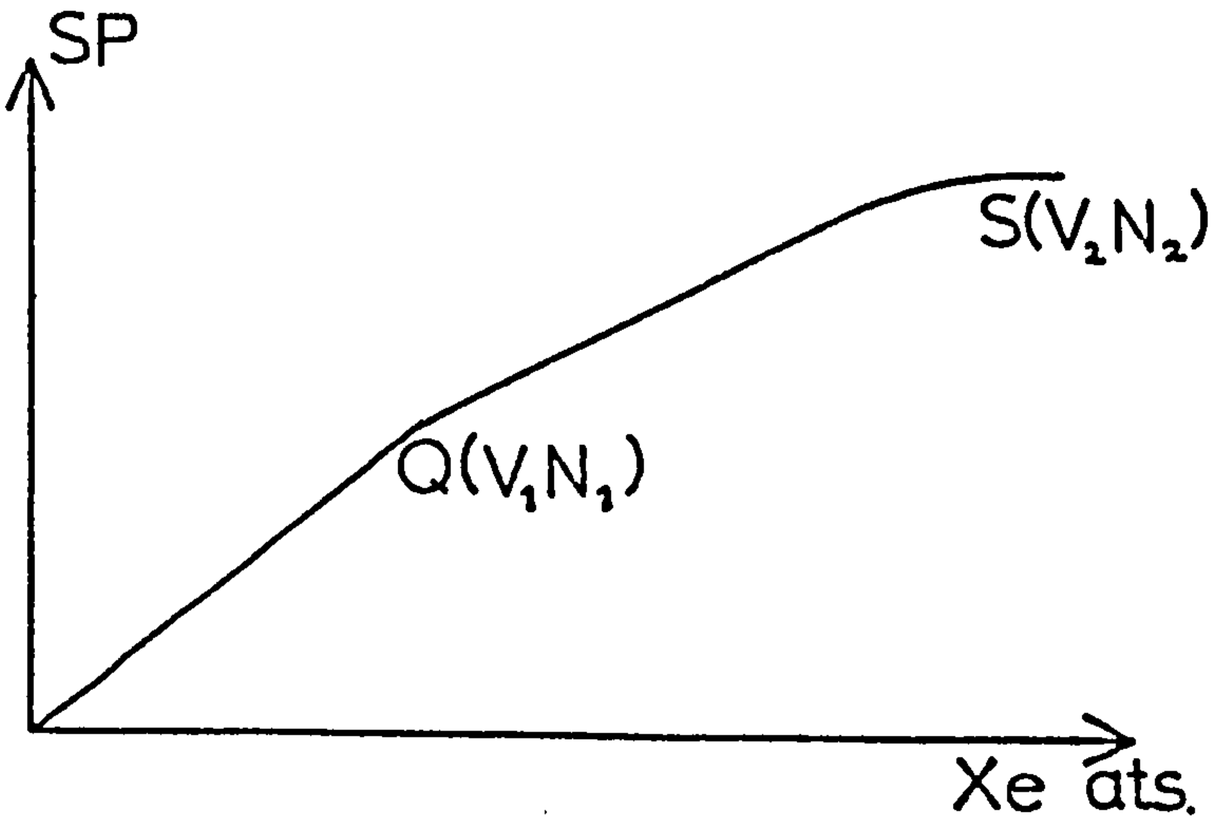

The graphs always showed the two intersecting straight line sections observed with silver films evaporated onto pyrex, and the curved section leading to a horizontal line at high coverages. The curved section at very low coverages was however entirely absent on all these films. The SP vs coverage data for these films is summarised in fig. 3.6, the equilibrium pressure of xenon varying with coverage exactly as described for films evaporated onto pyrex.

Fig. 3.6 Ag FILMS EVAPORATED ONTO B37

Film No.	Weight (mg.)	Sub-strate	SP(V_2) (mV)	N_2 (x10^{-16}ats)	Q(V_1) (mV)	Q(N_1) (x10^{-16}ats)
5	6.4	B37	+490	6	+340	3
6	6.15	"	+487	8.5	+260	4.3
7	6.7	"	+475	-	-	-

(iii) Gold evaporated onto B37

Four such films were studied, the graphs of SP vs coverage all having the shape characteristic of silver films evaporated onto B37. The curved section at low coverage was always absent. There was however one point of dissimilarity between the form of these graphs for gold and those for silver. In the case of all the silver films, the straight line sections of the graphs were remarkable for their almost ideal linearity, while all those for the gold films showed small but significant deviations from the mean straight line. These appeared not to be caused by random errors in the measuring process but to reflect small differences in

the surface potential change which resulted from the addition of each dose of xenon as the coverage of the surface increased. The effect is illustrated diagramatically in fig. 3.7.

Fig. 3.7 SP vs COVERAGE FOR Au/ B37

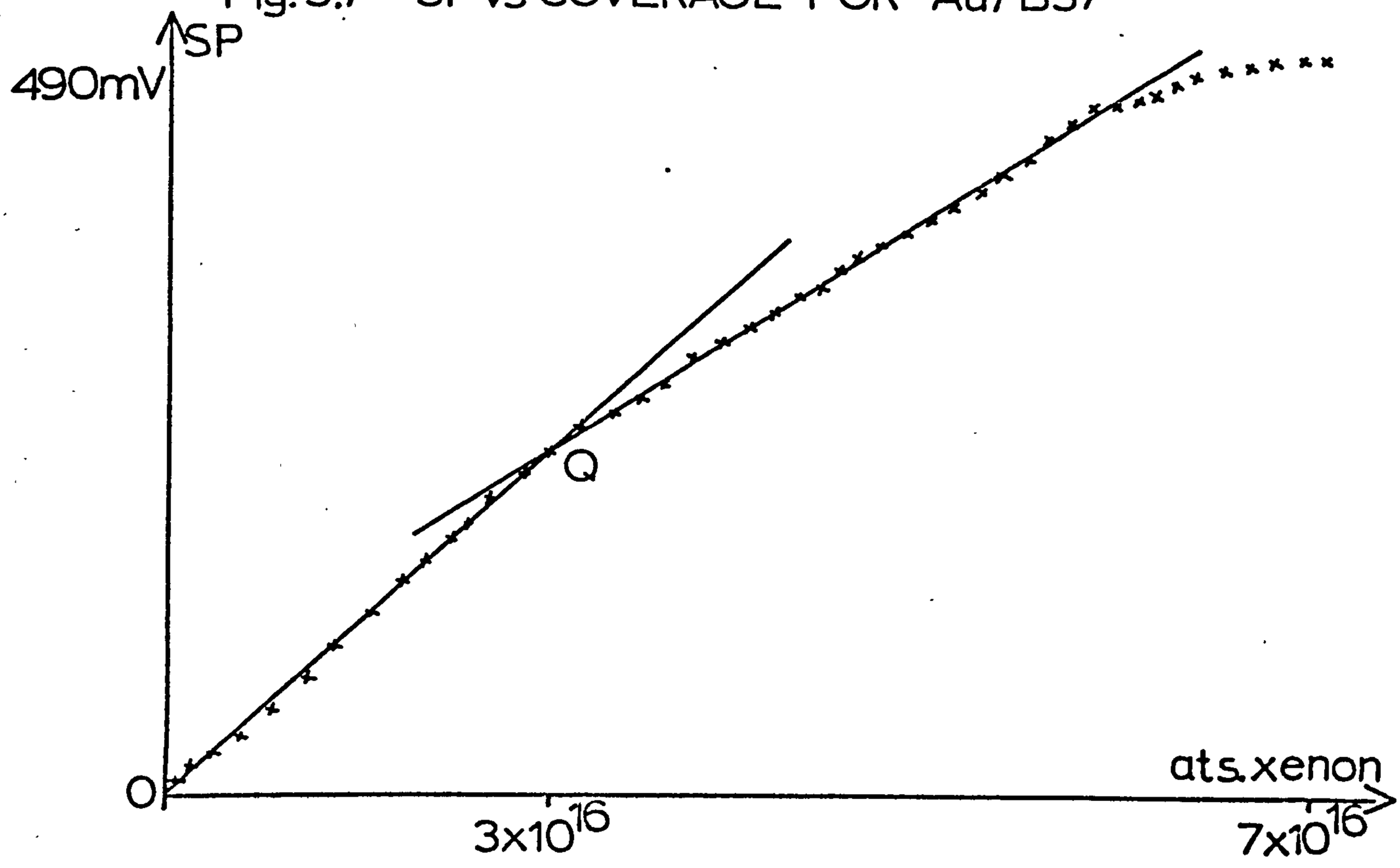

Careful checks were made to ensure that this effect was not caused by faults in the electrical systems associated with the measurement of surface potentials. The stability of the filament temperature stabiliser and Vibron electrometer were in particular carefully tested. It was felt that this behaviour possibly reflected some heterogeneity of the gold surface.

Surface potential data are summarised for these films in fig. 3.8. The equilibrium pressure varied with coverage exactly as for silver.

Fig.3.8 Au FILMS EVAPORATED ONTO B37

Film No.	Weight (mg.)	Sub-strate	SP(V_2) (mV)	N_2 ($\times10^{-16}$ats)	Q(V_1) (mV)	Q(N_1) ($\times10^{-16}$ats)
1	9.2	B37	+475	6.5	+270	2.5
2	11.2	"	+490 +470*	7	+270	3.5
3	11.5	"	+460	7	+260	3
4	15	"	+460	6.5	+250	2.5

* The lower value was recorded later in the life of the film (7th day).

The geometric area of the films was slightly less than those evaporated onto pyrex, but again approximately 100cm^2.

(iv) Gold evaporated onto pyrex

Preliminary measurements on one film were made for this system. Tentative conclusions included a maximum surface potential of 480mV and an intersection at point Q as described above. Equilibrium pressure against coverage plots were also similar.

3.3 Xenon Adsorption - Discussion

The significant features of the adsorption of xenon on gold and silver films may be summarised as follows:

(i) The maximum SP lay between +460 and 490mV: the mean value for silver was 480mV and that for gold, omitting the high value early in the life of film Au 2, was 472mV. Variations between films of the same metal were of the order of 10 to 20mV. A monolayer comprised approximately 7×10^{14} atoms per cm^2. on all the films. No correlation was observed between the surface potential or the monolayer number of

xenon atoms and the weight of the films.

(ii) The variation of equilibrium pressure with coverage was largely independent of the film material, weight and substrate and was as described in section 3.2(i).

(iii) The surface potential against coverage curve for every film studied, displayed two straight line sections which met at a quite sharp intersection Q . This point corresponded to the completion of one half monolayer of xenon atoms for silver on pyrex or B37, as indicated in fig. 3.9 but occurred somewhat earlier in the case of gold films. The slope of the second section was always less than that of the first and the slopes of both sections always remained constant for a given film. However the slopes varied from film to film as did the ratio of the slope of one section to that of the other. Little correlation could be perceived between these slopes and ratios of slopes and any other film properties.

Fig.3.9

THE RATIO OF N_1/N_2

Film no.		N_1/N_2
Ag	1	0.5
	2	0.5
	3	0.5
	4	0.47
	5	0.5
	6	0.51
	7	-
Au	1	0.38
	2	0.5
	3	0.43
	4	0.38
Au Pyrex		$<.5$

(iv) SP vs coverage graphs for silver films evaporated onto

pyrex always showed a curved section at low coverages which was slowly lost as the age of the film increased. This feature was always absent for silver films on B37 and was not observed on gold films.

(v) All SP vs coverage curves showed a curved section at high coverages leading to a horizontal line.

3.4

The monolayer surface potential of xenon is a quite sensitive indicator of the degree of contamination of gold and silver films by mercury which is by far the most likely contaminant in a mercury pumped system. Such contamination may occur either during the evaporation of the film or later during the course of adsorption experiments, the latter being particularly noticeable as it results in changes in the monolayer surface potential during the life of the film. Only in one case (film Au 2) was any significant change in this monolayer surface potential observed and this was probably at least partly due to a change in the structure of the film. Satisfactory agreement between the measured surface potentials and recently published values (2), particularly those of Ford and Pritchard who studied the effect of mercury on silver and gold films, strongly suggests that mercury contamination during evaporation was at a reasonably low level. Differences between the SP values recorded for the various films were small (approximately $\pm$ 2% $\overline{SP}$) and probably at least partly reflect structural differences in the films (cf section 3.6)

3.5

The form of the adsorption isotherms (P vs coverage) is highly characteristic of the formation of a well defined monolayer as has been discussed by several authors (5). The occurrence of the monolayer is identified with the point at which the pressure is rising tapidly above 10^{-6}torr and corresponds to the point where $\Delta SP \rightarrow 0$ on the SP vs coverage graph. The adsorption of approximately $7x10^{14}$ats. $cm.^{-2}$ for a monolayer suggests a surface roughness in the region of 1.3 (assuming bulk Xe - Xe separation of 4.37Å). Adsorption isotherms have been elegantly discussed in terms of a 2Dgas - 2Dsolid phase change by Suzanne et al (6), using results derived from the system xenon on (0001) graphite. It is interesting to compare their isotherms, obtained on a system widely regarded as possessing a high degree of homogeneity with those of this study:(fig. 3.10)

Fig 3.10 COMPARISON OF ADSORPTION ISOTHERMS FOR Xe/Ag or Au AND Xe/graphite(0001)

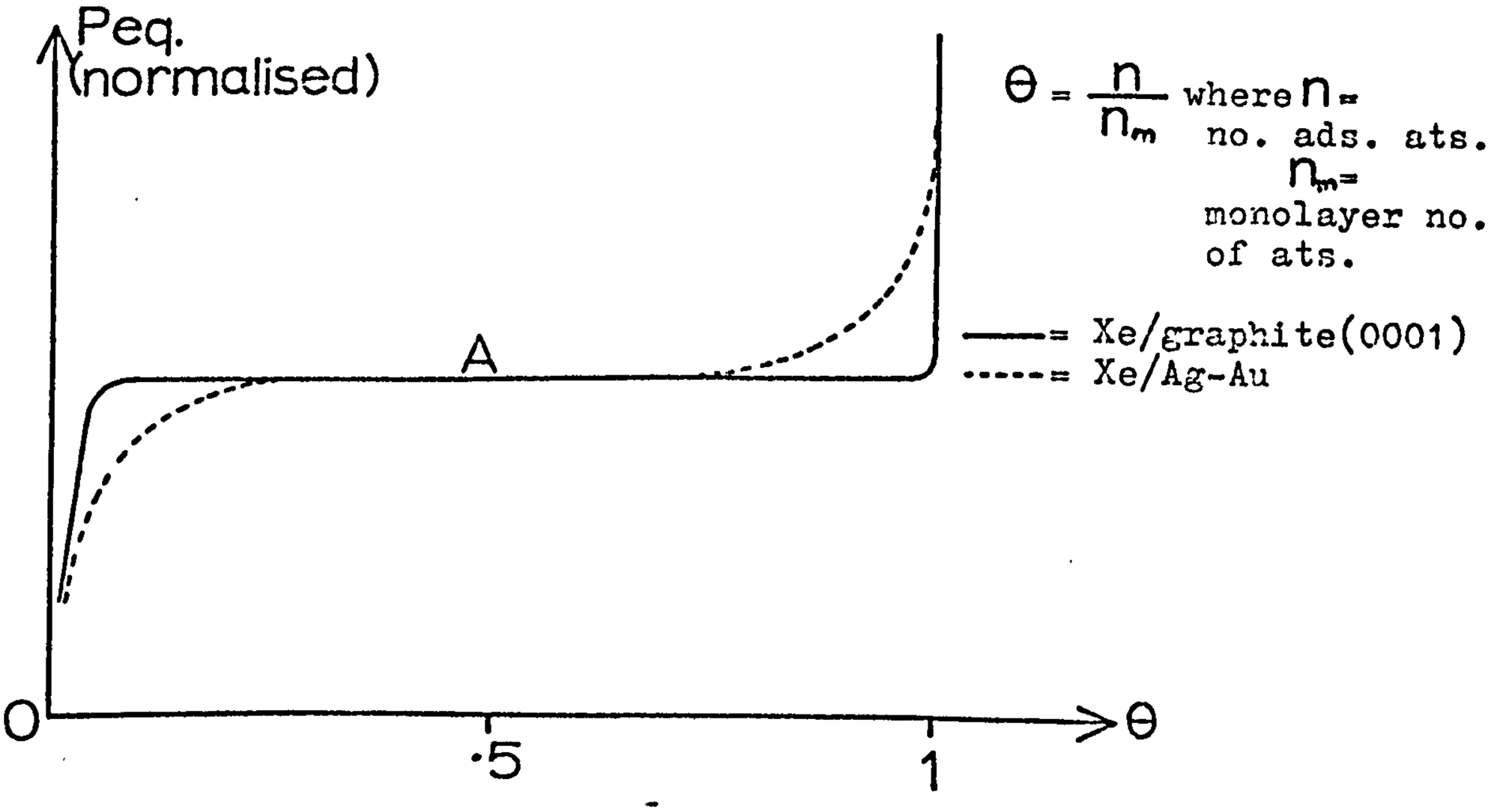

The rounding off of the Xe/Ag isotherm at high coverages is indicative of the heterogeneity of the gold and silver surfaces, the monolayer being formed at slightly different pressures on different patches of the film. A similar effect occurs at very low coverages, initial adsorption occurring at lower pressures on certain preferred portions of the film. Variations in the surface structure of the films may also be reflected in the different pressures recorded from film to film for the constant pressure region (A). By analogy with three dimensional systems (7) the form of this isotherm perhaps indicates a second phase change:

2D disordered gas——phase II——2D solid (monolayer)

the temperature during adsorption lying below the critical point for the coexistence of the first two phases at appropriate coverages. This point is discussed further below.

3.6

The behaviour of xenon at very low coverages reveals an interesting difference between films evaporated onto pyrex glass substrates and those evaporated onto B37. This behaviour which is described in section 3.2(i) (fig.3.3) was observed to occur only on silver films evaporated onto pyrex. It was entirely absent on silver films evaporated onto B37 and was not observed on gold evaporated onto B37. Since only preliminary measurements were made on gold films on pyrex, it is not possible to conclude whether or not this

behaviour occurs on this system. The SP vs coverage graphs indicate that for silver on pyrex, the addition of the first few doses of xenon produces a lower surface potential change than later doses at higher coverage. The effect was most marked on recently evaporated films and diminished with the increasing age of the film. The graphs also suggest that there is a corresponding reduction in the monolayer number of xenon atoms as the film ages. It is suggested therefore that on newly evaporated silver films on pyrex, there exists a small additional number of sites on which xenon is preferentially adsorbed and on which the surface potential change due to adsorption is reduced. These sites are removed by the very slow final sintering of the film. Knapp (4) has tentatively identified these sites with cavities in the film and this view accords well with the experimental evidence, it being reasonable to assume that xenon atoms adsorbed in such cavities would experience a less effective polarising field and hence cause at the very least a smaller surface potential than those adsorbed on a smooth surface. Xenon atoms are widely believed to be mobile on noble metal surfaces at 77^{o}K. and one can therefore envisage an equilibrium being set up between xenon atoms adsorbed on these preferred cavity sites and on sites elsewhere, resulting in the observed behaviour as the cavity sites are filled. This phenomenon of extraneous sites modifying xenon adsorption at low coverages has also been observed for xenon on tungsten (111) at 104^{o}K. (8). In this system of silver evaporated onto

glass however, perhaps the most interesting feature is the total absence of this behaviour on silver films on B37. Indeed, those graphs drawn for Ag/B37 whose first straight line section did not accurately pass through the origin implied an intersection with the SP axis (of approximately 5mV) as shown diagramatically in fig. 3.11, suggesting that extraneous sites on which xenon is preferentially adsorbed in this system experience enhanced electric fields.

Fig. 3.11

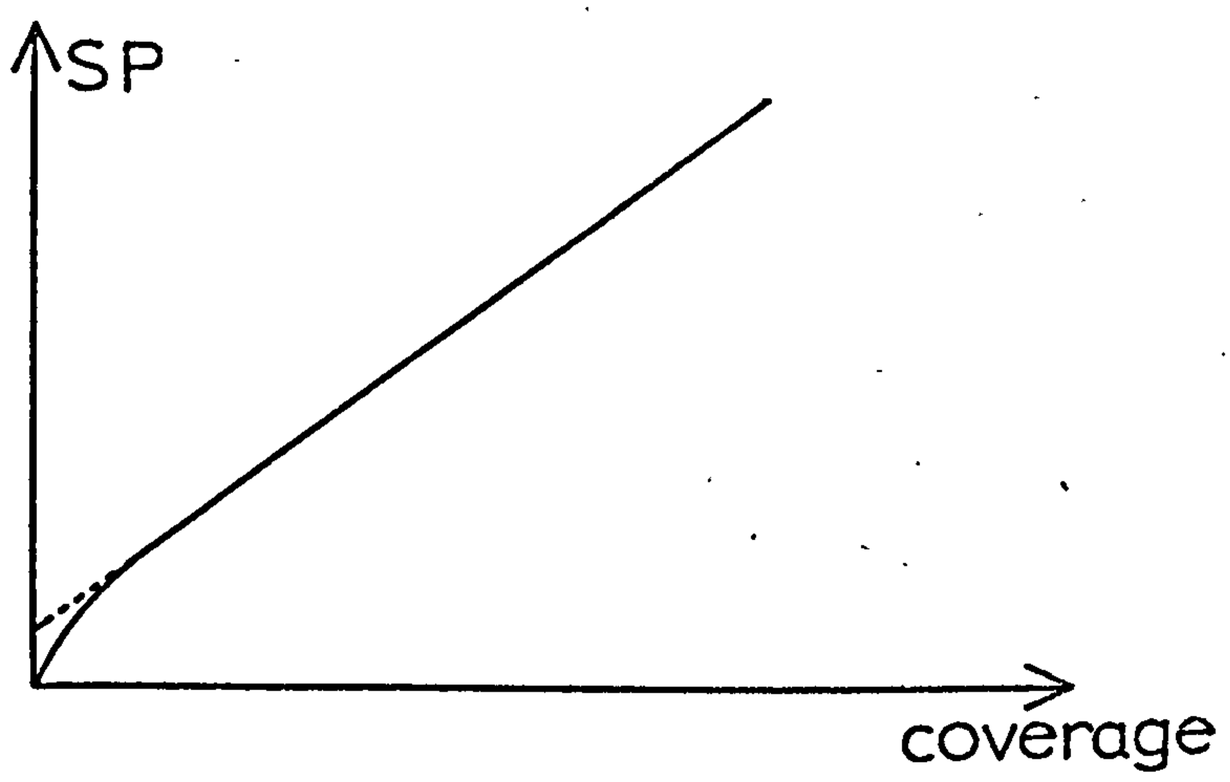

Such sites are probably asperities, no doubt also found on Ag/pyrex, where their presence is masked by the occurrence of cavities. The implication seems to be that despite their apparent similarity, differences between pyrex and B37 glass surfaces induce dissimilarities in the structure of silver films that are evaporated onto them. The fact that overall the properties of the films on the two types of substrate are very similar, and further that the dissimilarities diminish as the age of the film increases, suggests that the films possess many structural features in common and probably differ chiefly in the nature and concentration of defects at the surface. The defect concentration may be

expected to be reduced by sintering, differences in the initial concentration probably arising from the nucleation process during film evaporation. At the low rates of evaporation used in this study this nucleation process is very likely to be sensitive to the nature and state of the film substrate, i.e. the glass, as discussed in chapter 2. In this context it is perhaps worth noting that the sequence of colours exhibited by the silver films on pyrex and B37 during the very early stages of depcsition are not precisely identical and indeed the final colour of the gold films seen by reflection from the inside surface differs on the two substrates, showing a deeper red reflection on B37. It appears likely that the nature and condition of the glass substrate used in these experiments has a greater influence on the structure of films evaporated onto them at low deposition rates than was initially assumed, probably by influencing the nucleation of the film, and that variations in the state of the glass surface may be the cause of other apparently random variations in the film properties, for example in the maximum surface potentials (cf section 3.11, hydrogen adsorption).

3.7

In the absence of inter-atom interactions and effects such as those described in section 3.6, the dipoles induced in the adsorbed xenon atoms by the electric fields at the surface would be expected to cause a surface potential which is directly proportional to the number of atoms

per square centimetre (equation 14 section 2.9). This behaviour would give rise to an SP vs coverage graph of the form of fig. 3.12, the surface potential rising linearly with coverage until the adsorption abruptly ceases at the monolayer.

Fig. 3.12

"IDEAL" SP vs COVERAGE GRAPH

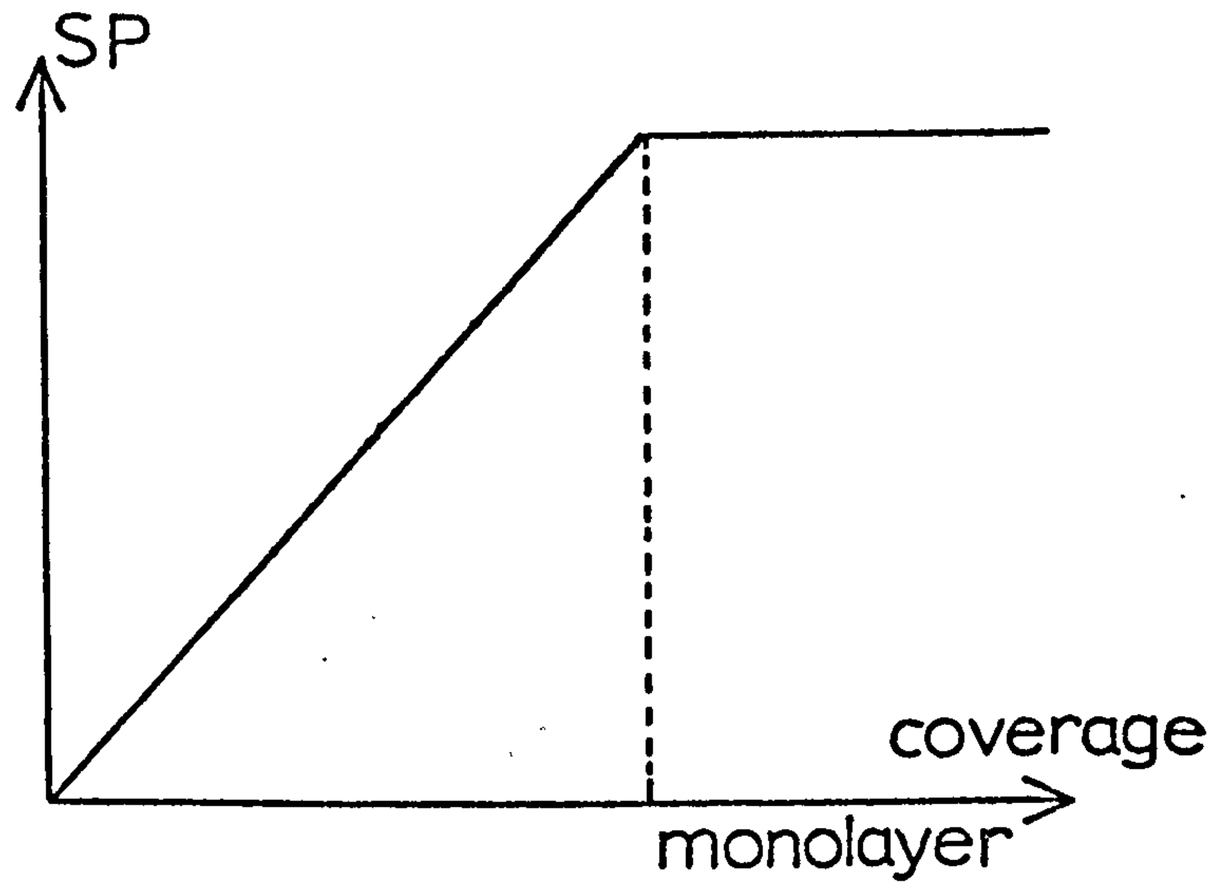

However the dipoles will themselves generate an electric field which causes mutual depolarisation. Attempts have been made to calculate the magnitude of this electric field and to estimate the extent to which depolarisation occurs as a function of coverage, i.e. ad-atom to ad-atom distance. The Topping model referred to in chapter 2 calculates the strength of the field by assuming a geometric array of dipoles and utilising a summation technique. More recently Schram (9) has obtained an alternative expression assuming a continuous sheet of dipoles (i.e. mobile ad-atoms and a simple integration). Both methods anticipate an SP vs coverage graph for physically adsorbed species whose slope monotonically decreases with increased coverage, as for example in fig. 3.13. However neither of these models has

Fig. 3.13

SP vs COVERAGE INCLUDING SIMPLE DEPOLARISATION EFFECT

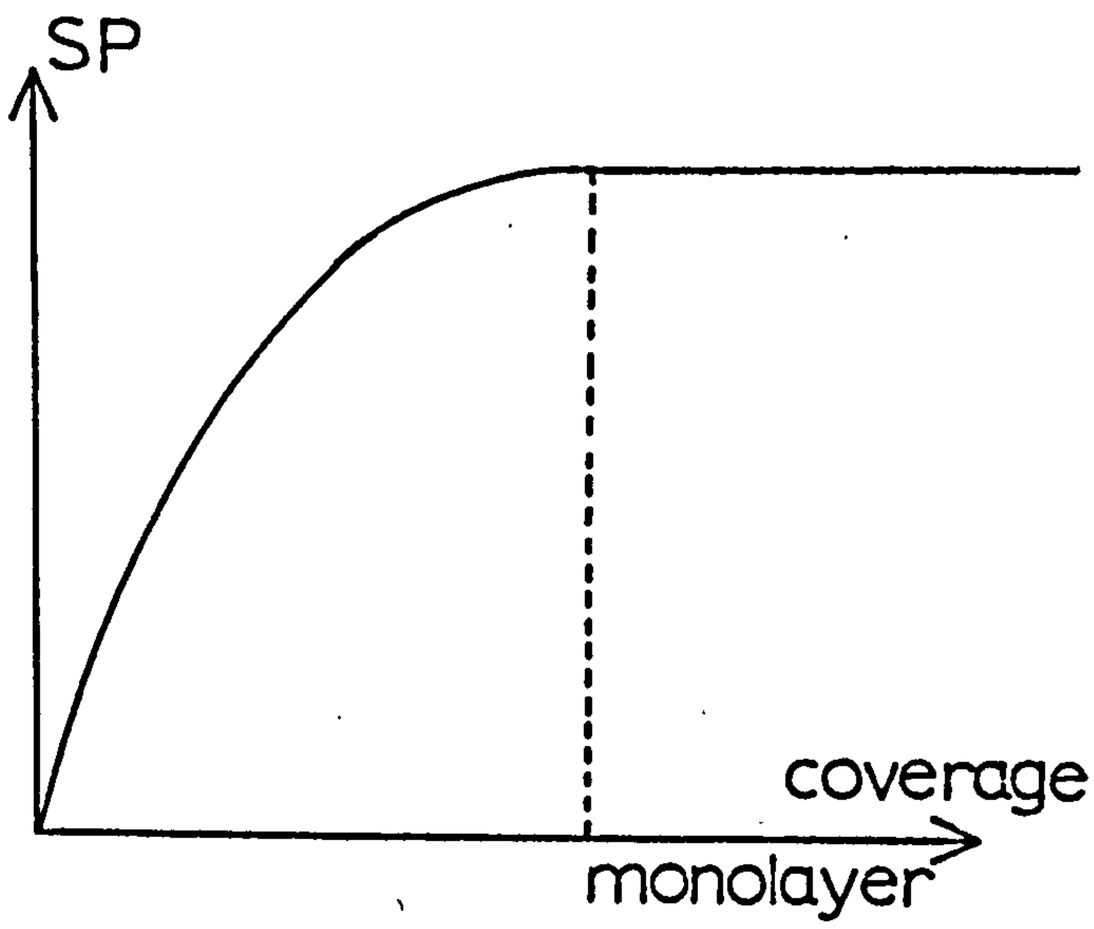

been verified for adsorption on films, and Palmberg's graph (10) illustrating the applicability of the Topping model to the Xe/Pd(100) system is open to reinterpretation. If the first experimental point is deleted from the graph in preference to the last two as implied by Palmberg, the remaining points form an elegant curve rather than the hoped for straight line. Clearly also, the SP vs coverage plots obtained in this study for xenon on gold or silver, as exemplified by figs. 3.2 and 3.5 do not fit either the Schram or Topping model. Neglecting for a moment the change of slope at point Q they much more closely ressemble the form of fig. 3.12, with depolarisation occurring only very near the monolayer. A number of possible explanations of this behaviour have been considered. Both the Schram and Topping models calculate the depolarising field for an isolated 2D array of dipoles and neglect the influence of the metal surface; exploratory calculations were therefore performed to include this perturbing effect. The solid was assumed to consist of a perfectly plane conducting body and the

field due to the dipole image of the adsorbate dipole was calculated. The results indicated that the variation of this field with coverage, i.e. xenon-xenon atom distance, was complex and although it could conceivably contribute to the behaviour observed, it was not felt to present a satisfactory explanation. The calculations did however indicate that both the Schram and Topping models are likely to be only first approximations to the depolarising field in an array of dipoles close to a metal surface.

In the rapidly changing and powerful fields close to the metal surface another effect will be very significant. It is anticipated that the surface electric field will decay in a distance of between 0.5 and 1.5Å from the surface, implying that only the outermost electrons in the large xenon atom are perturbed by the field and that since formally the field outside a double layer is zero, that the atom must penetrate this double layer. The negative charge of the induced dipole will then be closely associated with the electrons of the metal surface and the dipole moment must be regarded as essentially due to the excess charge on the xenon atom. The consequences of such a charge transfer are interesting, for while lateral repulsive interactions of electrostatic origin will remain very strong, varying according to a Z^{-n} law with n now less than 3, the lateral field will have a much reduced depolarising effect on the xenon atoms since it no longer acts in a direction normal to the metal surface. The extent to which mutual depolarisation of the adsorbed layer of inert gas atoms

occurs is therefore expected to be dependent on the nature of the interaction between the ad-atoms and the metal, in particular being sensitive to the magnitude of any charge transfer that may occur. In any system where charge transfer is appreciable very little depolarisation will be expected and it is tentatively suggested that this may be the case for xenon on silver or gold.

3.8

The abrupt change of slope of the SP vs coverage graph (point Q on figs. 3.2, 3.5 and 3.7) has not been reported for other systems. Knapp and Stiddard (2a) also observed the effect on Xe/Ag(pyrex) and the effect is implicit but not discussed in a paper by Ford and Pritchard (2b).

The change in slope implies an abrupt change in the effective induced dipole in the xenon atoms at a particular coverage, strongly correlated with the half monolayer on silver but occurring somewhat earlier on gold. Two models seem able to offer an explanation for this change of dipole moment.

(i) The surface may consist predominantly of two crystal faces with the xenon atoms adsorbing preferentially on one of these and having a different induced dipole on each face (Knapp (4)). An equilibrium will be set up between the xenon atoms adsorbed on each face such that

$$\frac{n_2}{n_1} = k \qquad \text{——————————} (1)$$

where n_1 = no. of adsorbed atoms on face 1

n_2 = no. of adsorbed atoms on face 2

k = equilibrium constant

Until the preferred crystal face is completely covered by xenon, the effective dipole will be given by the mean of the dipoles on each face

$$\sigma_a = \frac{(n_1\sigma_1 + n_2\sigma_2)}{n_1 + n_2} = \frac{(\sigma_1 + k\sigma_2)}{1 + k} \qquad (2)$$

where σ_1 = induced dipole on face 1

σ_2 = induced dipole on face 2

σ_a = apparent induced dipole for Xe atoms adsorbed before point Q .

After the filling of the preferred face is complete, the remaining xenon atoms can only be adsorbed on the second face, and these will have an apparent dipole of σ_2 . There are however several difficulties with this model:

(a) Since the point Q occurred at a substantially fixed coverage, particularly on silver, the model demands that the ratio of the surface areas of the two crystal faces be constant from film to film. In view of the heavy dependence of the film structure on the essentially random nucleation process, such a constant ratio seems to be an unlikely occurrence.

(b) The nature of the nucleation process (section 2) suggests that the formation of two crystal faces in anything like similar amounts is not likely.

(c) If point Q corresponds to the coverage of a crystal face, the effect may be expected to occur with other inert gases on silver or gold, independently of adsorption temperature to a first approximation. The effect was not

observed however for krypton on gold at 77°K. (fig. 3.14).

(d) Recent observations by Pritchard et al (1) suggest that xenon shows negligible crystal face sensitivity on silver:-

Surface:	Surface Potential:
Ag (111)	0.44V
Ag (110)	0.45V
Ag (211)	0.45V

(ii) The second possibility is that a change in the apparent dipole occurs as a consequence of a change in the form of the functions describing interactions between adsorbate atoms, or between adsorbate and surface atoms. Such an abrupt discontinuity might occur if the xenon atoms underwent a 2D phase change. Phase relationships in 2D have been studied extensively in recent years following Onsager's (11) theoretical treatment of 2D disorder ⟶ lattice gas phase transitions, which are predicted to occur near the half monolayer. Well characterised 2D phase transitions have been reported (12) especially for helium (13), xenon (12) and krypton (14) on extoliated graphite and graphite single crystals, and it seems not unreasonable to anticipate that similar transitions may occur on noble metal surfaces. The shape of the adsorption isotherms for xenon on silver and gold (section 3.5) is analogous to that of Thomy and Duval (14) for krypton on graphite, in the region below the critical point for the coexistence of the disordered gas and the second phase and is also analogous to 3D behaviour

in the same region (gas-liquid) (7). Several experiments that were performed in which krypton was adsorbed on gold at 77°K. are interesting inthis context: the results are summarised in section 3.9. They show an isotherm typical of the region above this critical point, and an SP vs coverage plot which consists of a smooth line with no indication of an abrupt discontinuity. It seems therefore that there may be a correlation between the slope of the isotherm and the observation of a discontinuity in the surface potential data, adding support to the tentative assignment of the SP discontinuity to a phase change. The most appropriate candidate for this intermediate phase between disordered gas and monolayer would seem to be a lattice gas since this is expected to occur near half coverage. The existence of such a state in no way implies the formation of an immobile ad-atom structure at 77°K., but simply that an additional term which contains periodic variations has been added to the interaction functions of the adsorbate. At sufficiently low temperatures this may lead to the formation of an immobile phase, but at higher temperatures it would simply increase the lifetime of the xenon atoms in certain positions. At still higher temperatures its effect may be negligible. Confirmation of this phase change hypothesis must await specific heat measurements on this system, but a series of SP vs coverage plots at different temperatures may well prove interesting as may SP vs coverage plots on other systems showing similar isotherms.

3.9 Adsorption of Krypton on Gold

Preliminary measurements were made at 70°K. and indicated a maximum surface potential of approximately 3.25V. No SP vs coverage data were obtained at this temperature.

Surface potential and equilibrium pressure measurements at 77°K. are summarised in fig. 3.14.

Very large corrections were necessary to obtain the number of atoms adsorbed as a result of the high equilibrium

Fig 3.14 SP and EQUILIBRIUM PRESSURE — Kr on Au

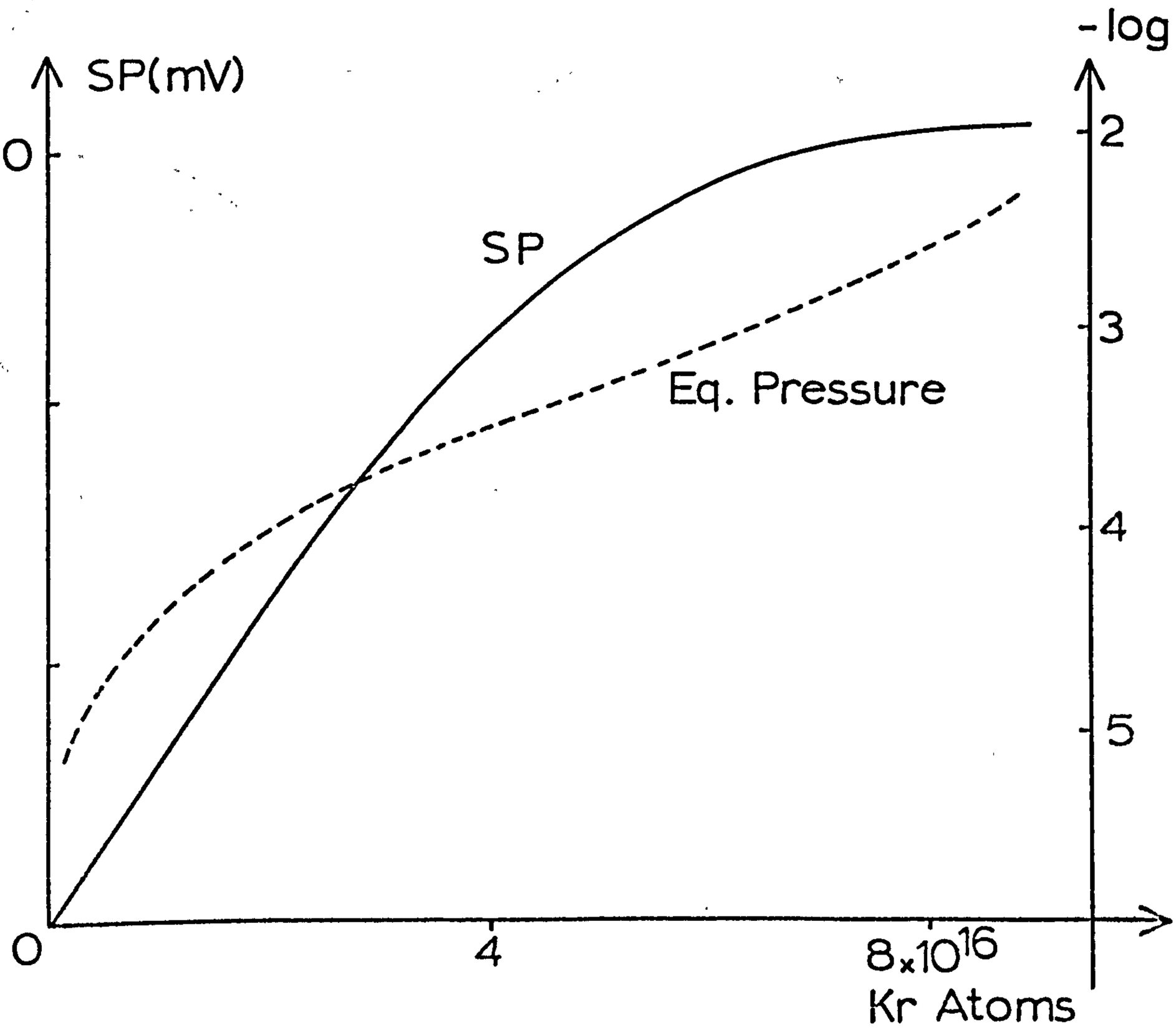

pressure (cf section 3.2(i)) and hence the errors in the recorded values are large. The form of the graphs is probably reasonably accurate however.

Fig 3.15 COMPARISON OF ISOTHERMS and SP vs COVERAGE PLOTS FOR Kr and Xe on GOLD

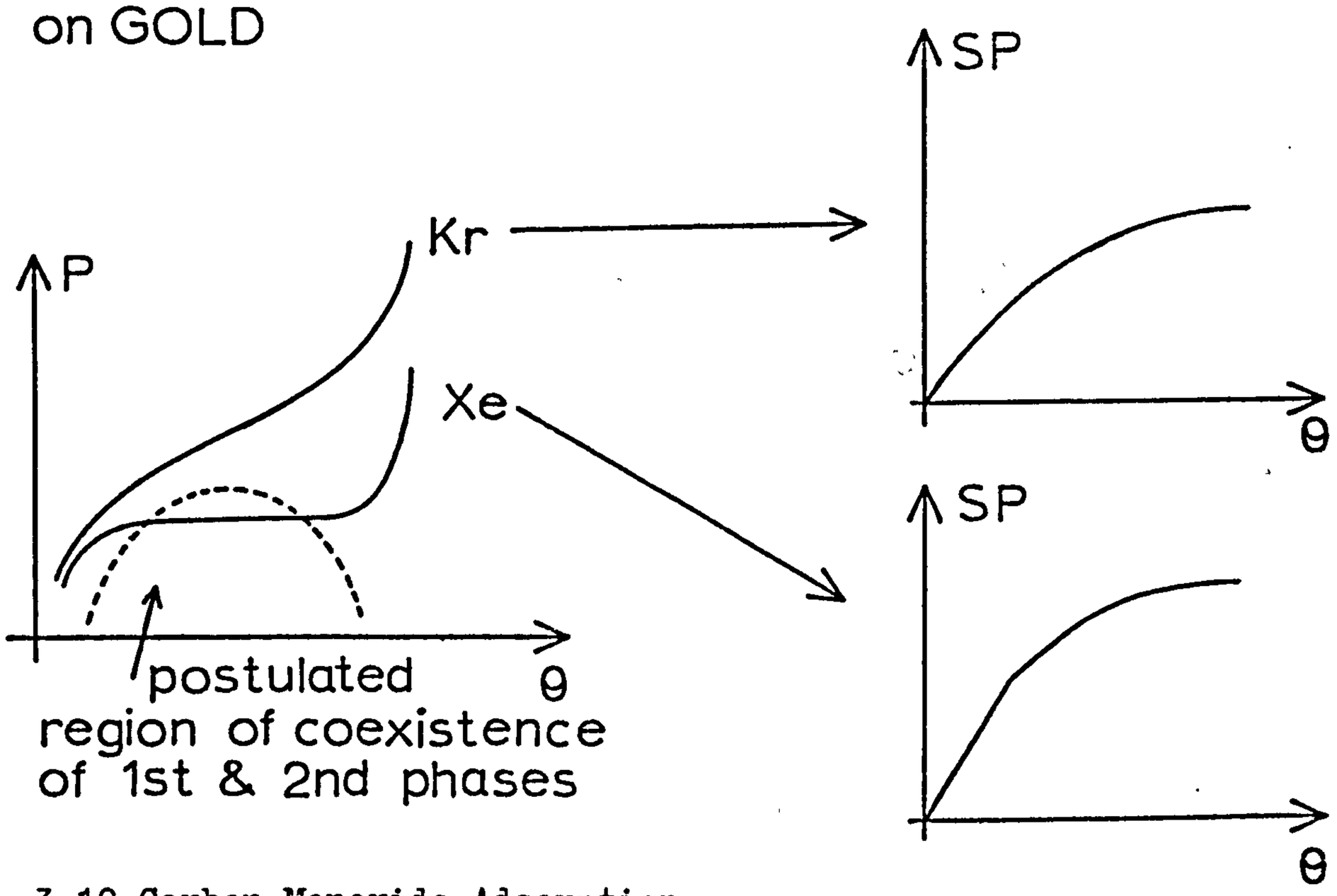

3.10 Carbon Monoxide Adsorption

The adsorption of carbon monoxide was studied on both gold and silver films including silver films evaporated onto pyrex and B37. The results indicated a maximum surface potential of about 460mV on silver and 660mV on gold. The equilibrium pressure of carbon monoxide over the surfaces was very high even at comparitively low coverages while at high coverages addition of further carbon monoxide to the diode resulted in large changes in this equilibrium pressure with little adsorption and only small changes in the surface potential. Large corrections were therefore necessary to

obtain the amount of carbon monoxide adsorbed and in consequence, as for krypton adsorption, the values recorded are not very accurate. In addition the surface potential values almost certainly fell short of the maximum possible at $77^{o}K$. since measurements were not extended to equilibrium pressures above $5x10^{-4}$torr. The maximum surface potentials obtained and the number of carbon monoxide molecules adsorbed (N) are recorded in fig. 3.16 and typical SP and equilibrium pressure vs coverage plots for silver and gold shown in fig. 3.17.

Fig 3.16 SP DATA for CO ADSORPTION

Film No.	Weight (mg)	Substrate	Max. SP (mV)	N ($x10^{-16}$ats.)
Ag 2	5.8	Pyrex	+450	3.4
Ag 5	6.4	B37	+480	3.2
Ag 6	6.15	"	+460	4.0
Au 1	9.2	"	+678	3.0
Au 4	15.0	"	+660	3.1

The maximum surface potentials recorded on both silver and gold films are rather low compared to values in the literature, the values for silver comparing with reported values of approximately 500mV (4)(15) and those for gold with reported values of 736mV (16) and 920mV (17). Such discrepancies may be due to differences in the structure of the films arising as a consequence of the rather low evaporation rates used in this work (section 2.4), or alternatively to contamination

Fig 3.17 CO ADSORPTION

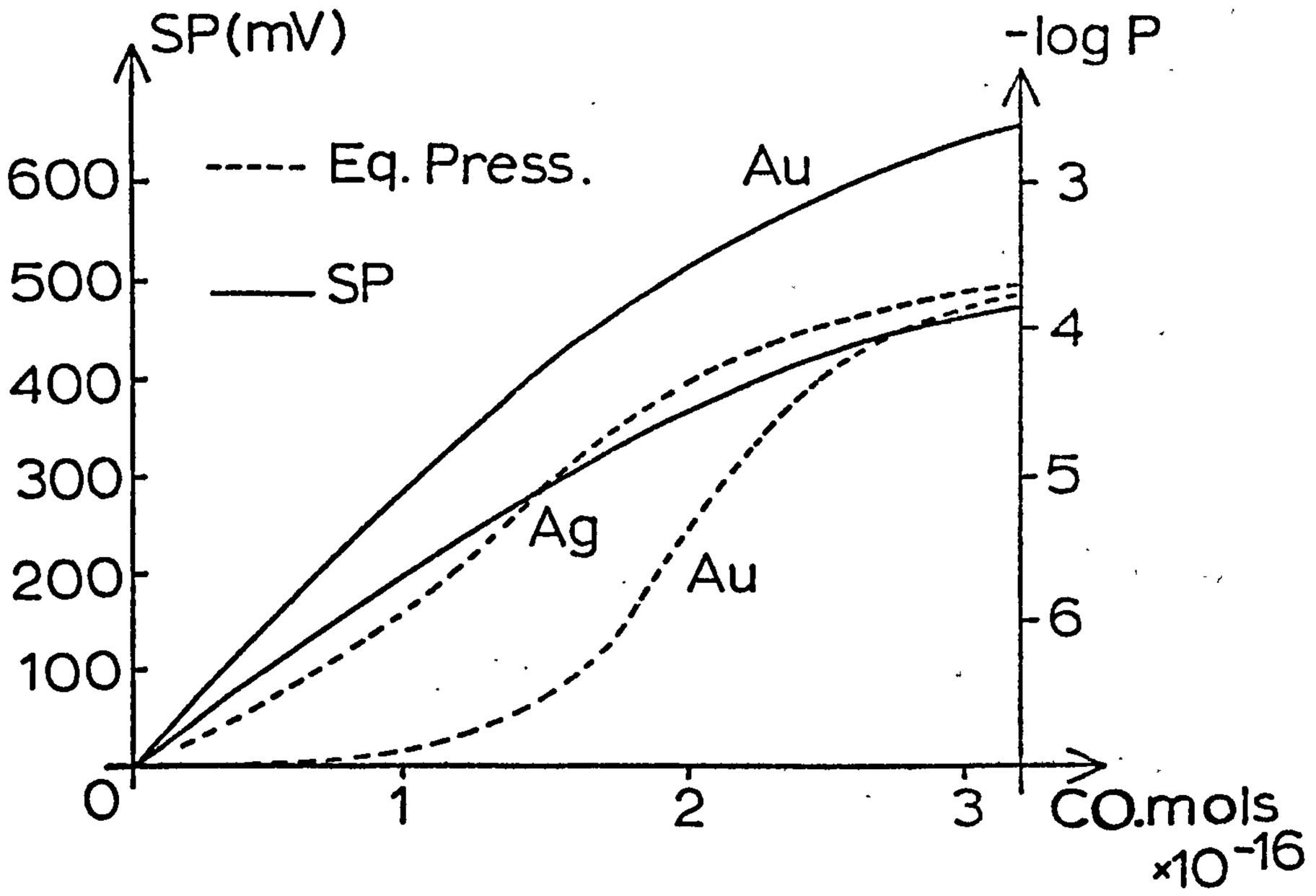

especially by oxygen which is known to reduce the maximum surface potential of carbon monoxide on silver (4). However, oxygen contamination cannot account for the observed result on gold, and in addition both silver and gold films were repeatedly exposed to atomic hydrogen, a procedure which has been shown to remove deliberate oxygen contamination (18). Furthermore xenon and hydrogen (section 3.11) surface potentials on these films compare favourably with literature values.

The large surface potentials recorded for carbon monoxide on silver and gold suggest a quite strong interaction between the adsorbate and the metal surface. Simple calculations indicate that the effects of polarisation of the carbon monoxide molecule plus its permanent dipole are unable to account for the observed surface potential and that some further interaction beyond polarisation must be occurring. However the high equilibrium pressure below maximum coverage

implies just the reverse, suggesting that the carbon monoxide is quite weakly bound. A large proportion of the adsorbed carbon monoxide can in fact be removed from the surface merely by pumping at 77°K.

Quite a simple model can be postulated that offers an explanation of this apparent contradiction. It is widely believed that carbon monoxide may be bound to some metal surfaces in at least two distinct states having different heats of adsorption, surface potentials etc. Evidence for this may be found in flash desorption experiments (19) and from surface potential measurements during carbon monoxide adsorption on copper where the surface potential rises to a maximum value near the half monolayer, and then decreases.(16) (cf 3.11).

It is suggested that adsorption of carbon monoxide on silver and gold similarly involves the formation of two states, one of which is strongly bound to the surface and produces a large surface potential, the other being much more weakly bound and producing at most a small positive surface potential. If we now allow that these are in rapid equilibrium with each other then the system may be represented as follows:

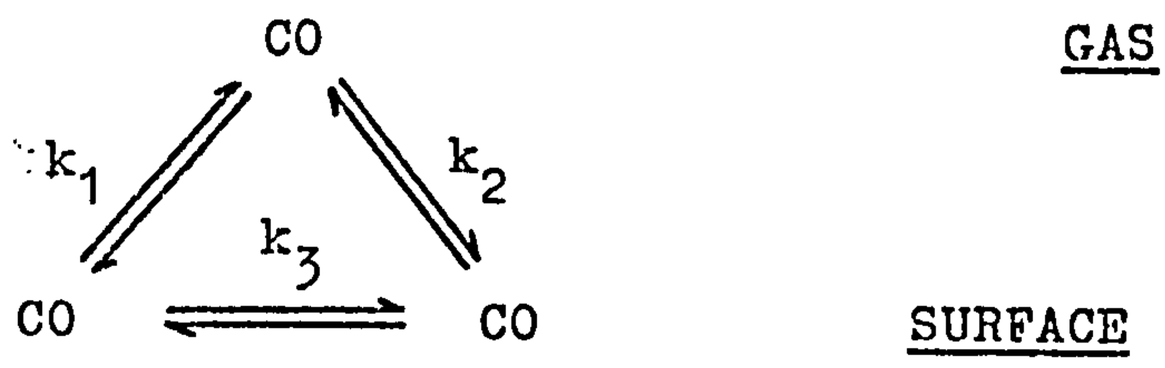

State 1
Strongly bound
High SP

State 2
Weakly bound
Low SP

$$k_1 = \frac{CO(g)}{CO(1)} \ll 1$$

$$k_2 = \frac{CO(g)}{CO(2)} \gg 1$$

Providing that the two adsorbed states are in rapid equilibrium with one another, then regardless of the strength of the bonding between the surface and state (1) the carbon monoxide will appear to be weakly bound to the metal and will be readily removed. Such a system is also consistent with the observed shape of the SP vs coverage curve, producing an effect similar to simple depolarisation as the surface coverage is increased (cf hydrogen adsorption).

3.11 Hydrogen Adsorption

(i) Silver: The adsorption of molecular hydrogen was not observed at either 77°K. or at room temperature. Raising the filament temperature to a value sufficient to produce atomisation of the molecular hydrogen caused initially rapid adsorption to occur on films cooled to 77°K. The variation of this initially high rate of adsorption with coverage is described in chapter 4. The maximum surface potential observed on any given film was substantially constant throughout the life of the film, nevertheless, quite wide variations in maximum surface potential were observed from film to film: mean values for each film are recorded in fig.3.18 together with the number of atoms of hydrogen adsorbed, and for comparison, the number of xenon atoms adsorbed on the same film. Some measurements were also made with deuterium on one film and these are also recorded

in the table. The form of the variation of surface potential with coverage was identical on each film and a typical example is shown in fig. 3.19.

Fig 3.18 SP DATA for H ADSORPTION - Ag

Film No.	Weight (mg)	Substrate	Max. SP (mV)	N_H ($\times 10^{-16}$)	N_{Xe} ($\times 10^{-16}$)
Ag 2	5.8	pyrex	-284	10	7
Ag 3	8.6	"	-320	10.3	7.5
Ag 4	9.4	"	-316	10.2	7.5
Ag 6	6.15	B37	-265(H) -250(D)	9(H_2&D_2)	8.5
Ag 7	6.7	"	-240	8.8	-

Fig 3.19

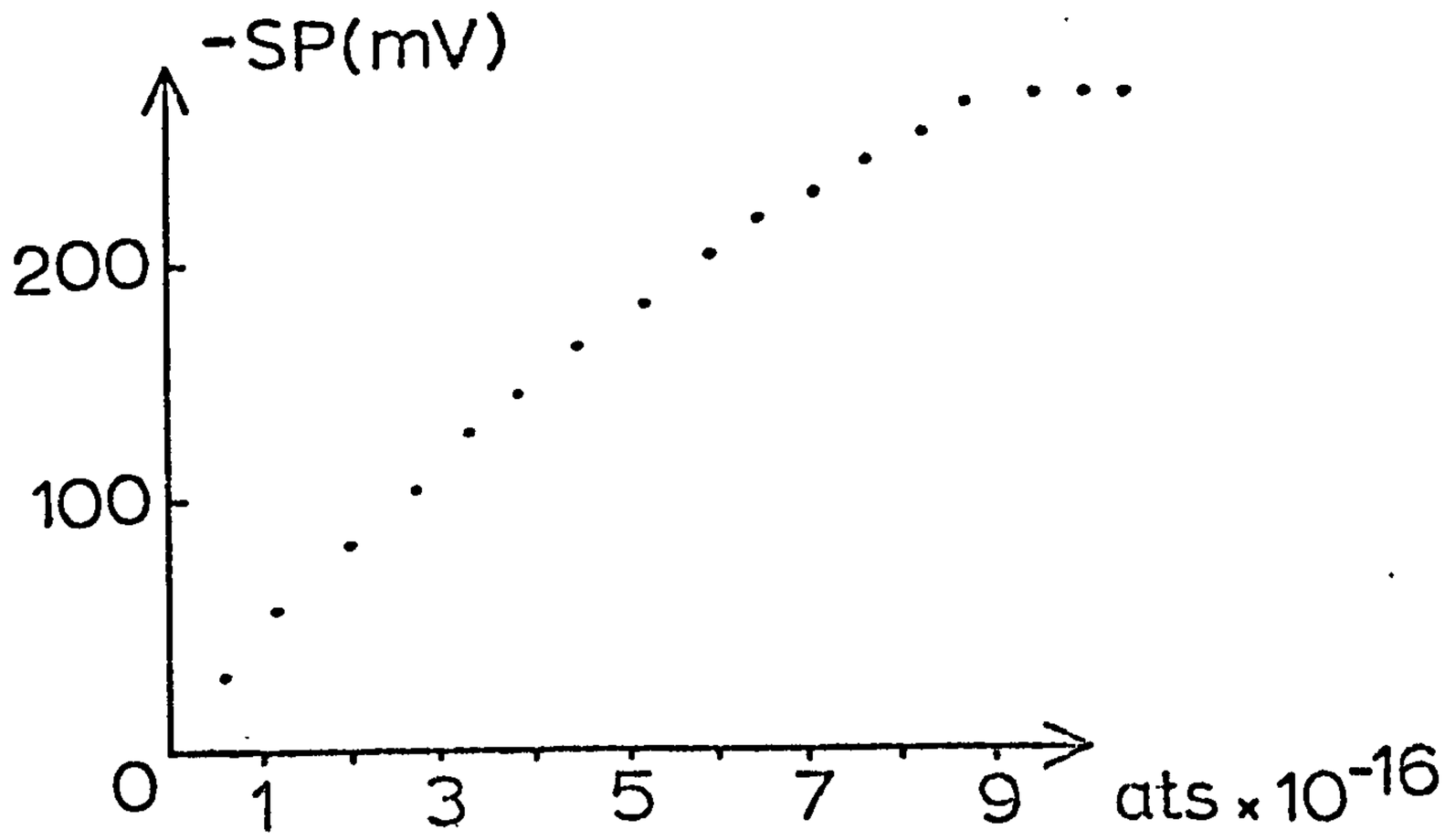

The value of the maximum surface potentials compare favourably with those of Knapp (4) and Pritchard and Tomkins (20), however it is clear that the surface potentials on films evaporated onto B37 substrates are consistently lower than

those evaporated onto pyrex. In view of the discrepancies between the adsorption of xenon on silver/ pyrex and silver/B37, it seems reasonable to attribute this observation to a similar phenomenon, namely that the structure of the films is not precisely identical on the two different substrates and the surface potential of hydrogen atoms on silver is sensitive to this difference.

(ii) Gold: The adsorption of hydrogen atoms on gold, while in many respects similar to that on silver (chapter 4), was marked by quite dissimilar surface potential data. In addition the behaviour differed significantly from that found by Pritchard (16). A typical SP vs coverage plot is shown in fig. 3.20.

Fig 3.20 SP vs COVERAGE — H on Au/B37

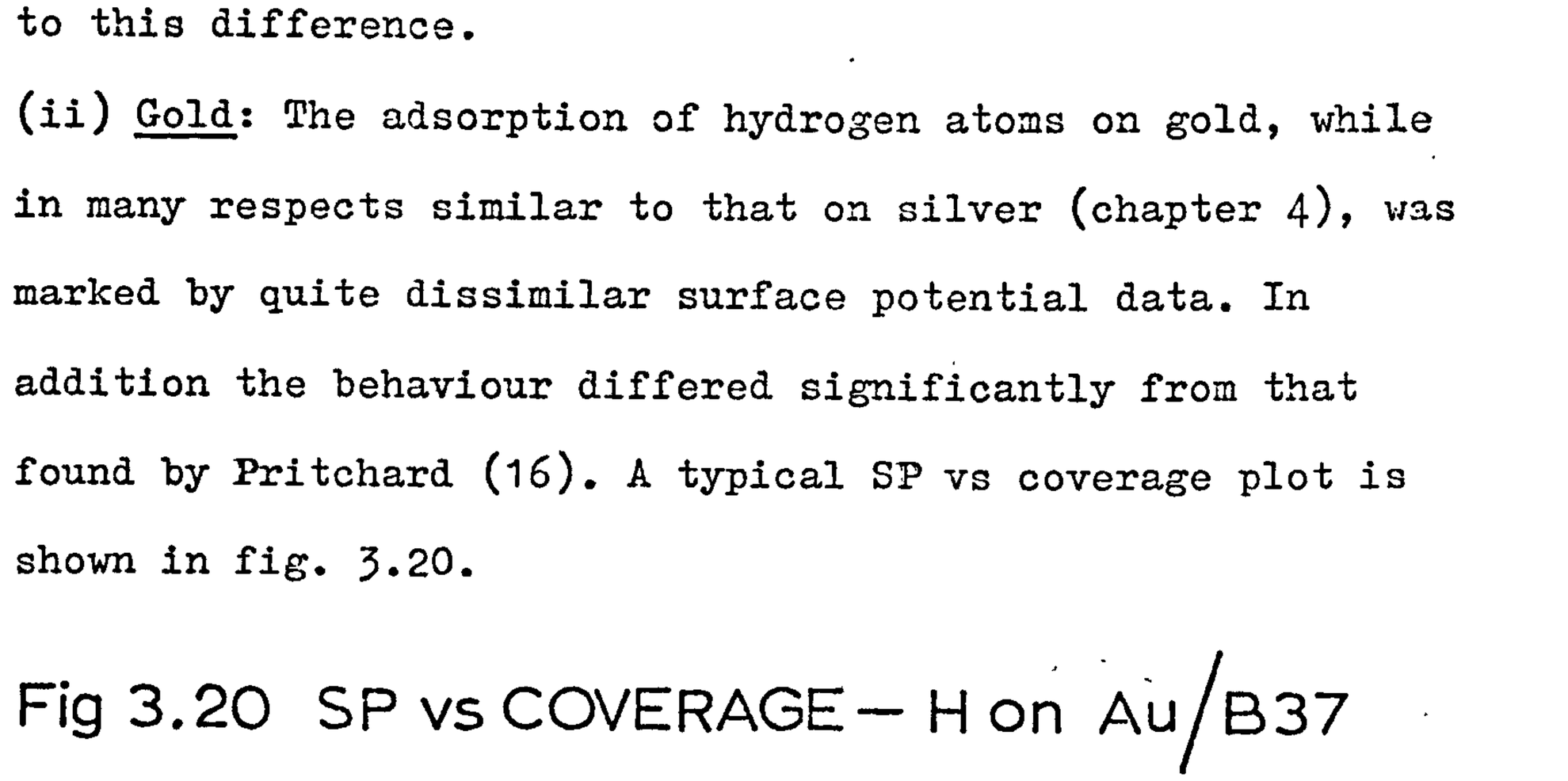

This shows that after reaching a (negative going) maximum at about 3.4×10^{16} atoms, the surface potential decreases, finally reaching a constant value. The total adsorption of hydrogen atoms at this point is less than that of hydrogen atoms on

silver. Surface potential data in the form of the coordinates of X and Y in fig. 3.20 are given in fig. 3.21 for a number of gold films.

Fig 3.21 SP DATA for H ADSORPTION–Au / B37

Film No.	Weight (mg)	X SP (mV)	X N ($\times10^{-16}$ats)	Y SP (mV)	Y N ($\times10^{-16}$ats)	N_{Xe} ($\times10^{-16}$ats)
Au 1	9.2	- 98	2.9	-72	6.4	6.5
Au 2	11.2	-104	3.6	-72	7.0	7.0
Au 3	11.5	- 90	3.4	-64	6.0	7.0
Au 4	15.0	- 92	3.0	-60	6.4	6.5

The equilibrium pressure of hydrogen measured by the pirani gauge first became significant shortly after the adsorption of an amount of hydrogen equivalent to point X . Any hydrogen added after this stage could be removed by pumping at 77°K., producing a smooth increase in surface potential until a value close to that of point X was reattained, after a few minutes pumping.

An additional effect was also noted to occur near X . During the adsorption of the two or three doses following point X , when the surface potential was decreasing towards its final value at Y , the surface potential would decrease rapidly (by about 6 to 10mV) immediately after the adsorption of the dose commenced, and then rise slowly to the recorded value (approximately 3mV higher). The overall effect is shown diagramatically in fig. 3.22.

Fig 3.22

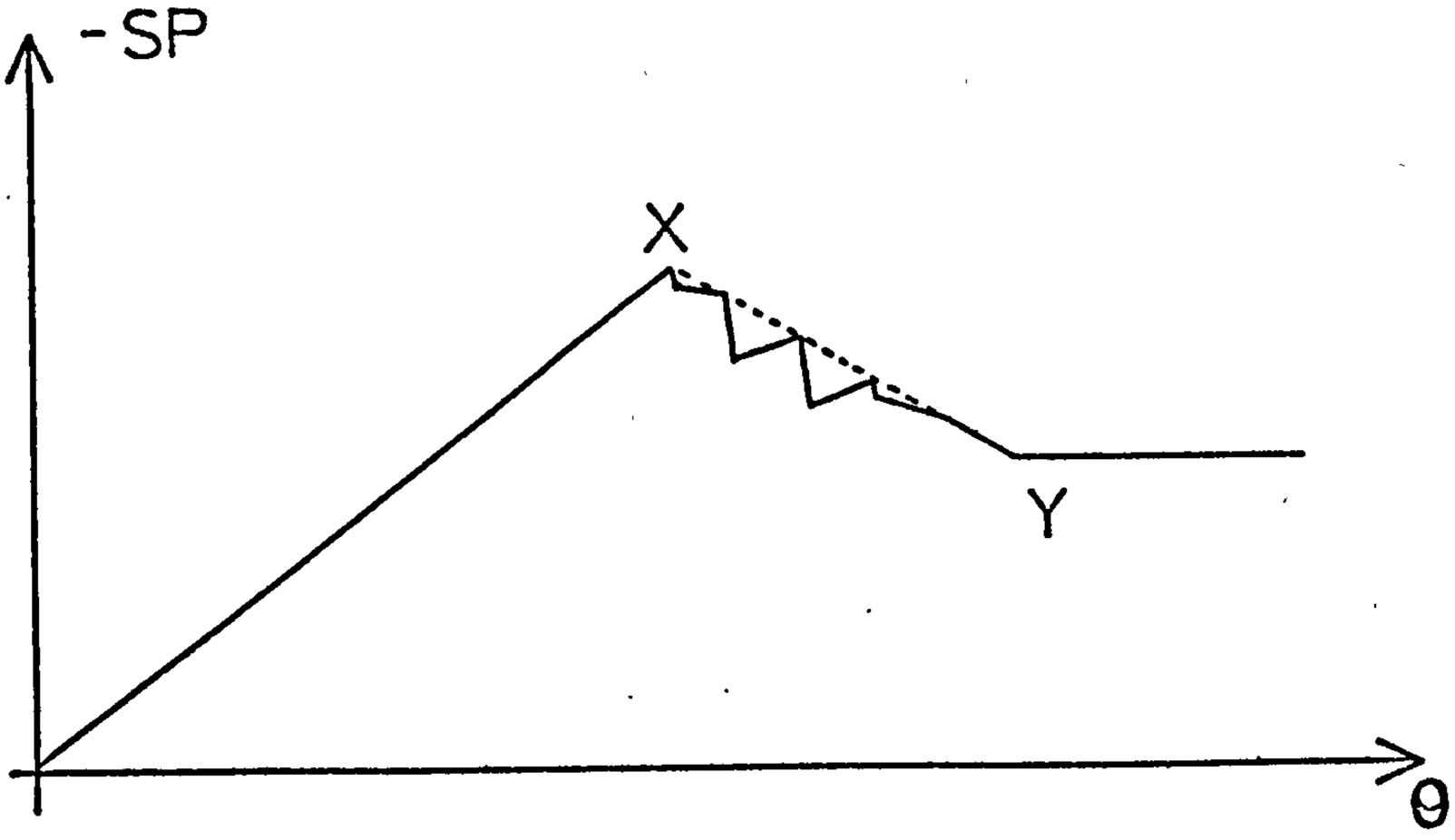

Horinto and Toya (21) have discussed the chemisorption of hydrogen atoms on metal surfaces and conclude that two types of adsorption state are possible which they term r and s . r ad-atoms are bonded to the surface directly above the metal surface atom but outside the electron cloud of the adsorbant metal, and result in a negative surface potential while s ad-atoms are partially embedded in the electron cloud between metal atoms and produce a positive surface potential. The implication of the experimental results on gold seems to be that at low coverages type r adsorption predominates and that this gives way at higher coverages to type s . It is possible that some form of equilibration occurs between the two states r and s which causes the observed "overshoot" behaviour.

The reduction in the slope of the SP vs θ curve for hydrogen on silver at high coverages perhaps indicates the

emergence of this type of behaviour on silver.

3.12 Mixed Gases

The experiments described in chapter 4 involved the sequential addition of gases to the surface, xenon or carbon monoxide followed by hydrogen. The surface potential data collected during these experiments are presented in this section, being summarised for silver in figs. 3.23, xenon followed by hydrogen, and 3.24, carbon monoxide followed by hydrogen.

Fig 3.23

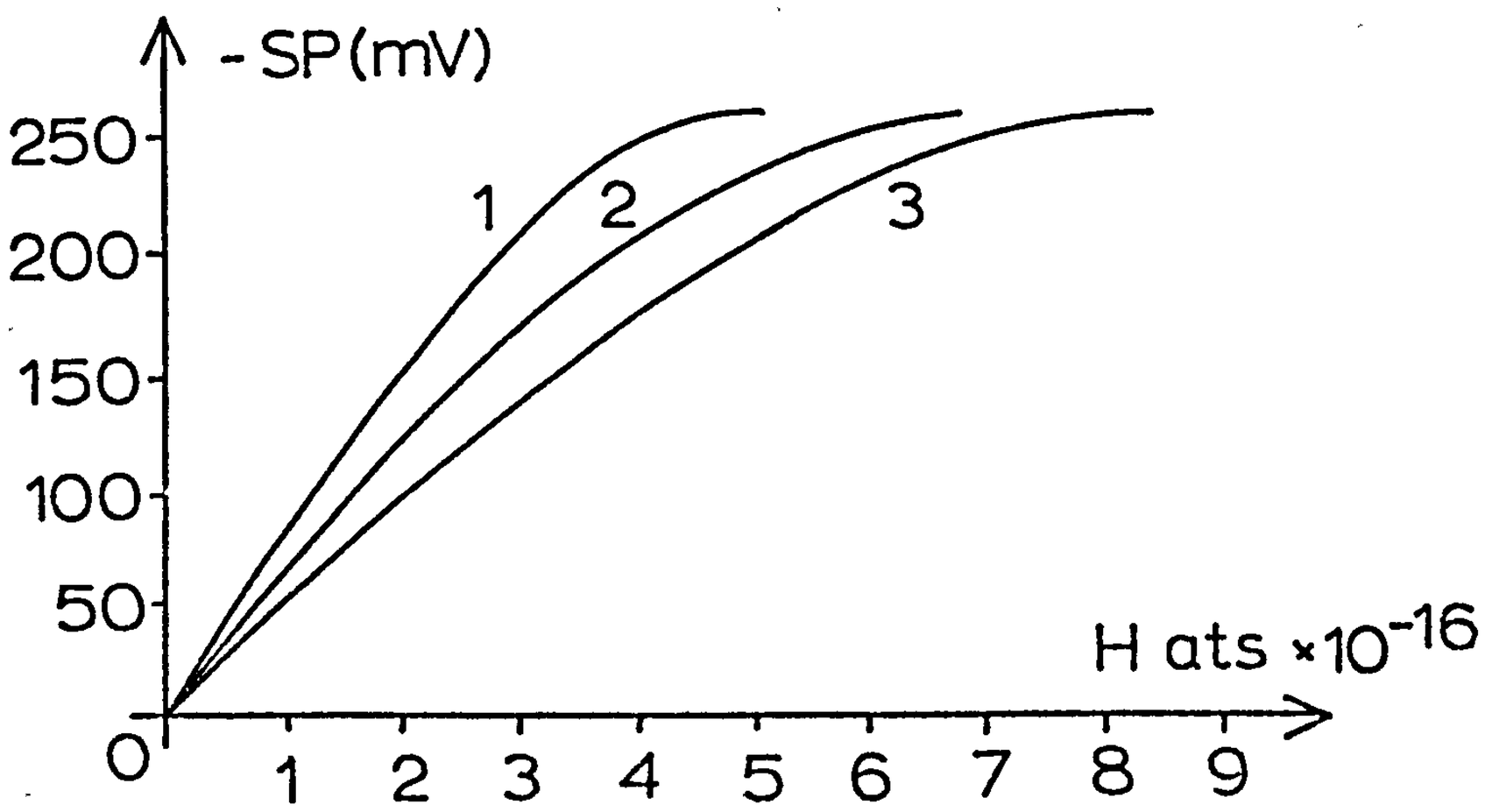

SP vs COVERAGE for 1) clean silver film
2) half monolayer Xe
3) full coverage Xe

Figs. 3.23 and 3.24 show results obtained on film six. A substantially identical effect was observed on every film studied. The maximum surface potential was found to be independent of the presence of pre-adsorbed xenon; the number of adsorbed hydrogen atoms fell by about 40% however, on a film plus xenon monolayer. The interaction

between the hydrogen and xenon on the surface must therefore lead to either a decrease in the xenon dipole or to an increase in the metal-hydrogen dipole.

Fig 3.24

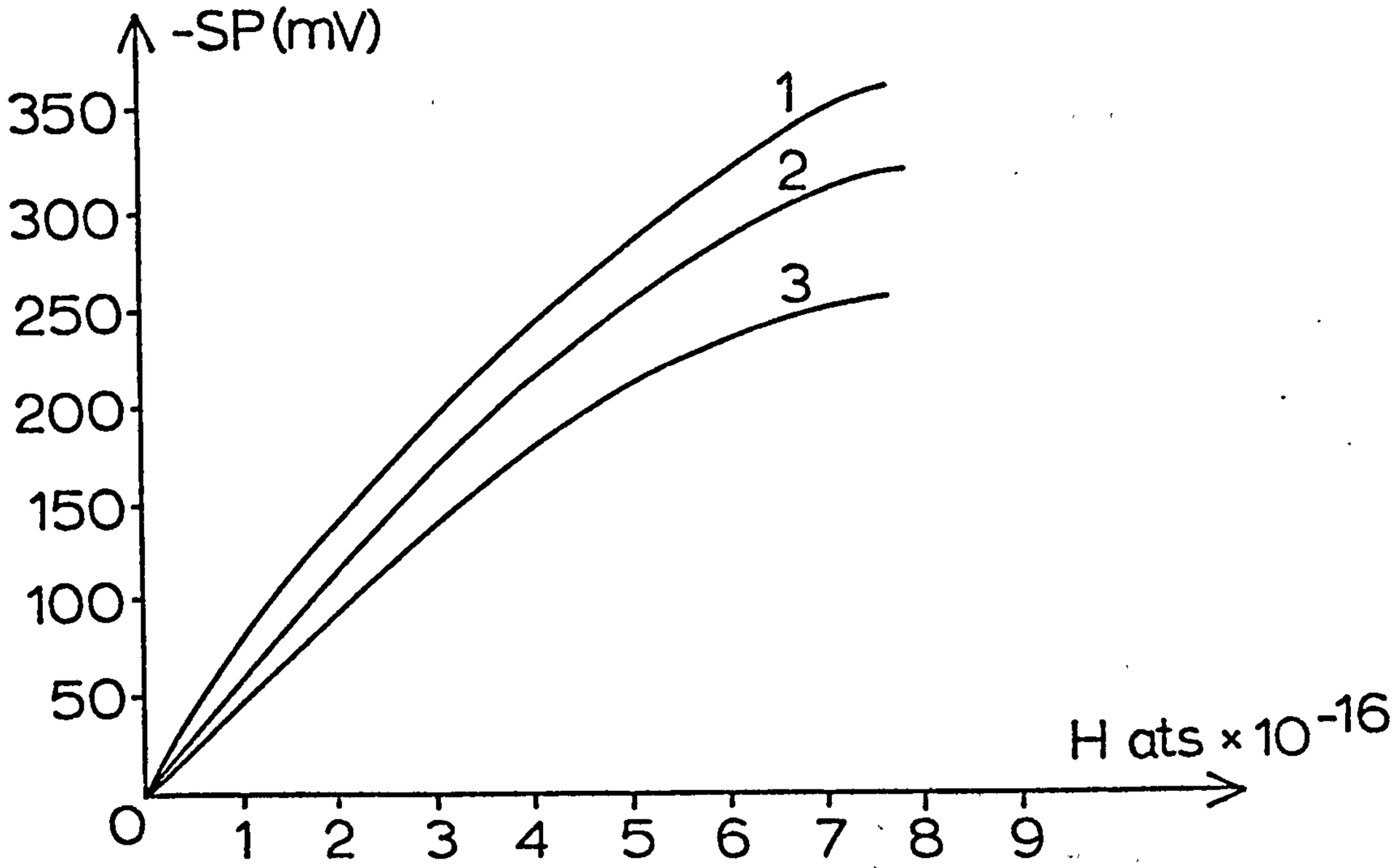

SP vs H COVERAGE for 1) full coverage CO
2) half coverage CO
3) clean silver film

In the presence of pre-adsorbed CO a different behaviour is observed (fig. 3.24). While the number of hydrogen atoms adsorbed remains constant i.e. is independent of the presence of CO on the surface, the hydrogen surface potential changes markedly, rising by some 30% on a film plus a full coverage of carbon monoxide. Interestingly, the interaction has again led to an apparent increase in the hydrogen-metal dipole.

The situation on gold films is less clear and requires further investigation. As on silver films the effect of pre-adsorbed xenon was to cause a progressive reduction in the number of hydrogen atoms adsorbed. This appeared to occur entirely at the expense of those hydrogen atoms which cause the surface potential to decrease at high coverages (between X and Y, fig 3.20) so that at high coverages of xenon the hydrogen surface potential rose smoothly to a value near that of X. Further addition of hydrogen produced little adsorption and no further change in surface potential. Again as on silver, pre-adsorbed carbon monoxide did not significantly alter the number of hydrogen atoms adsorbed, but the surface potential due to these atoms was markedly reduced. In addition, the surface potential continued to drift upward by a total of a few mV for some sixty seconds after the pressure change accompanying adsorption had ceased. The "overshoot" effect (fig. 3.22) and the overall decrease in surface potential at high hydrogen coverages were both suppressed when a large number of carbon monoxide molecules are adsorbed on the gold surface.

3.13 Summary

Some differences have been observed in the properties of films deposited on pyrex and B37 glass substrates, which are attributed to variations in their structure. The behaviour of xenon, hydrogen and carbon monoxide has been observed on these films and some simple models proposed to describe the observations. Subtle and complex interactions have been observed between xenon or carbon monoxide and hydrogen adsorbed

onto silver and gold surfaces.

Although the overall behaviour of the films was always found to be reproducible, variations in points of detail were found to occur from film to film, particularly in the case of gold. It was felt that these variations arose from the sensitivity of the adsorption processes studied towards the detailed structure of the film, which it is believed is a function of the conditions during film deposition. While these were controlled as far as was practicable, dissimilarities inevitably occur in the glass substrates, and the effect of these on adsorption processes was felt to be significant.

References

(1) M.A.Chesters, M.Hussain and J.Pritchard:
Surface Sci. 35, 161,(1973)

(2) a) A.G.Knapp and M.H.B.Stiddard:
J. Chem. Soc. Faraday Trans. I. 68, 2139, (1972)

b) R.R.Ford and J.Pritchard:
Trans. Faraday Soc. 67, 216, (1971)

c) B.E.Nieuwenhuys, R.Bouwman, and W.M.H.Sachtler:
Thin Solid Films 21, 51, (1974)

(3) J.Pritchard: Nature 194, 38, (1962)

(4) A.G.Knapp: PhD Thesis U.of London (1971)

(5) S.Brunauer, L.S.Deming, W.E.Deming and E.Teller:
J. Am. Chem. Soc. 62, 1723, (1940)

(6) J.Suzanne, J.P.Coulomb et M. Bienfait:
Surface Sci. 44, 141, (1974)

(7) Glasstone and Lewis: Elements of Physical Chemistry, Macmillan, London, p118, (1946)

(8) M.J.Dresser, T.E.Madey, and J.T.Yates Jr. : Surface Sci. 42, 533, (1974)

(9) A.Schram: Adsorption Desorption Phenomena, Ed. F.Ricca Academic Press, London, p57, (1971)

(10) P.W.Palmberg: Surface Sci. 25, 598, (1971)

(11) L.Onsager: Phys. Rev. 65, 117, (1944)

(12) J.J.Lander and J.Morrison: Surface Sci. 6, 1, (1967)

(13) R.J.Rollefson: Phys.Rev.Letters, 29, 410, (1972)

(14) A.Thomy and X.Duval: Colloq. Int. Centre Nat. Rech. Sci. 152, 81.

(15) A.M.Bradshaw and J.Pritchard: Proc. Roy. Soc. A316, 169, (1970)

(16) J.Pritchard: Trans. Faraday Soc. 59, 437, (1963)

(17) R.V.Culver and F.C.Tomkins: Advan. Catal. 11, 67, (1959)

(18) Blogaert, D'Or and Mignolet: J. Chim. Physique, 54, 74, (1957)

(19) a) P.Hirst: Private Comm.
b) C.S.Goymour and D.A. King: Surface Sci. 35, 246, (1973)

(20) J.Pritchard and F.C.Tomkins: Trans. Faraday Soc. 56, 540, (1960)

(21) J.Horiuti and T.Toya: Solid State Surface Sci. 1, 1,(1969)

Chapter 4

Rates of Adsorption

4.1

The adsorption of individual gases on clean metal surfaces has been quite extensively studied. However it is only in recent years that there has been a similar interest in the interaction between gases co-adsorbed on such surfaces. The co-adsorption of oxygen and carbon monoxide on silver has been studied by Engelhardt et al (1) and other authors have also reported work on this system (2)(3). Knapp and Stiddard have studied the interaction between xenon and pre-adsorbed hydrogen on a silver surface (4). Other systems studied in recent years include oxygen and carbon monoxide on tungsten (5), oxygen and xenon on tungsten (6) and hydrogen and carbon monoxide on nickel (7).

The experiments described in this chapter were performed to investigate the rates at which gases are adsorbed onto gold and silver surfaces as a function of coverage. Results will be reported for xenon and hydrogen individually, but the primary interest lay with the subtle interaction between hydrogen atoms and pre-adsorbed xenon or carbon monoxide that was revealed by these measurements. The effect of the interaction on the surface potential of hydrogen has been reported in section 3.12.

4.2

The rate of adsorption data were obtained by a static technique as has been outlined in section 1.15. After the addition of each small dose of gas to the UHV section, the

change in pressure as adsorption proceeded was followed either using the fast response pirani gauge (xenon and hydrogen) or the ion gauge (xenon only). The geometry of the diode cell is quite well suited to this type of measurement. Since xenon is mobile when adsorbed at 77°K. its rate of adsorption is relatively insensitive to the cell geometry, however hydrogen atoms are substantially immobile and must be supplied to the film at a rate which is uniform over its entire surface. This requirement is elegantly met in the spherical diode cell where the hydrogen atoms are produced by thermal dissociation at a centrally mounted filament.

Preliminary measurements indicated that the rate of adsorption of xenon and hydrogen was high and the fast response pirani gauge (section 1.6) was therefore constructed. The response rate of the whole system, comprising the gauge, its control unit, amplifier and chart recorder, the conductance of the tubing connecting gauge and diode cell, and the automatic filament temperature stabiliser (section 1.9) was tested in pressure-jump experiments, and permissible maxima established for rates of pressure change during measurements.

4.3 Rates of Xenon Adsorption

The rate of adsorption of xenon was found to be substantially independent of coverage on both silver and gold films, except near the monolayer. In the pressure range 5×10^{-7} to 4×10^{-4}torr plots of log P vs time for each dose were found to give straight lines.

A check was made at this stage of the conductance of the

tubing between the gauge and diode cell. The conductance (Q) of a tube is given by : (8)

$$Q = (2.3 \times 10^{21} \times d^3 . \Delta P) \Big/ (M^{\frac{1}{2}} . l) \qquad (1)$$

where d = tube diameter

l = tube length

M = molecular weight of gas

ΔP = pressure difference across the length of tube.

If ΔP is in torr and l and d are in cm., then Q will be in atoms.seconds^{-1}.

For xenon, M = 131.3 and l and d were estimated to be approximately 25cm. and 1cm. respectively. The highest rate of flow of gas, limited only by the conductance of the tubing, will occur if the pressure in the diode is zero when that indicated by the gauge was the maximum recorded xenon pressure. The value of ΔP in equation (1) was therefore put at 4×10^{-4}torr.

Hence $\underline{Q = 5 \times 10^{15} \text{atoms.sec.}^{-1}}$.

At 4×10^{-4}torr the rate of decrease of pressure at the ion gauge was 5×10^{-6}torr.sec.$^{-1}$ which, assuming a gauge volume of approximately 100cm^3, implies that xenon is leaving the gauge at a rate of approximately 2×10^{13}atoms.sec.$^{-1}$

It is therefore very unlikely that at any time the rate of adsorption is limited by the conductance of the tubing. Exactly analogous calculations were later performed for hydrogen and these prompted the same conclusion for that gas.

4.4 Rate of Hydrogen Adsorption

Investigations by several authors (9) have established that the rate of production of hydrogen atoms (R_H) at an incandescent tungsten filament may be expressed in the form:

$$R_H = K_n P^n \text{ atoms.sec.}^{-1} \qquad (2)$$

where P = pressure of hydrogen

n = 1 or $\frac{1}{2}$, dependent on the value of P and the filament temperature

K = constant, function of n, the filament temperature and its dimensions

and hence if the sticking coefficient for hydrogen atoms on the surface is s , then the rate of change of pressure during adsorption will be given by:

$$-\frac{dP}{dt} = sK_n P^n \qquad (3)$$

During the addition of a small dose of gas to the surface, the sticking coefficient will remain sensibly constant and hence equation (3) may be integrated to give:

$n = \frac{1}{2}$ $$2(P_o^{\frac{1}{2}} - P^{\frac{1}{2}}) = sK_{\frac{1}{2}}t \qquad (4)$$

$n = 1$ $$2.303(\log_{10}P_o - \log_{10}P) = sK_1 t \qquad (5)$$

It was found experimentally that plots of $\log_{10}P$ against t gave excellent straight lines at pressures of less than 10^{-4}torr and consequently this pressure was not exceeded during measurements. Some examples of those plots for a silver film are shown in fig. 4.1. Values of sK_1 were obtained from the slopes of these graphs and were plotted

against the number of adsorbed hydrogen atoms.

Fig. 4.1 LOG P vs t for H ADSORPTION

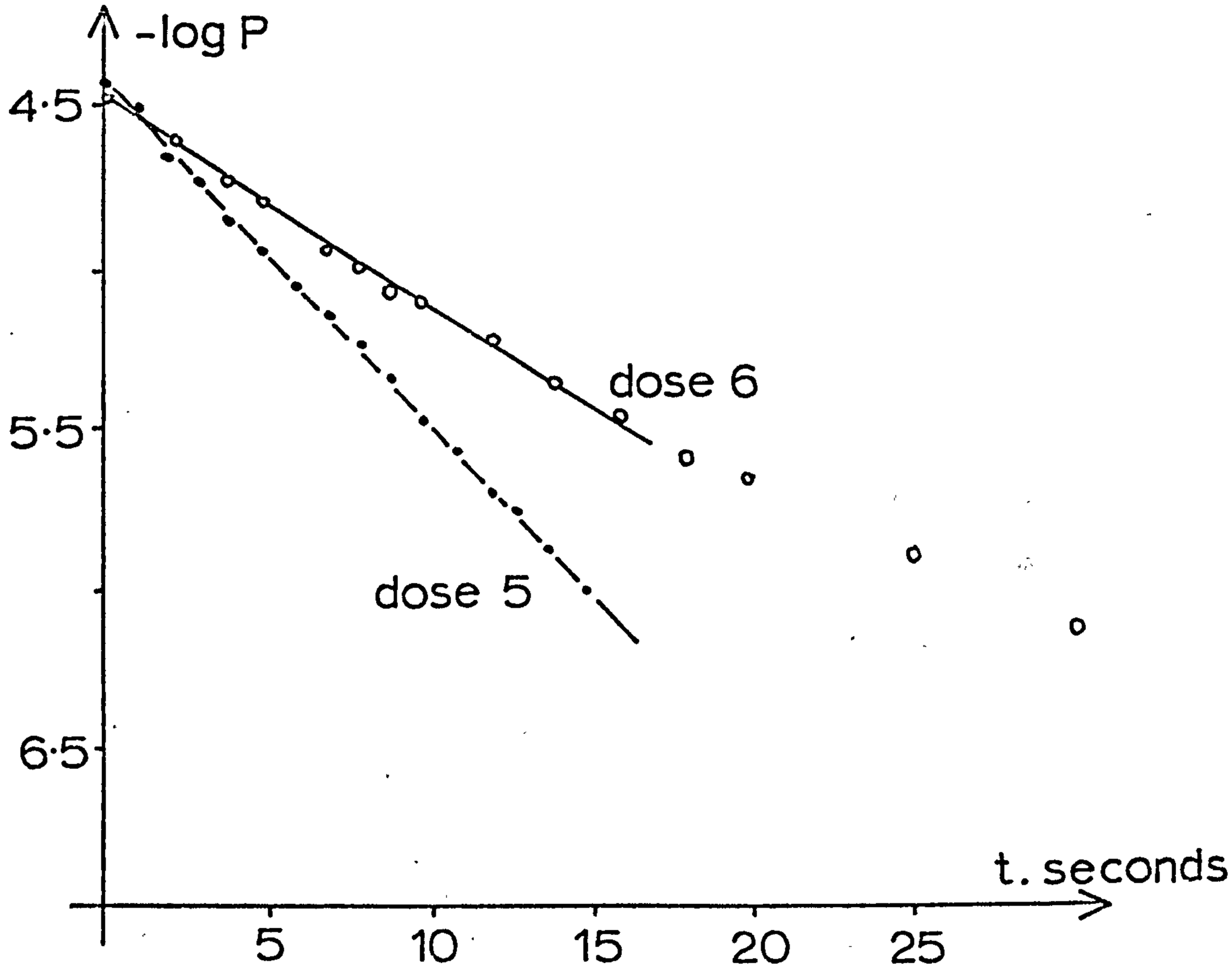

Fig. 4.2 shows how the value of sK_1 fell linearly with increasing hydrogen coverage, reflecting a linear decrease in sticking coefficient. Essentially similar results were obtained for both silver and gold films. At high coverage the sticking coefficient fell to a nearly constant value corresponding to a very low rate of uptake of hydrogen, which however was not accompanied by any change in surface potential. Quite large amounts of hydrogen were involved in this slow uptake which is believed to be due to a slow

Fig. 4.2 sK_1 vs HYDROGEN COVERAGE

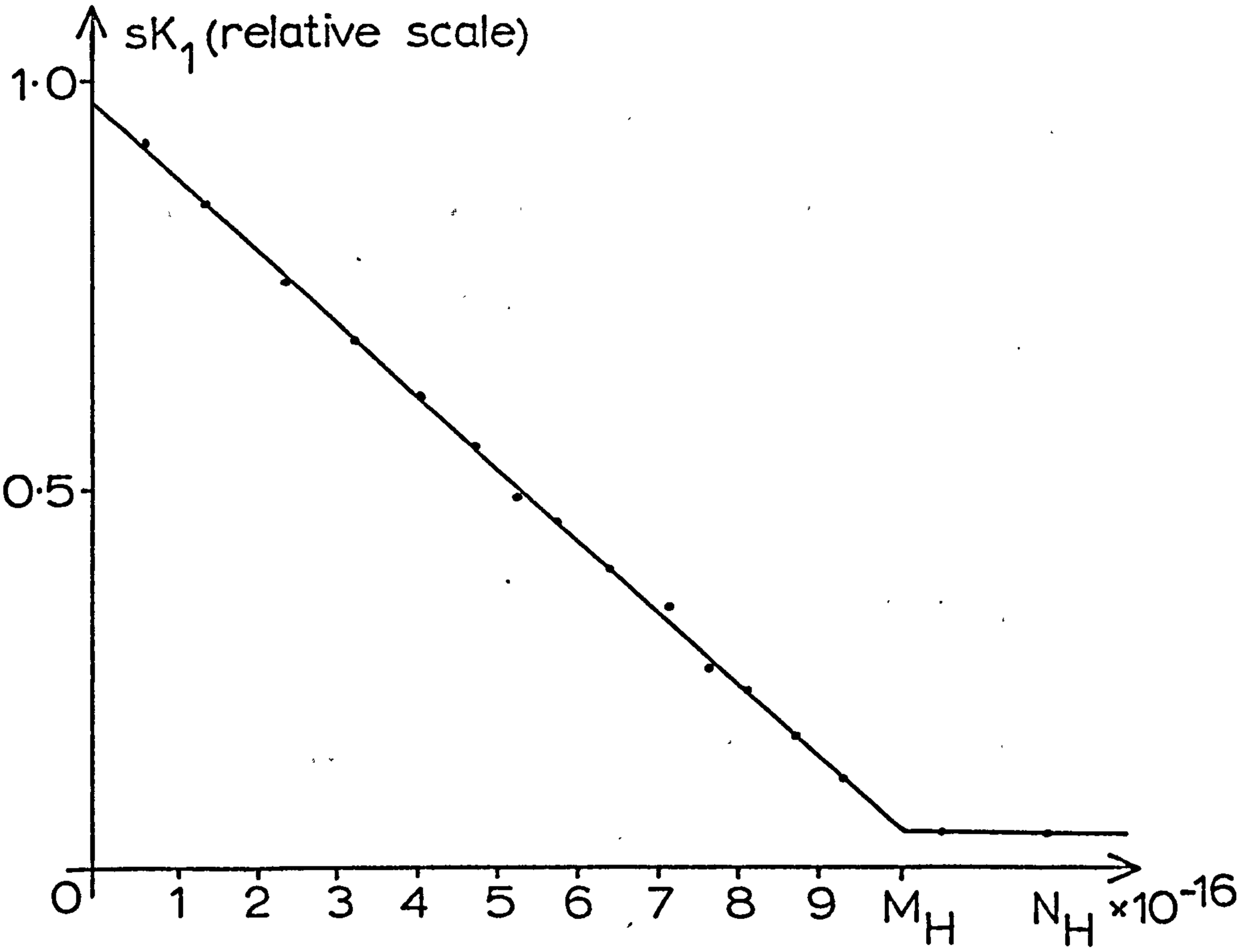

diffusion of hydrogen into the bulk metal of the film. Neglecting this final slow uptake, the form of the variation in the sticking coefficient may be described by:

$$s(N_H) = s_o\left(1 - \frac{N_H}{M_H}\right) \qquad (6)$$

where s_o = sticking coefficient for the clean film

N_H = number of adsorbed hydrogen atoms

M_H = maximum number of adsorbed hydrogen atoms (fig. 4.2)

4.5 Hydrogen plus Pre-adsorbed Xenon - Results.

The adsorption of hydrogen on silver films covered with N_{Xe}

pre-adsorbed xenon atoms produced graphs of sK_1 vs N_H typified by fig. 4.3

Fig. 4.3 THE RATE OF H ADSORPTION AS A FUNCTION OF N_H AND XENON PRE-ADSORPTION

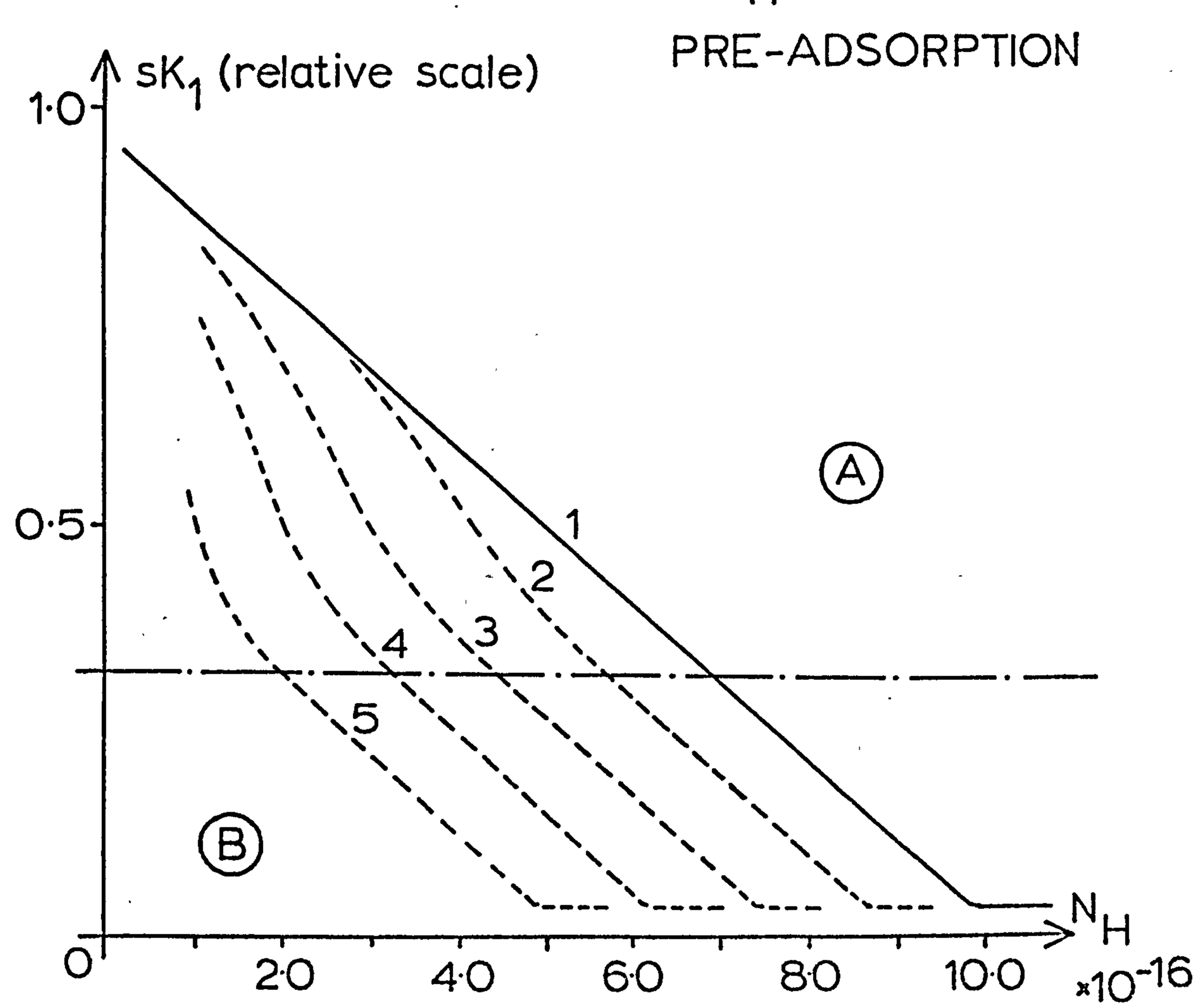

1 rate of hydrogen adsorption on an initially clean film

2 ¼ xenon coverage

3 ½ xenon coverage

4 ¾ xenon coverage

5 xenon monolayer

The effect of the pre-adsorbed xenon was to reduce the rate

of adsorption of hydrogen atoms. In the region of the graph marked **B** the plots of sK_1 vs N_H for different amounts of pre-adsorbed xenon tended quite accurately, particularly at high xenon coverage, to a family of parallel straight lines as shown. Also in this region the reduction in sK_1 at constant N_H was found to be proportional to N_{Xe} as is shown by

fig. 4.4

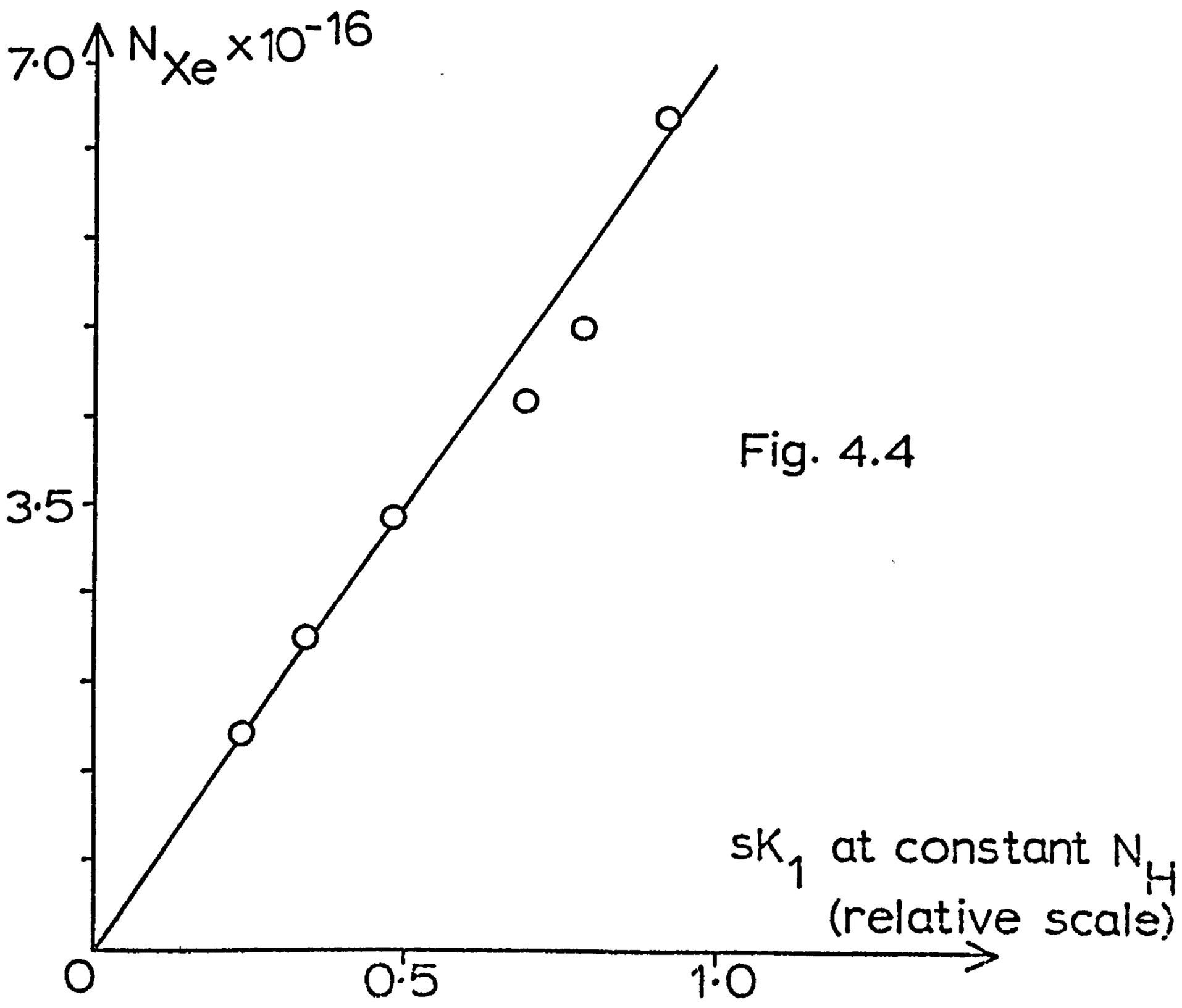

Fig. 4.4

The slope of this line varied slightly from film to film.

The maximum number of hydrogen atoms adsorbed was reduced by an amount proportional to N_{Xe} culminating for a film plus a monolayer of xenon in a reduction of 40-50% M_H. The area of the graph marked **A** appears to be a region of transition between the behaviour towards hydrogen of a clean

film, and that of a film plus pre-adsorbed xenon. The form of the graphs implies that the adsorption of the first few atoms of hydrogen occurs at a rate which is close to that of the clean film and independent of xenon coverage, while the rate for succeeding doses falls rapidly, particularly at high N_{Xe}, until region B behaviour is attained. The onset of region B behaviour for a film plus a monolayer of xenon occured at approximately 20-30% M_H and at proportionally higher $\%M_H$ for lower coverages of xenon. There was some small variation in the point of transition from type A to type B behaviour from film to film and this plus the variation in the slope of fig. 4.4 was sufficient to mask any distinction between silver films evaporated onto pyrex and those on B37. Gold films were found to show very similar behaviour to silver, except that the transition from region A to region B occured rather earlier and the slope of fig. 4.4 for gold was greater.

4.6 Hydrogen and pre-adsorbed Xenon - Discussion

The form of the variation in $s(N_H)$ given by equation 6 is consistant with two models for the adsorption of hydrogen atoms on silver or gold surfaces. The first, due to Langmuir, suggests that a hydrogen atom can only be adsorbed at sites not already occupied and that the probability of its sticking, should it hit a vacant site is constant:

$$H + S \xrightarrow{k_1} HS \qquad \text{(a)}$$

$$HS + H \xrightarrow{k_1 \frac{N_H}{M_H}} HS + H \qquad \text{(b)}$$

and hence the overall rate (R) will be given by:

$$R = k_1\left(1 - \frac{N_H}{M_H}\right).P_H \qquad (7)$$

where P_H = pressure of hydrogen atoms

which is of the required form.

The second model shares an essentially similar adsorption step, it being assumed that the probability of an H atom sticking to any site is constant:

$$H + S \xrightarrow{k_1} HS$$

However it is then suggested that any gas phase hydrogen atom approaching or being adsorbed within some small constant distance of an adsorbed hydrogen atom will combine with it and the resulting hydrogen molecule will be desorbed:

$$\begin{array}{c} H \quad H \\ | \quad | \\ S-S \end{array} \xrightarrow{k_2 \frac{N_H}{M_H}} S-S + H_2 \qquad (c)$$

The overall rate R will now be:

$$R = \left[k_1 - k_2\frac{N_H}{M_H}\right].P_H \qquad (8)$$

which is again of the required form.

While both of these models are able to offer an explanation for the variation of sK_1 with N_H, the first seems inadequate in one respect; there is no mechanism implicit within it which permits the recombination of hydrogen atoms. Since there is no process operating in the diode cell outside of the model which can provide a recombination route at a rate comparable to the rate of hydrogen atom formation (gas phase

collisions for example occur at a rate some 10^{10} events.sec^{-1} lower than the rate of hydrogen atom production), high standing pressures of hydrogen atoms will result as sK_1 falls to a low value and this is clearly not realistic. Furthermore a recombination step of the form of (C) is essential for a full description of the interaction between pre-adsorbed gases and hydrogen. It is of course entirely possible that step (b) may occur in competition with the recombination reaction, but presumably at a rate which is slow in comparison. Its occurrence would be reflected in the value of k_2.

That the interaction between xenon and hydrogen results in a family of parallel lines in an sK_1 vs N_H plot (fig. 4.3) must imply that the rate of the recombination reaction is not influenced by the interaction in this region, since a change in k_2 would change the slope of the plot (equation (8) and fig. 4.5)

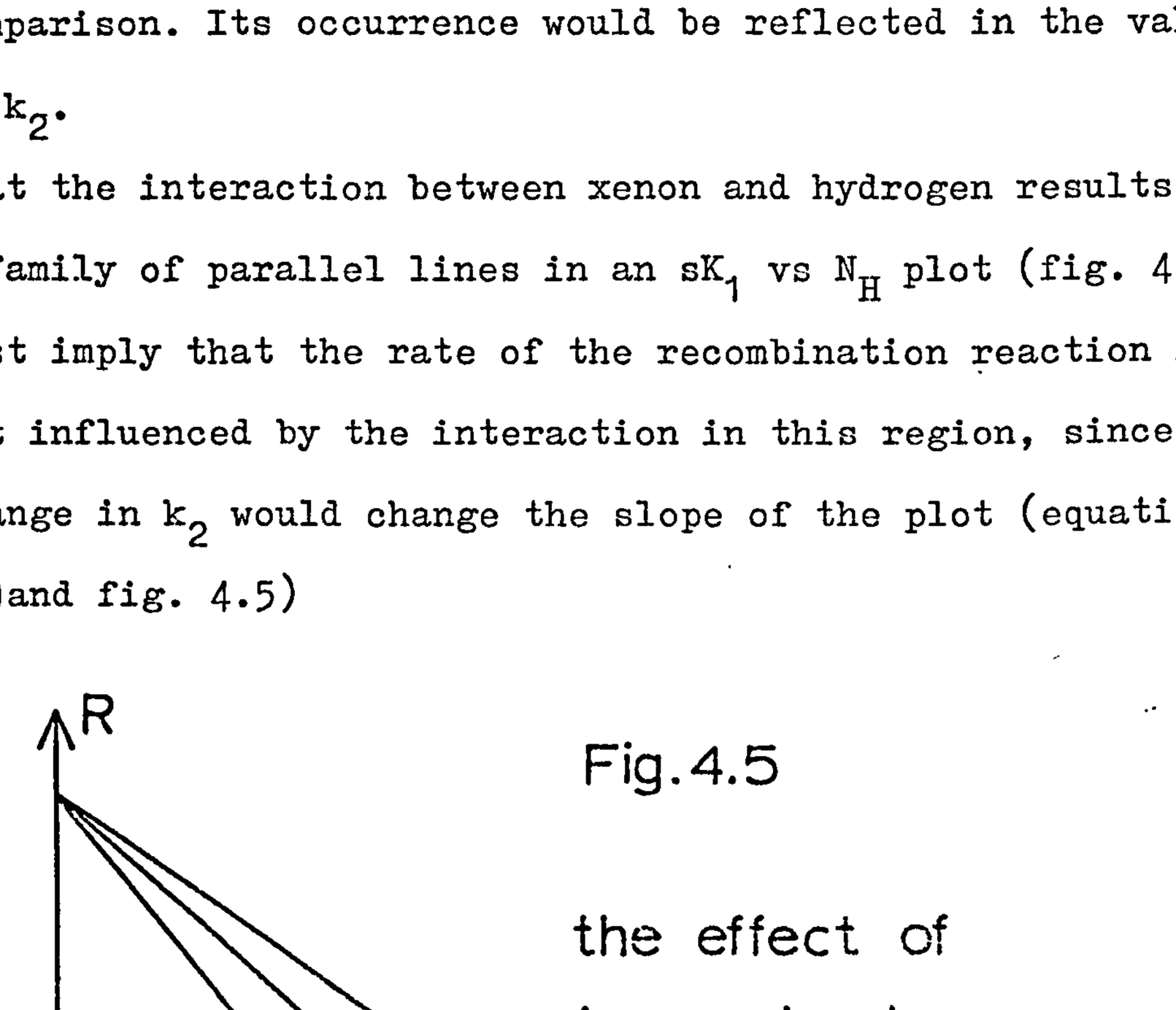

Fig. 4.5

the effect of

If the interaction results in a reduction in k_1 however, the desired family of parallel straight lines will be produced, the reduction in the rate of adsorption due to the presence of the xenon now being independent of N_H. Since,

$$R \longrightarrow 0 \quad \text{as} \quad k_2 \frac{N_H}{M_H} \longrightarrow k_1$$

a reduction in M_H

is also implied. It is tempting to suppose that the presence of adsorbed xenon atoms on the surface reduces k_1 by merely reducing the number of sites on the surface available for the adsorption of hydrogen atoms. However this is not compatable with the observed surface potential data as described and discussed in section 3.12. It is not possible unfortunately, to elucidate further the nature of the interaction between xenon and hydrogen with the data available. The events which lead to the observed behaviour in region A of fig. 4.3 i.e. before the parallel straight line regime is established, are equally difficult to rationalize. The extent of this region is undoubtably sensitive to the nature of the surface, being much attenuated on gold surfaces for example. Additionally the interaction between xenon and very low surface concentrations of hydrogen atoms may be more complex than hitherto imagined. While clearly there is a need for further experiments to elucidate the behaviour in this region, perhaps on more closely defined single crystal surfaces, it is felt that the existence of this transition zone between clean and xenon precovered surface behaviour in no way detracts from the description of the behaviour at

higher coverages.

An interesting effect is also implicit in this second (recombination) model. The system allows for a constant recycling of hydrogen atoms between the gas phase and surface in a kind of equilibration:

Fig. 4.6

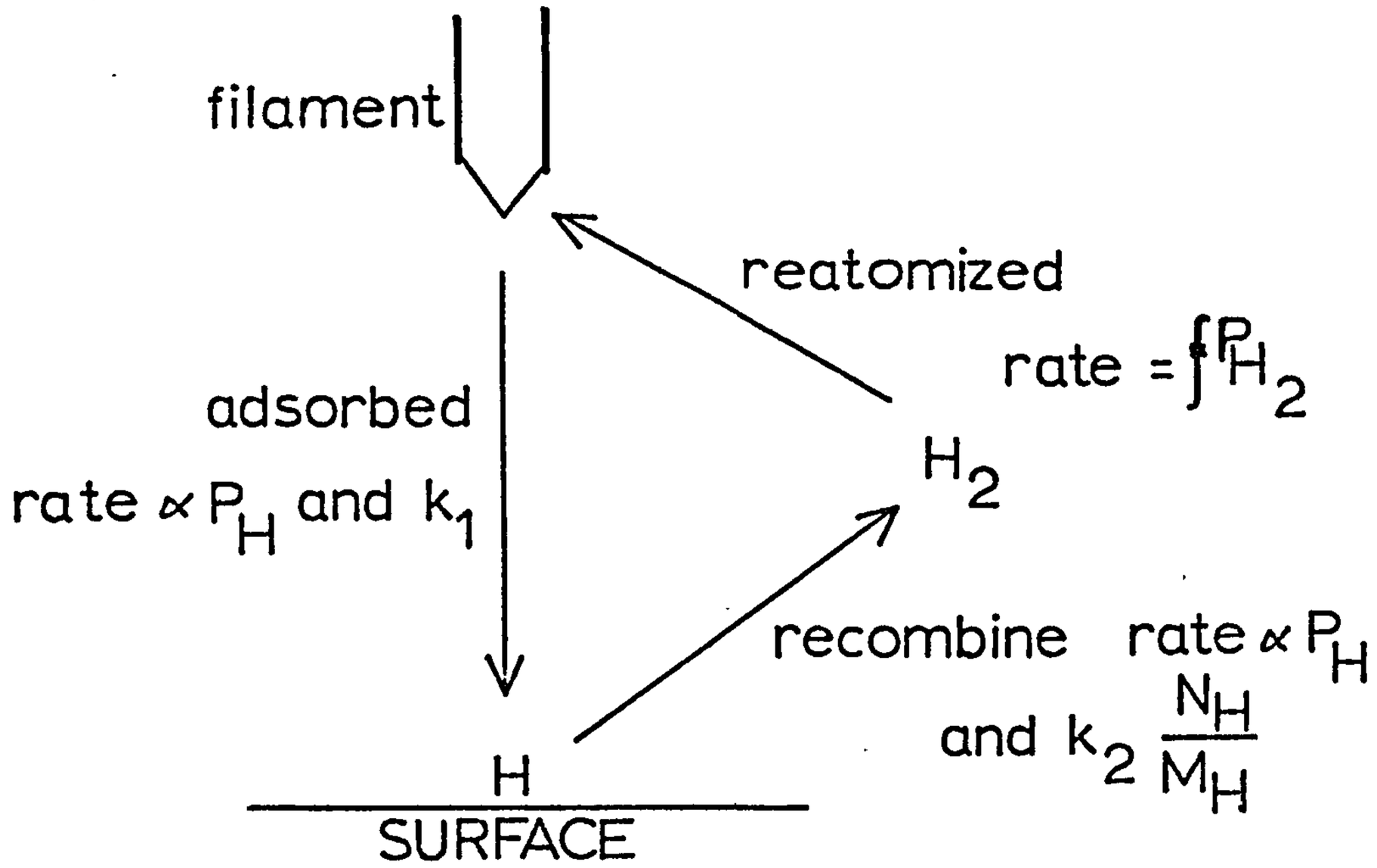

At any particular value of N_H, the rate of the adsorption and recombination reactions will be equal at some value of P_H. In the presence of an atomising filament this is itself a function of the pressure of hydrogen molecules. The reduction of k_1 (i.e. the rate of the adsorption reaction) by the addition of xenon to the hydrogen covered surface will disturb the position of equilibrium, since the rate of the recombination reaction will not be altered. Desorption of hydrogen will occur until P_H and N_H/M_H have reached values such that the rates of the adsorption and recombination reactions are again equal. Behaviour exactly consistant with

this model has been observed by Knapp and Stiddard (4). It is interesting and undoubtably significant that they report that desorption only occurs at values of N_H greater than 30% M_H i.e. only in the parallel line region (B fig.4.3).

4.7 Hydrogen plus pre-adsorbed Carbon Monoxide

Exactly similar experiments to those described above were carried out in which the xenon was replaced by pre-adsorbed carbon monoxide. The analogous graphs of sK_1 vs N_H are typified by fig. 4.7 (silver).

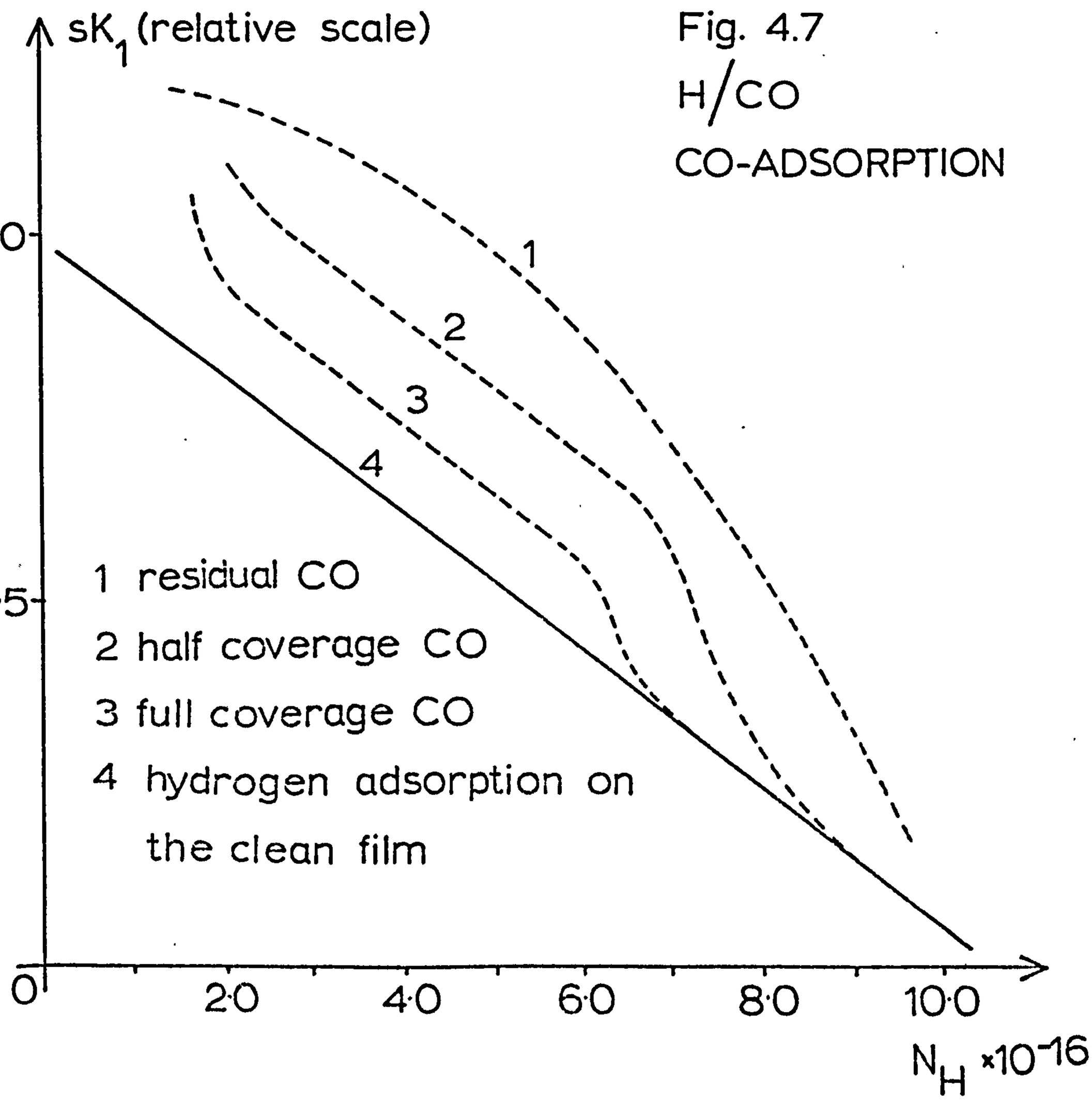

Fig. 4.7
H/CO
CO-ADSORPTION

The effect of the pre-adsorbed carbon monoxide was to increase the rate of uptake of hydrogen atoms and to cause a departure from the linear behaviour of hydrogen on a clean film. However, least departure from linearity was observed in the presence of large amounts of carbon monoxide. The maximum effect was produced by a small amount of carbon monoxide which is labeled "residual". Unlike say hydrogen which can be removed completely from the system at room temperature by pumping to a background pressure of about 1×10^{-9}torr, adsorbed carbon monoxide cannot be removed in this manner. Even after an extended period of pumping at room temperature, equilibrium pressures of carbon monoxide in the range $1\text{-}2 \times 10^{-8}$torr were recorded. It is these vestigially adsorbed species that have the maximum effect in promoting the rate of hydrogen atom adsorption, but without influencing the final maximum coverage M_H. The addition of further carbon monoxide to the surface reduces the rate of hydrogen uptakein a manner very similar to that of xenon. It is anticipated that these larger amounts of carbon monoxide reduce the rate of uptake of hydrogen via a similar mechanism i.e. reduction of the rate of the adsorption reaction (k_1) since parallel straight line behaviour is again observed. A desorption effect on adding additional carbon monoxide identical to that with xenon is also observed. The initial promotion of the rate of hydrogen uptake must result from a more complex interaction however. It appears possible that the effect might operate through a decrease in the rate of the recombination reaction, perhaps by an increased

stabilization of the hydrogen atom to surface bond since this could be imagined to produce an enhanced rate of uptake without corresponding increase in M_H.
The results for gold were in every way similar to those on silver, the initial promotion of hydrogen atom adsorption being somewhat lower however (fig. 4.8)

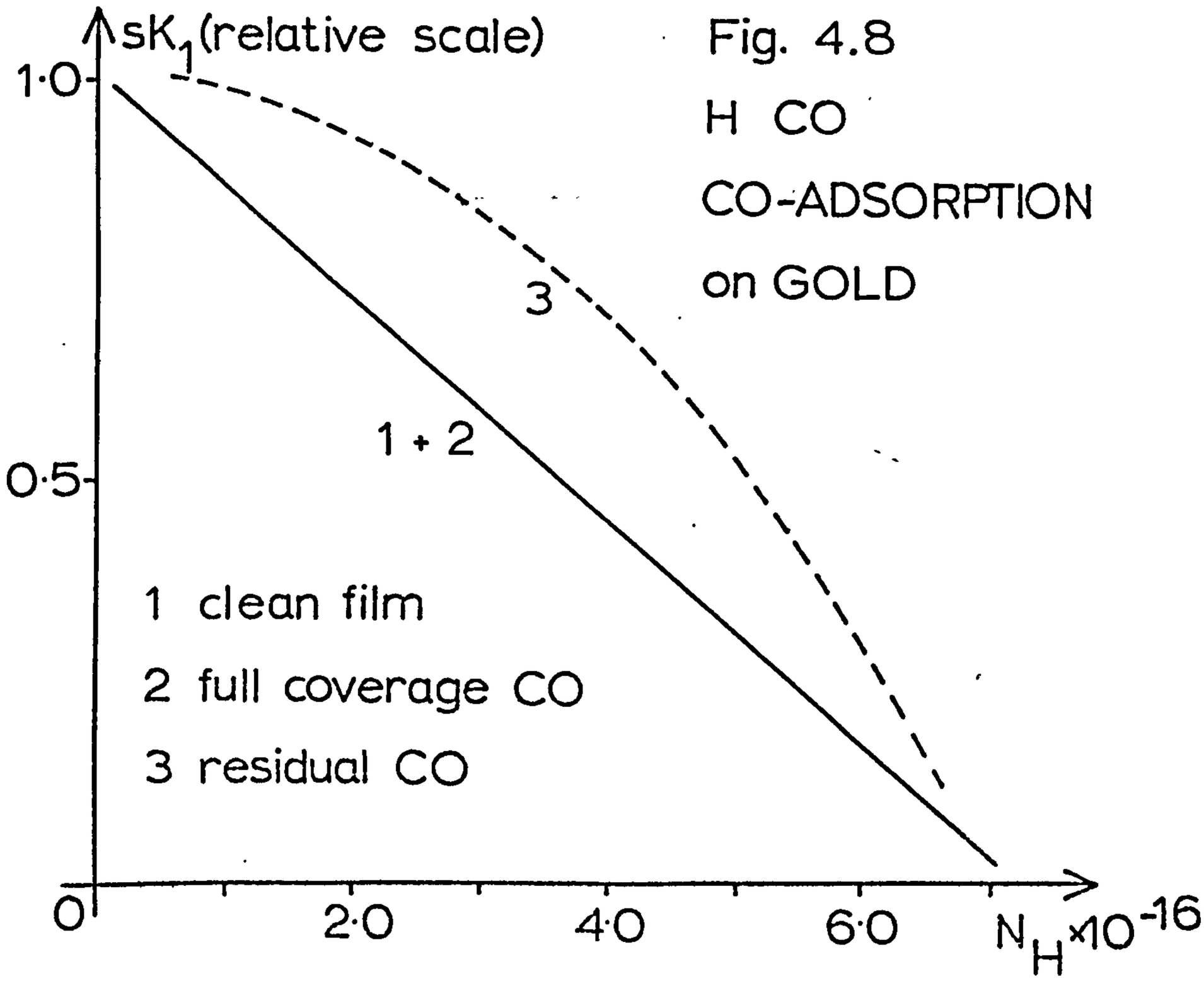

Fig. 4.8
H CO
CO-ADSORPTION
on GOLD

4.8 Summary

The rates at which xenon and hydrogen are adsorbed onto clean silver and gold films have been investigated, and two models for the observed linear variation of sticking coefficient with coverage for hydrogen discussed. One of these (the recombination model) has been shown to satisfactorily explain some features of the interaction between hydrogen

and pre-adsorbed gases on these surfaces.

It is clearly desirable at this stage to seek some independent confirmation of this model, and a particularly interesting experiment would be one in which a beam of deuterium atoms was allowed to hit a film covered with pre-adsorbed hydrogen and the desorbed gas analysed. An understanding of the role of the surface in these interactions would be facilitated by experiments in which the film was replaced by a more closely defined single crystal surface.

References

(1) H.A.Engelhardt, A.M.Bradshaw, and D.Menzel:
Surface Sci. 40, 410, (1973)

(2) G.W.Keulks and C.C.Chang: J. Phys. Chem. 74, 2590, (1970)

(3) G.W.Keulks and A.Ravi: J. Phys. Chem. 74, 783, (1970)

(4) A.G.Knapp and M.H.B.Stiddard:
J. Chem. Soc. Faraday Trans. I. 68, 2139, (1972)

(5) C.G.Goymour and D.A.King: Surface Sci. 35, 246, (1973)

(6) M.J.Dresser, T.E.Madey and J.T.Yates Jr. :
Surface Sci. 42, 533, (1974)

(7) A.M.Horgan and D.A.King: Adsorption Desorption
Phenomena, Ed. F.Ricca Academic Press, London, p329 (1972)

(8) J.Yarwood: High Vacuum Techniques, p152.

(9) D.Brennan: Adv. Catal. 16, 1, (1964)